Fall 2017

Experimental investigations of natural circulation in a separate-and-mixed effects test facility mimicking prismatic modular reactor (PMR) core

Mahmoud M. Taha

Department: Chemical and Biochemical Engineering

EXPERIMENTAL INVESTIGATIONS OF NATURAL CIRCULATION IN A SEPARATE-AND-MIXED EFFECTS TEST FACILITY MIMICKING PRISMATIC MODULAR REACTOR (PMR) CORE

by

MAHMOUD MOHAMED TAHA MOHARAM

A DISSERTATION

Presented to the Faculty of the Graduate School of the

MISSOURI UNIVERSITY OF SCIENCE AND TECHNOLOGY

In Partial Fulfillment of the Requirements for the Degree

DOCTOR OF PHILOSOPHY

in

CHEMICAL ENGINEERING

2017

Approved by:

Muthanna H. Al-Dahhan, Advisor
Shoaib Usman, Co-advisor
Jee-Ching Wang
Fateme Rezaei
Joshua P. Schlegel

PUBLICATION DISSERTATION OPTION

This dissertation consists of the following four articles which have been submitted for publication as follows:

Paper I: Pages 28-73 have been submitted to the Nuclear Engineering and Design Journal.

Paper II: Pages 74-109 have been submitted to the International Journal of Thermal Sciences Journal.

Paper III: Pages 110-141 have been submitted to Experimental Thermal and Fluid Sciences Journal.

Paper IV: Pages 142-185 have been submitted to International Journal of Heat and Mass Transfer Journal.

ABSTRACT

After the Fukushima Daiichi nuclear power plant accident in 2011, significant attention was directed to investigate natural circulation thermal-hydraulics in Prismatic Modular Reactors (PMRs). Natural circulation is employed as a passive safety feature that passively removes the decay heat released after the loss of flow accidents (LOFA). Several computational studies have addressed such phenomena, however, validation of Computational Fluid Dynamics (CFD) is needed by providing high-quality data obtained from separate test facilities designed with reference to the corresponding reference PMRs. To address this need, a separate effects Plenum-to-Plenum Facility (P2PF) was designed and developed with dual channels and plena for experimental investigations of naturally driven gas thermal and velocity fields under different circulation intensities. Thermal and velocity measurements have been characterized by implementation of advanced sophisticated measurement techniques such as: (1) the hot wire anemometry (HWA), (2) flush-mounted micro-foil sensors, and (3) thermocouples that are capable of providing local measurements at different axial and radials positions along both channels. These measurement techniques have been integrated in a novel way so that the thermocouple readings are not disturbed by the HWA sensor, and vice versa. This proposed work has a significant impact on advancing the knowledge and understanding of the plenum-to-plenum (P2P) natural circulation thermal-hydraulic phenomenon and provides high-quality benchmark data that are much needed for verification and validation (V&V) of computational fluid dynamics (CFD) models and codes. Therefore, computational simulations can be reliably used in designing PMRs passive safety systems and in safety analysis and assessment.

ACKNOWLEDGEMENTS

First and foremost, thanks and praises to ALLAH for his kindness and blessing. Thanks for giving me faith to believe in myself and guidance to overcome my weakness. Thanks for granting me patience through the hard times and thankfulness through the good times.

I wish to express my deep gratitude and thanks to my advisor, Dr. Muthanna H. Al-Dahhan, and my co-advisor, Dr. Shoaib Usman. Dr. Muthanna H. Al-Dahhan introduced me to Missouri University of Science and Technology and encouraged me to pursue my Ph.D. under his guidance with his research team at this great university. Also, I would like to thank Dr. Shoaib Usman for his support and affording me in the early stages of the research until I gained the required skills to understand and complete the work independently. In addition, I would like to thank all my colleagues for their support, help; and I want to say that I will never forget the hard and fun times we have faced together during these years of friendship, study, and work. I am very lucky to be a member of such a team, and hope to keep our friendship forever. Warm and special thanks are due to my family: Mohamed Taha Moharam, Nadia Mohamed Abelghani, Fatma Mohamed Taha, Abdelrahman Ahmed Elramsisi, Zeinab Mahmoud Elemary, and Ahmed Abdelrahman Elramsisi for their encouragement throughout these years. Finally and forever, I don’t find words to thank my lovely wife, Nourhan. Thanks for believing in me and for supporting our dream which today comes true as a result of her sacrifices. As I head towards other places to meet other peoples, I hope I left a good memory as I gathered many.

TABLE OF CONTENTS

LIST OF ILLUSTRATIONS

SECTION Page

PAPER III

PAPER IV

LIST OF TABLES

SECTION Page

PAPER III

PAPER IV

NOMENCLATURE

Abbreviations	Description
IPCC	International Panel on Climate Change
Gen-IV	Generation IV nuclear reactors
NGNPs	Next Generation Nuclear Plants
GIF	Generation IV International Forum
SERs	Fast neutron reactors cooled by sodium (Sodium-cooled fast reactors)
LFRs	Fast neutron reactors cooled by lead (Lead-cooled fast reactors)
GFRs	Fast neutron reactors cooled by helium gas Gas-Cooled fast reactors)
VHTRs	Very High-Temperature Gas-cooled Reactors
SCWRs	Supercritical Water-cooled Reactors
MSRs	Molten Salt Reactors
GCRs	Gas-cooled Reactors
HTGRs	High-Temperature Gas-cooled Reactors
PMRs	Prismatic Modular Reactors
PBR	Pebble Bed Reactor
PBMR	Pebble Bed Modular Reactor
AVR	Arbeitsgemeinschaft Versuchsreaktor reactor
FSV	Fort St. Vrain reactor
THTR-300	Thorium High-Temperature Reactor
JAERI	Japan Atomic Energy Research Institute
HTTR	High-Temperature Engineering Test Reactor

HTR-10	High-Temperature Gas-Cooled Reactor Test Module
INET	the Institute of Nuclear Energy Technology
GA	General Atomics
GT-MHR	Gas Turbine-Modular Helium Reactor
HTR-Module	Modular High-Temperature Gas-cooled Reactor
TRISO	Tri-Structural Isotropic or Tri-Isotopes
NHDD	Nuclear Hydrogen Development and Demonstration
DOE	U.S. Department of Energy
NNSA	National Nuclear Security Administration
OKBM	Experimental Design Bureau of Mechanical Engineering
KI	Kurchatov Institute
VNIINM	A.A. Bochvar All-Russian Scientific Research Institute for Inorganic Materials
RCCS	Reactor Cavity Cooling System
HTR-TN	High-Temperature Reactor–Technology Network
GTHTR300C	Gas Turbine High-Temperature Reactor 300
KAERI	Korea Atomic Energy Research Institute
CFD	Computational Fluid Dynamics
INL	Idaho National Laboratory
ORNL	Oak Ridge National Laboratory
ANL	Argonne National Laboratory
DBA	Design Basis Accidents
PCC	Pressurized Conduction Cool-down
LOFA	loss of forced cooling accident

DCC	De-pressurized Conduction Cool-down
LOCA	loss of coolant accident
GT	gaseous tracer
RTD	residence time distribution
OSU-HTTF	Oregon State University High-Temperature Test Facility

1. INTRODUCTION

The 5th Assessment Report (AR5) of the International Panel on Climate Change (IPCC) suggests that under current policies, CO emissions from the energy sector could double or triple by 2050. Reducing emissions to a level unlikely to cause dangerous climate change will require a significant drop in the energy intensity of global economies, along with the rapid reduction in the use of fossil fuels (Schneider 2014). This suggestion is consistent with the US energy policy for reducing carbon emissions and increasing energy independence (Chapin 2004) through extensive and comprehensive studies undergo to investigate the performance characteristics and safety features of the proposed Generation IV nuclear reactors (Gen-IV), or Next Generation Nuclear Plants (NGNPs), as operating nuclear reactors releases CO_2-free emissions. These NGNPs are the evolutionary development of past nuclear generations that have evolved into four distinct generations as shown in Figure 1.1.

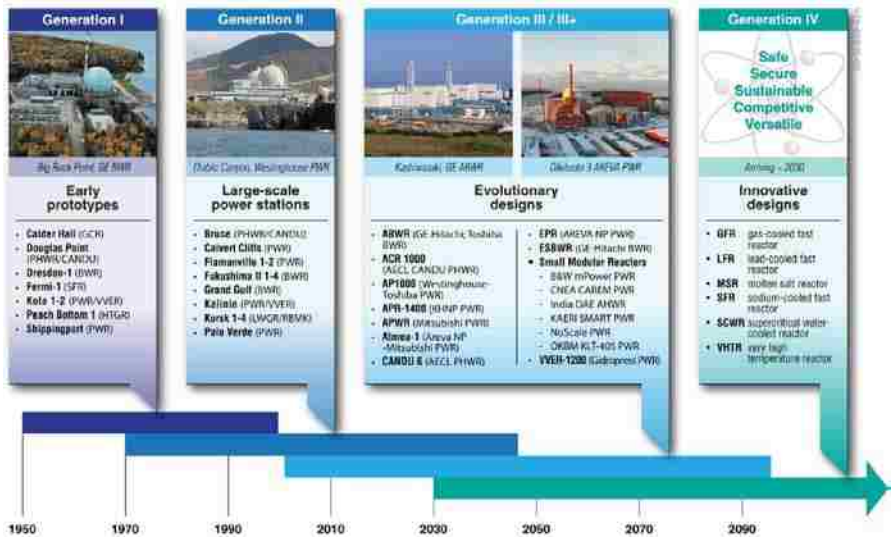

Figure 1.1. Different generations of nuclear generation systems (Kelly 2013)

- 1st generation: consists of early prototypes and demonstrates safe generation of electricity by nuclear means. All the prototypes in this generation were retired or improved to the next following two generations.
- 2nd generation: consists of current operating plants that went under power-up-rating and life extension.
- 3rd generation: consists of deployable improvements to current reactors mainly passive safety systems were used.
- 4th generation: known as Gen-IV or NGNP and consists of new advanced reactor systems.

The NGNPs are a set of theoretical designs currently being searched. This generation involves six designs released by the Generation IV International Forum (GIF) in 2000 among over 200 proposed designs. These systems include fast neutron reactors cooled by sodium (SFRs), lead (LFRs), or helium gas (GFRs); Very High-Temperature Gas-cooled Reactors (VHTRs); Supercritical Water-cooled Reactors (SCWRs) and Molten Salt Reactors (MSRs), as mentioned previously in Figure 1.1 (Kelly 2013). The operating conditions and design specifications for different NGNPs proposed systems are shown in Table 1.1. The current status and different project arrangements for NGNPs, different designs, are shown in Table 1.2.

The NGNPs are deployed to be more safe, secure, sustainable, competitive, and versatile than previous generations. Enhanced safety is one of the major design criteria for this new generation, and it focuses on developing inherent safety features and designs to remove the decay heat naturally, in case of accidents, so there is no risk of releasing large amounts of radioactive material that would necessitate the evacuation of the surrounding

public of the site. Sustainability means that this generation has the ability to meet the present and future needs for energy. Economic goals focus on reducing operating and capital costs through increased efficiency, design simplifications, and advances in fabrication and construction techniques. This generation will help to generate 100:300 times more energy yield from the same amount of nuclear fuel relative to current nuclear power plants. Also, this generation provides the ability to utilize existing nuclear waste in the production of electricity (Chapin 2004).

Table 1.1. NGNP operating conditions and design specifications (Abdulmohsin, 2013)

The energy policy act of 2005 designates that the NGNPs will be based on a Very High-Temperature Reactors (VHTRs) (also called High-Temperature Gas-cooled Reactors "HTGRs") (Sato et al. 2010). It is worth mentioning that the VHTR term refers to any reactor with an outlet temperature of 1000 ℃ or above. This achievable high temperature

affords high-efficiency electrical generation and the use of nuclear power for potential process heat utilization, specifically carbon-free hydrogen production using nuclear heat via thermos-chemical processes, coal gasification, etc. (Chapin 2004, Sato et al. 2010). These VHTRs are advanced designs of Gas-Cooled Reactors (GCRs). Generally, GCRs are nuclear reactors that use graphite moderator and carbon dioxide or helium gas as a coolant. Graphite moderator is used to slow down the movement of neutrons emitted from the fuel for a certain time to permit the nuclear fission to occur. Helium is more preferable than CO_2 as is it more efficient and highly resistant to corrosion, but CO_2 is much cheaper. On the other hand, helium purification prior to entering the reactor is of paramount importance as the presence of impurities may cause direct corrosion at very high temperatures. The U.S. Department of Energy (DOE) is exploring the potential for VHTRs, which will be either Prismatic Modular Reactors (PMR) or Pebble Bed Reactors (PBR) (Chapin 2004, Abdulmohsin 2013, Sato et al. 2010, Khane 2014). A brief history of GCRs covering the design features of both types of VHTRs is shown in the succeeding parts.

Table 1.2. Gen-IV different design current status and project arrangements (Kelly 2013)

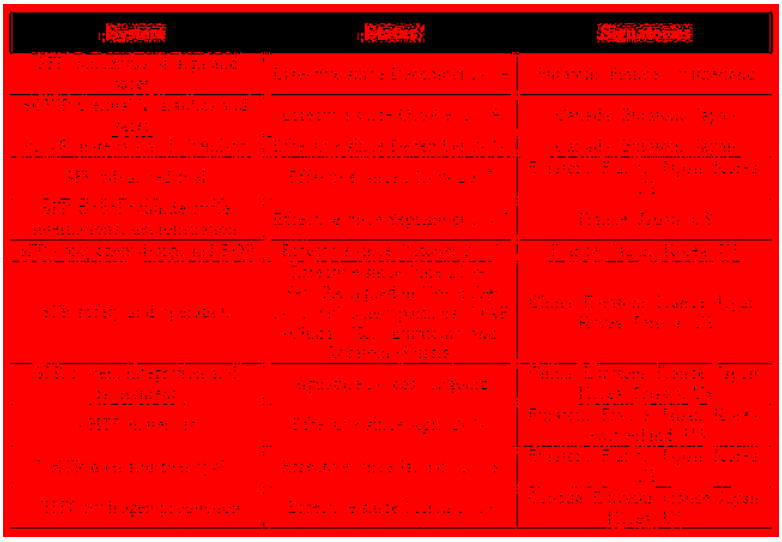

1.1. THE HISTORY OF GCRs

The history of GCRs begins with the X-10 reactor in Oak Ridge, Tennessee, which was attained critically in 1943. It was a graphite-moderated and air-cooled reactor capable of generating 3.5 MW. The first HTGR prototype was the Dragon reactor commissioned in the UK. The project started in 1959, completed in 1964, reached its full-power of 20 MW by 1966, and operated until 1974. It produced 20 MW of heat and did not have an electricity generator circuit. In Germany, the Arbeitsgemeinschaft Versuchsreaktor (AVR) plant construction, which was based on pebble bed concept, also started in 1959. It was a 15 MW power plant and operated for 12 years until cancellation. The first prototype in the United States, which was based on the design in which the fuel is prismatic, was Peach Bottom Unit 1. It was commissioned in 1967 and operated until 1974, generating 40 MW of electricity. The USA was the first country to generate electricity using HTGR power plant. Following the successful prototype HTGR plants, larger plants were constructed to further study the commercial viability of the HTGR concept. Also, in the United States, the Fort St. Vrain (FSV) began to produce electricity in 1976 but was not declared commercial until 1979. In Germany, the successor nuclear plant, which is Thorium High-Temperature Reactor (THTR-300), was ordered in 1970. It was based on the pebble bed concept. In 1985, it was connected to the electrical grid, producing 300 MW of electricity, and operated until 1989 when it was subsidized by the government because of the safety regulator and other technical problems encountered during plant operation, although all repairs were completed in February 1989. Afterwards, Japan Atomic Energy Research Institute (JAERI) began construction of the High-Temperature Engineering Test Reactor (HTTR) in Japan in 1991. In 2000, the construction of the High-Temperature Gas-Cooled

Reactor Test Module (HTR-10), developed by the Institute of Nuclear Energy Technology (INET), was completed in China. Both reactors are considered state of the art in HTGRs design, with the HTTR using prismatic block fuel and the HTR-10 using pebble fuel concept, which is discussed later. The most recent attempt to develop a commercial VHTR based on pebble fuel concept started in South Africa in 1998, but in 2010, the final closure of the project was declared after the expenditure of a large amount of South Africa public money on it. On the other hand, the U.S. General Atomics (GA) and Russian Federation program cooperated to develop the prismatic fuel based GT-MHR and brought it into operation by 2010. The HTGRs' coolant temperatures for previously mentioned different reactors are shown in Figure 1.2. (Doug Chapin 2004, Thomas 2011, McDonald 2014).

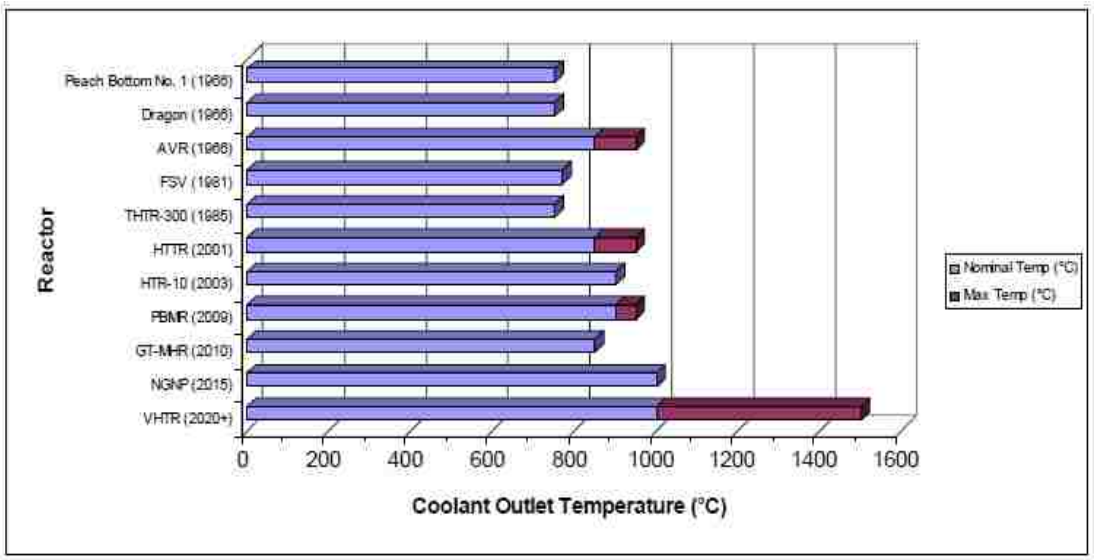

Figure 1.2. HTGR Coolant Outlet Temperatures (Chapin 2004)

The interest in GCRs has renewed, and a number of HTGRs designs have been developed for near-term deployment (i.e., generation III+ reactors). These include the

Pebble Bed Modular Reactor (PBMR) project, led by Eskom, and the Gas Turbine-Modular Helium Reactor (GT-MHR), which is composed of a prismatic core, developed by General Atomics. The GT-MHR and PBMR are the basis for the prismatic-and-Pebble VHTRs, respectively. The renewal interest is attributed to the successful commercial scale of carbon dioxide gas cooled reactor developed in the UK that motivates subsidy of the VHTRs. A summary of the key specifications for different types of HTGRs mentioned above is listed in Table 1.3. It is worth mentioning that this study is concerned with studying PMR.

Table 1.3. Key specifications for HTGRs (Beck 2011)

Reactors	Dragon	Peach Bottom	AVR	FSV	THTR	HTTR	HTR-10	AGRs	MHTGR	GT-MHR
Thermal Power (MW(t))	21.5	115	46	842	750	30	10	1500	350	600
Power Density (MW/m^3)	14	8.3	2.6	6.3	6	2.5	2	6	5.9	6.5
Primary Coolant	He	He	He	He	He	He	He	CO_2	He	He
Secondary Coolant	Steam	Steam	Steam	Steam	Steam	He/ Press. Water	Steam	Steam	Steam	—
Primary Coolant Pressure (MPa)	2	2.3	1.1	4.8	4	4	3	4.1	6.4	7
Primary Coolant Flow Rate (kg/s)	9.62	60*	13	110	512	10.2-12.4	3.2-4.3	3790	158	320
Reactor Inlet Temperature (°C)	350	327	275	404	250	395	250	278	258	491
Reactor Outlet Temperature (°C)	750	700-726	950	777	750	850-950	700	635-675	686	850
RPV Material	Carbon Steel	Carbon Steel	steel and concrete building	PCRV** with Liner	PCRV	2-1/4Cr-1Mo Steel	C-Mn-Si Steel	PCRV	Steel	Mod 9Cr-1Mo Steel
Core Structure Type	Graphite	Graphite	Graphite / Ceramic	Graphite	Graphite	Graphite	Graphite	Graphite	Graphite	Graphite
Fuel Element Type	Prismatic block	Prismatic block	Pebble bed	Prismatic block	Pebble bed	Prismatic block	Pebble bed	Prismatic block	Prismatic block	Prismatic block
Fuel	(U,Th,PuO$_2$) TRISO	(U,ThO$_2$) BISO	(U,ThO$_2$) BISO; the TRISO	UO$_2$ & ThO$_2$-UO$_2$ TRISO	(U,ThO$_2$) BISO	UO$_2$ TRISO	UO$_2$ TRISO	UO_2	UCO TRISO	Possible use of various
Enrichment (wt%)	3.5	93	93	93	93	3-10 (avg 6)	17	2.5-3.5	19	Avg 19
Circulator Size (kWe)	75	1417	220	3954	2300	Two @ 260, one @ 190	165	1171-5370	3210	
Circulator Quantity	6	2	(blowers) 2	4	6	3	1	8-Apr	1/module	
Years Operational	1964-1975	1966-1974	1967-1988	1976-1989	1985-1991	1998-Present	2000-Present	1962-Present	---	—
Primary Coolant	He	He	He	He	He	He	He	CO_2	He	He

*Total flow is divided equally between two loops, **Prestressed Concrete Reactor Vessel

1.2. THE PEBBLE BED REACTORS (PBRs) DESIGN

The first design of PBR was the AVR plant which started in 1959 in Germany. The design and dimensions of pebbles in this reactor is the same for all successor pebble bed designs (Thomas 2011). The design features of this reactor are explained in great detail (Schulten 1978, Frewer 1985, Schulten 1985). Recent research regarding PBRs took place for 12 years in South Africa to develop PBMR, but eventually, the project was abandoned in 2010 (Koster 2003, Thomas 2011). The HTR-10 experimental reactor constructed in China with the guidance of AVR and PBMR in South Africa is considered state of the art for pebble-based VHTRs in NGNP proposed designs.

The Modular High-Temperature Gas-cooled Reactor concept which was proposed originally as the ‘HTR-Module' by Siemens German in 1979 (shown in Figure 1.3) was applied to the HTR-10 as well, shown in Figure 1.4. These preliminary design features involve the use of spherical pebbles (i.e., have the size of a tennis balls usually 6 cm in diameter) and are capable of retaining all radiologically relevant fission products up to fuel element temperatures of 1600 ℃. The structural material of the core is made of graphite for its low neutron absorption, strong resistance to radiation, excellent heat resistance, and good thermal conductivity characteristics. Thus, graphite has the ability to moderate the fast emitted neutrons so as to the nuclear fission reactions are maintained. Furthermore, owing to its high thermal capacity, graphite also serves to mitigate rapid temperature increases during an accident. In HTR-Module, graphite is embedded in core areas with high temperatures (i.e., fuel elements and core internals). The noble gas helium, which is neutral from a chemical and neutron physical viewpoint, is used as a coolant. Helium has thermal and chemical stability, and good compatibility with the core graphite material and

metallic material of the primary system at the high-temperature condition; in addition, there is no phase transition. (Lohnert 1990, Steinwarz 1990, Xu 2002, Wu 2002, Zhang 2002, Abdulmohsin 2013, Khane 2014).

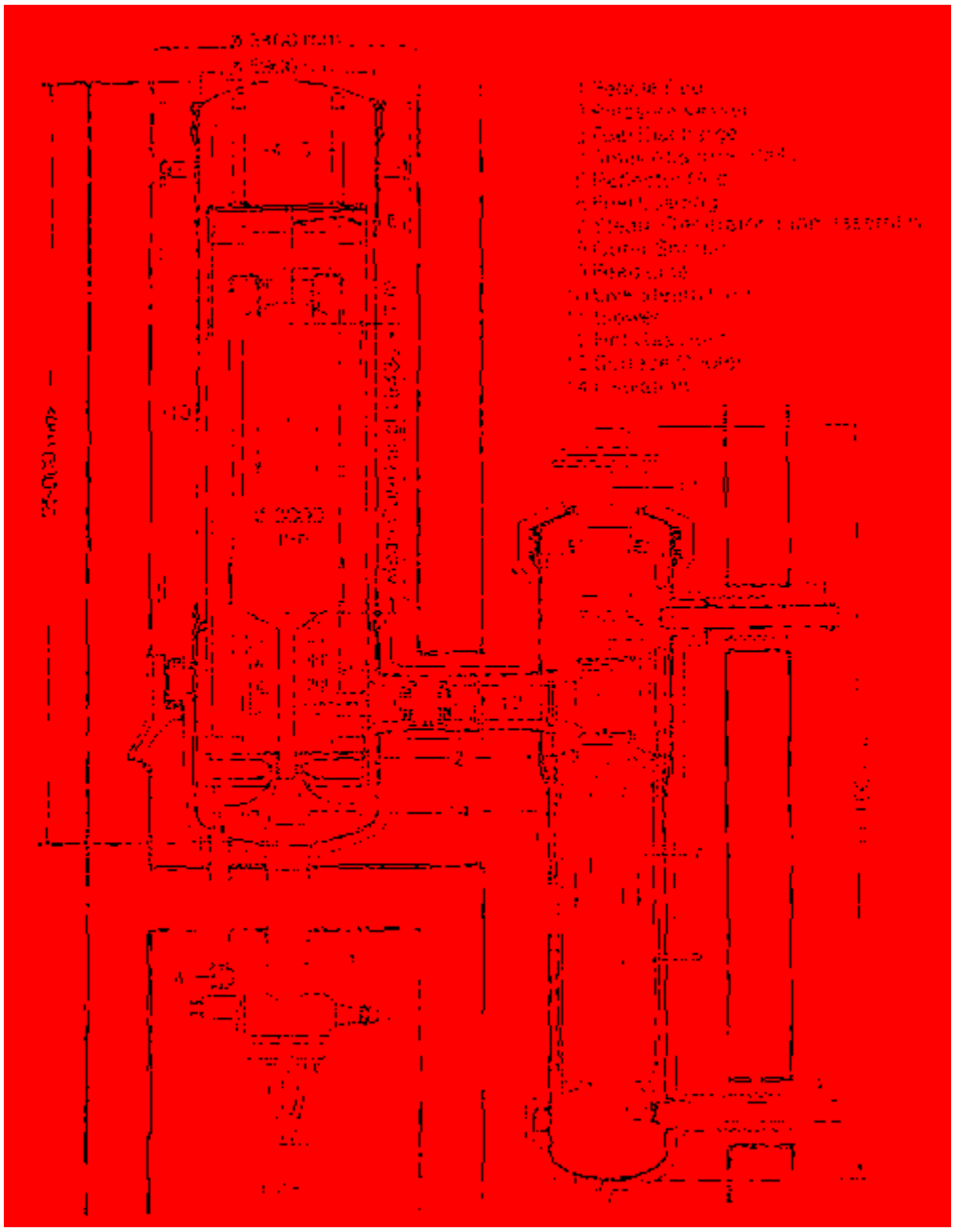

Figure 1.3. Cross section of the HTR-module (Wu 2002)

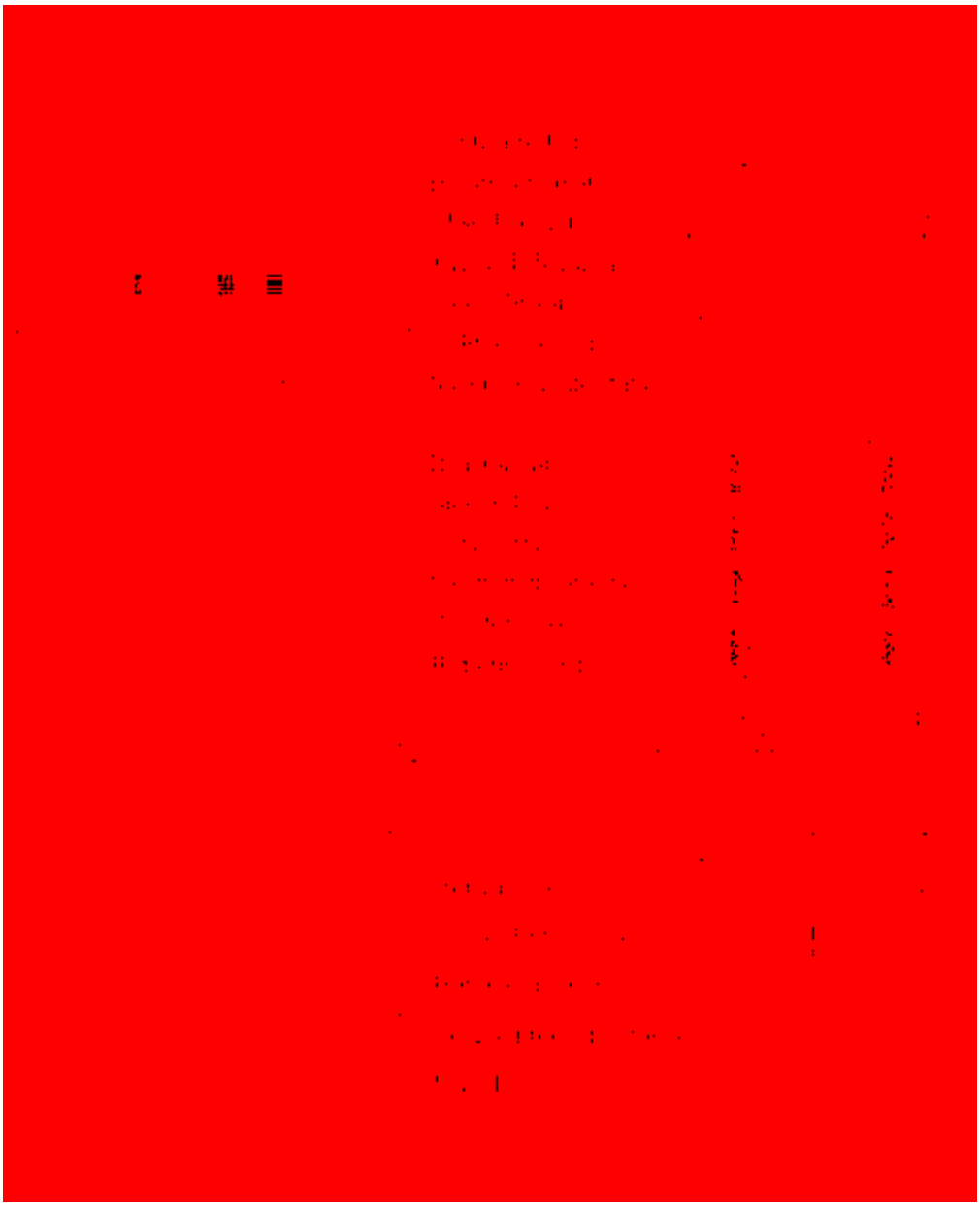

Figure 1.4. The HTR-10 reactor and steam generator arrangement in the primary cavity (Wu 2002)

The reactor core has a “double-zone” configuration (i.e., there are two cores: an inner blind core of graphite spheres at the center and an outer annular active core with fuel spheres), as shown in Figure 1.5. The core of the HTR-10 is formed as a pebble bed with

27000 spherical fuel elements. The pebble bed reactor is considered for its merit of continuous discharge of spent spherical fuel elements without shutting down the reactor, which can increase the reactor operation availability. The spherical fuel elements with Tri-Structural Isotropic or Tri-Isotopes (TRISO) coated particles are used in HTR-10. The low-enriched uranium dioxide (UO_2) fuel kernel particles are coated with ceramic layers, namely the inner buffer layer with less dense pyro-carbon, the dense pyro-carbon, the Silicon Carbide (SiC) coating and the outer layer of dense pyro-carbon as shown in Figure 1.6. It worth mentioning that TRISO fuel kernel may be composed of low-enriched uranium dioxide (UO_2), sometimes uranium oxycarbide (UCO), and it has diameter of 0.5 mm (Lohnert 1990, Steinwarz 1990, Wu 2002, Abdulmohsin 2013, Khane 2014).

Helium gas moves downwards through a complex interconnected network of voids formed between pebbles and removes the heat from the fuel (Yang 2009, Khane 2014). The fuel pebbles drop into the reactor core and move downward under the gravitational effect and then discharge from the bottom of the reactor. Then, the fuel pebbles pass through a defective fuel separator and the burn-up measurement facility one by one. These defective fuel elements and the scrap fragments should be sorted and dropped into the scrap contained. Fuel elements that have not reached the burn-up target (i.e., the amount of fissile materials in it) will be recirculated into the reactor core, and the spent fuel elements excessing the burn-up target will be discharged and transported into the spent fuel discharge tank. New fuel elements could be loaded into the reactor core with no need to shut down the reactor (Lohnert 1990, Steinwarz 1990, Wu 2002, Abdulmohsin 2013, Khane 2014). The advantages and disadvantages of PBR are mentioned in Table 1.4.

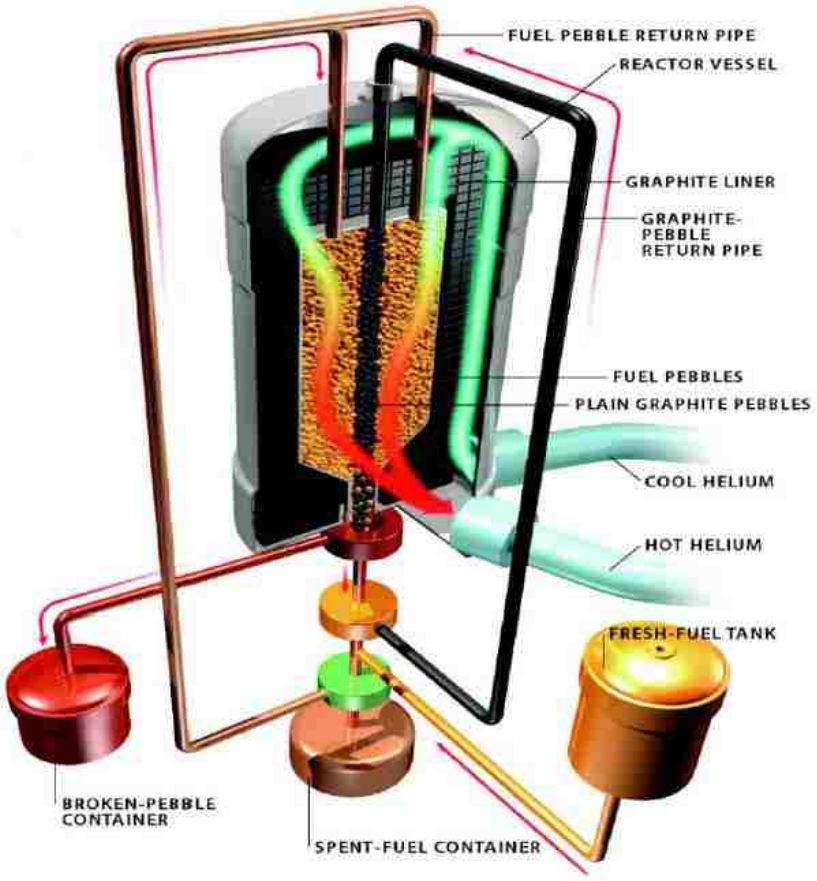

Figure 1.5. Schematic Diagram of the Pebble-Bed Nuclear Reactor (Rycroft 2007)

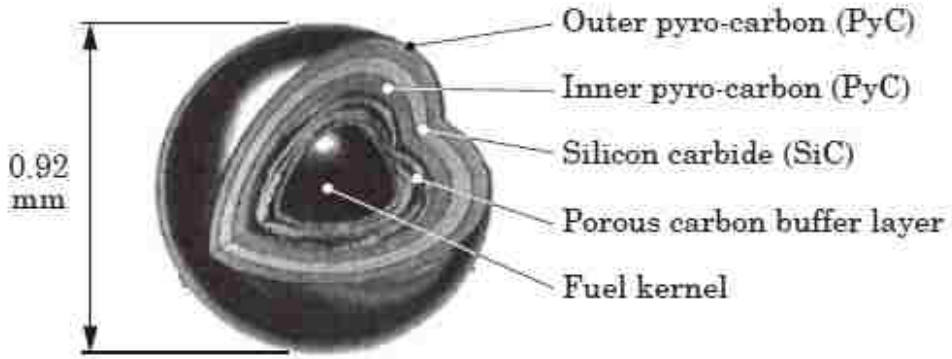

Figure 1.6. Coated fuel particle (Espinosa-Paredes 2014)

Table 1.4. Advantages and disadvantages of PBR (Abdulmohsin 2013)

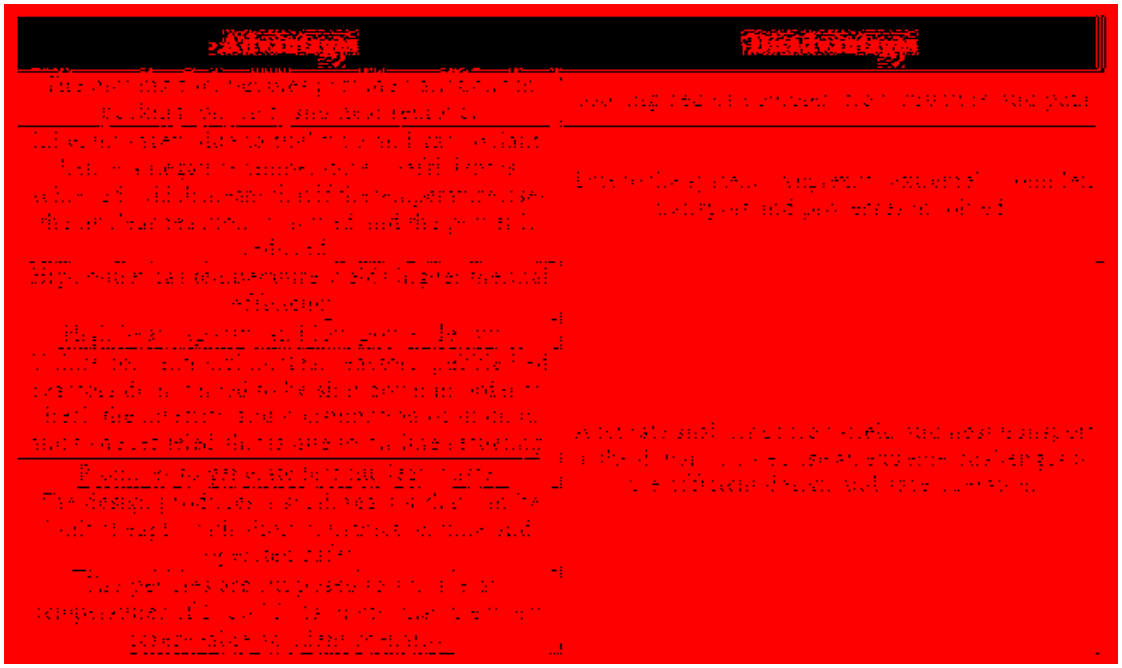

1.3. THE PRISMATIC MODULAR REACTORS (PMRs) DESIGN

There are currently five concepts for the prismatic VHTRs under consideration by different Generation IV International Forum (GIF) nations: the Gas-Turbine Modular Helium-cooled Reactor (GT-MHR), the Russian GT-MHR, AREVA HTR-VHTR design (ANTARES), the Modular High-Temperature Reactor Technology Network (HTR-TN), High Temperature Test Reactor (HTTR), and Nuclear Hydrogen Development and Demonstration (NHDD). The GT-MHR, also called Modular High-Temperature Gas Reactor (MHTGR), was developed in the USA by the General Atomics (GA), is a 600 MW-thermal plant with options for cogeneration of electricity and process heat. In cooperation with the GA and the U.S. Department of Energy (DOE) National Nuclear Security Administration (NNSA), the Experimental Design Bureau of Mechanical Engineering (OKBM) in Nizhniy-Novgorod with partners at the Kurchatov Institute (KI)

and the A.A. Bochvar All-Russian Scientific Research Institute for Inorganic Materials (VNIINM) in Moscow is designing a Russian version of the General Atomics (GA) GT-MHR. In France, the Areva prismatic-fuel, indirect cycle, water-cooled Reactor Cavity Cooling System (RCCS), filtered confinement Modular High-Temperature Reactor (HTR) (designated ANTARES) where Areva is also partnered with other EURATOM participants in the High-Temperature Reactor–Technology Network (HTR-TN). The Japan Atomic Energy Agency (JAEA) continues development work begun under the former Japan Atomic Energy Research Institute (JAERI) on the Gas Turbine High-Temperature Reactor 300 for Cogeneration (GTHTR300C), which will scale up the technology from the JAEA 30 MW-thermal High-Temperature Test Reactor (HTTR). However, deployment of the GTHTR300C is not envisioned until after 2030 (Moses 2010). The last concept was led by the Korea Atomic Energy Research Institute (KAERI), who is pursuing the Nuclear Hydrogen Development and Demonstration (NHDD) project, which will be limited to a 200 MW-thermal project (Moses 2010). The GT-MHT or the MHTGR is considered the reference reactor for a PMR and also a candidate for the DOE-funded NGNP, so its design features will be considered in detail below (Sato et al. 2010).

- Design features of GT-MHR (or MHTGR)

General Atomics (GA) Gas Turbine-Modular Helium Reactor (GT-MHR) meets the Generation IV nuclear programme goals, including passive safety, competitive economics, enhanced proliferation resistance, and improved water disposal characteristics (Moses 2010). It couples a gas-cooled modular helium reactor (MHR), contained in one vessel, with a high-efficiency Brayton cycle gas turbine (GT) energy conversion system contained in the other vessel, as shown in Figure 1.7. The reactor and power conversion vessels are

interconnected with a short cross-vessel and are located in a concrete silo below ground level as shown in the fully embedded reactor design in Figure 1.8.

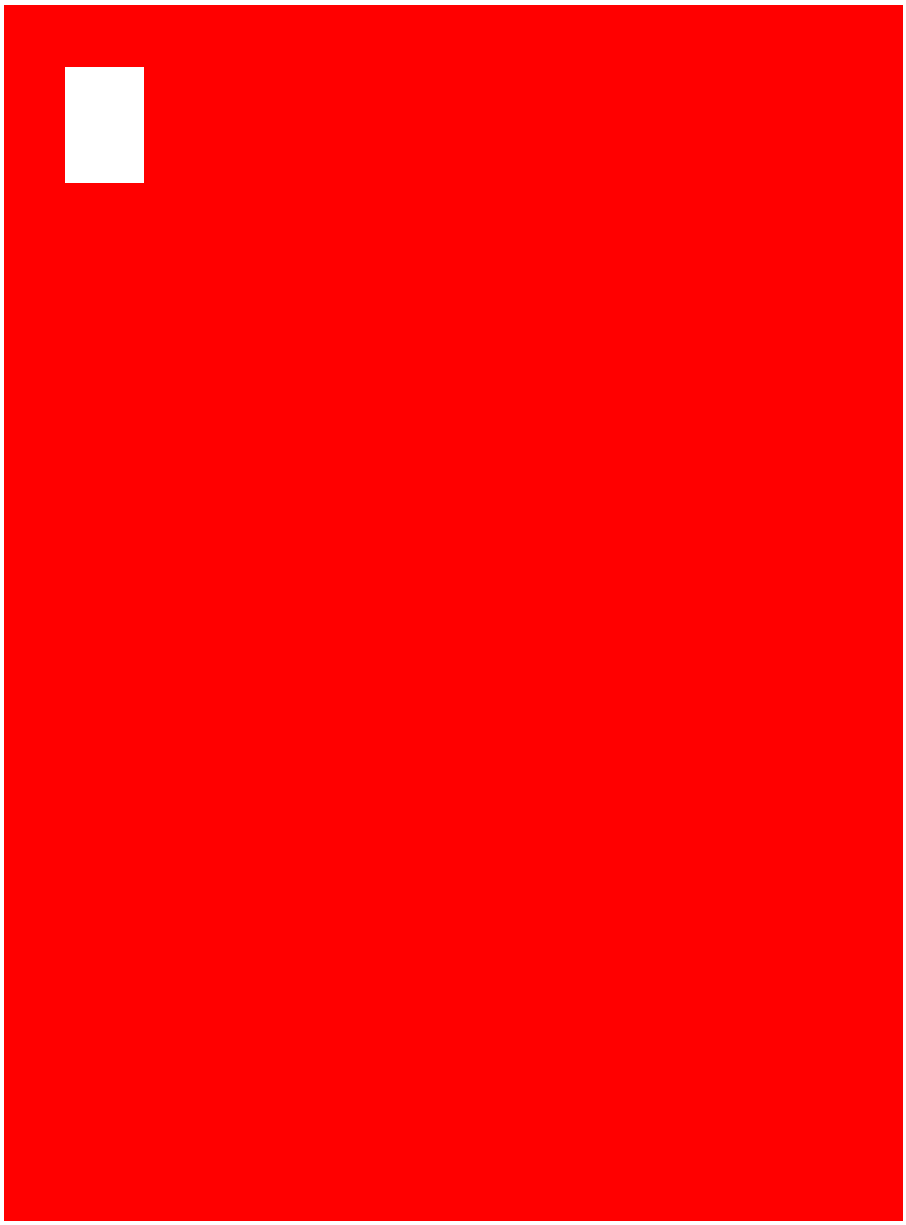

Figure 1.7. The GT-MHR vessel system (LaBar et al. 2004)

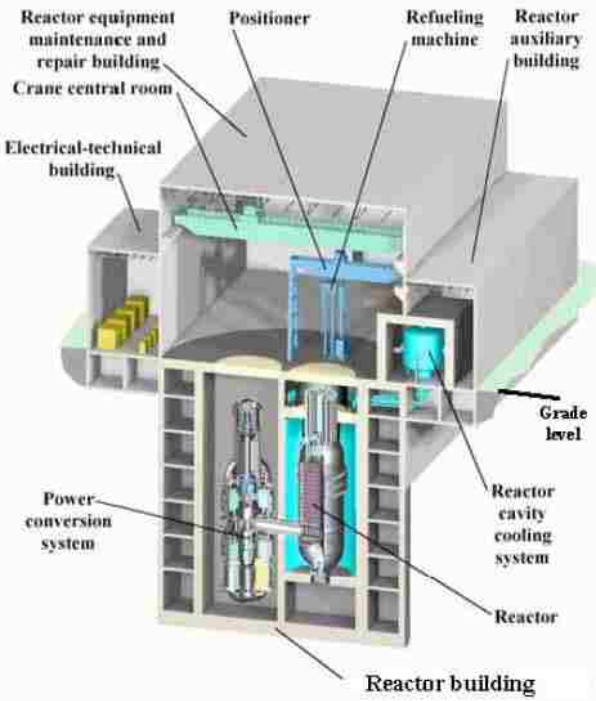

Figure 1.8. GT-MHR fully embedded reactor building (Moses 2010)

The GT-MHR is a helium-cooled, graphite-moderated, thermal-neutron-spectrum reactor with a 600 MW (thermal) power and other key specifications shown in Table 1.5. Figure 1.9 shows a cutaway view of the reactor, including the reactor core, upper and lower plena and annular inlet/outlet pipe; the annulus is the inlet, and the inner pipe is the outlet for the reactor vessel. The GT-MHR core consists of hexagonal graphite blocks one-third of which are fuel blocks arranged annularly; the other two-thirds of the blocks are neutron reflector blocks arranged inside and outside of the fuel blocks, as shown in Figure 1.10. The fuel elements consist of TRISO-coated particles with the same constituents previously mentioned. Fuel columns consist of ten layers of fuel blocks and are installed between removable upper and lower reflector blocks. Control rods and reserve shutdown system

channels are located in the annular fuel block region of the core. The average width and height of a block are 360 and 793 mm, respectively. Each fuel block has 102 and six flow channels with diameters of 15.88 and 12.70 mm, respectively, and 210 fuel channels. The blocks are vertically connected with dowel pins.

Table 1.5. Major specifications of the GT-MHR (Sato et al. 2010)

Specifications	Values
Reactor power (MWt	600
Reactor inlet/outlet temperature (°C)	490/850
Reactor pressure (MPa)	7.0
Power density (W/cc)	6.5
Reactor mass flow rate (kg/s)	320
Effective core height (m)	7.93
Number of fuel blocks	1020

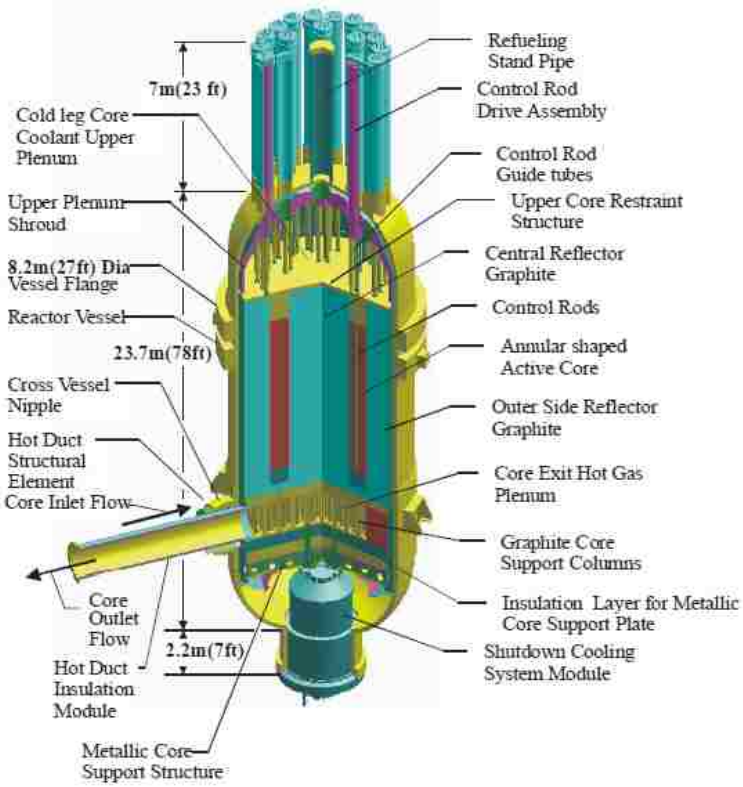

Figure 1.9. GT-MHR reactor vessel cutaway showing the arrangement of the reactor vessel (Southworth et al. 2004)

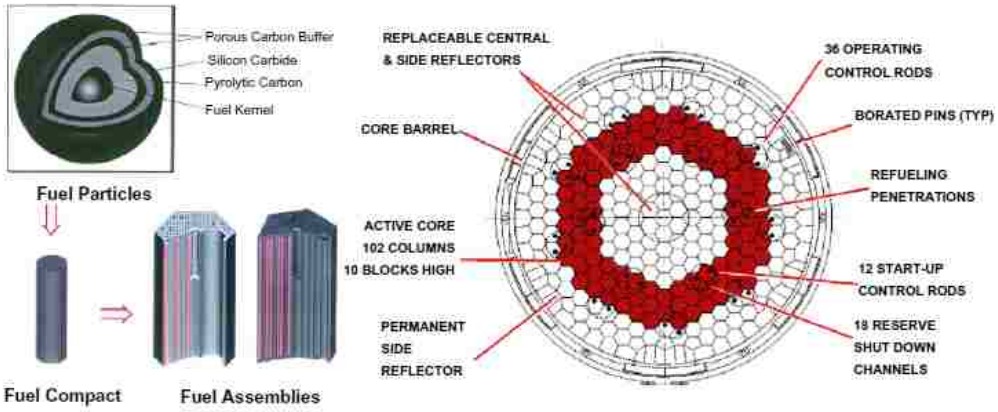

Figure 1.10. Cutaway view of fuel and fuel blocks and cross-section of a core (LaBar et al. 2004, Southworth et al. 2004, Sato et al. 2010)

Helium coolant enters the reactor pressure vessel through the annular inlet, flows upwards through the reactor pressure vessel and core barrel, enters the upper plenum, and then flows downwards through coolant channels in the hexagonal core. The coolant temperature increases as it flows downward through the coolant channels in the graphite columns joins at the lower plenum and exits the vessel through the outlet pipe. Afterwards, heated helium from the reactor expands through the gas turbine to drive the generator and gas compressors. Then, helium passes through recuperators before returning to the reactor. The use of the direct Brayton cycle helps to produce electricity and results in a net plant efficiency of approximately 48%. Additionally, there is bypass flow and cross flow through interstitial gaps between the graphite columns. The flow through these gaps varies because of variations in gap-width, which occurs because of tolerances in manufacturing and inexact installation. In addition, the nonuniform neutron fluences and temperature distributions in the actual core cause non-uniform deformations in the graphite block over

its lifetime, creating complex bypass flow pathways (Doug Chapin 2004, Sato et al. 2010, Kim et al. 2011, Yoon et al. 2011, Yoon et al. 2011, Lee et al. 2014).

Safety is achieved through a combination of inherent safety characteristics and design choices such as the following:

- Helium coolant is a single phase, inert, and has no reactivity effects
- Graphite core provides high heat capacity and slow thermal response, and structural stability at very high temperatures
- Refractory TRISO-coated particles fuel retain fission products at temperatures much higher than normal operation and postulated accident conditions
- An annular low power density core is an uninsulated steel reactor vessel surrounded by a natural circulation rector cavity cooling system, as mentioned earlier, in Figure 1.8.

The GT-MHR has two heat removal systems, the heat power conversion system and a shutdown cooling system, which can be used for removal of decay heat. In the event that neither of these systems is available, an independent passive means is provided for the removal of decay heat. This is the reactor cavity cooling system (RCCS) surrounding the reactor vessel. The core power density and the annular core configuration have been designed such that the decay heat can be removed by induction, thermal radiation, and natural convection without exceeding the fuel particle temperature limit. Even if the RCCS is assumed to fail, passive heat conduction from the core, thermal radiation from the vessel, and conduction into the walls is sufficient to maintain peak core temperatures below the design limit. The use of passive systems can eliminate the costs associated with the installation, maintenance, and operation of active systems that require multiple pumps with

independent and redundant electric power supplies. Also, the large heat capacity of graphite core structure is an important inherent characteristic that significantly contributes to maintaining core temperatures below damage limits (LaBar et al. 2003, LaBar et al. 2004, Choi et al. 2011).

As mentioned above, natural circulation is one of the passive safety features of prismatic VHTRs to remove core decay heat during off-normal shutdown and accident scenarios. The main postulated design basis accident scenarios (DBA) are pressurized conduction cool-down (PCC) and depressurized conduction cool-down (DCC). In a DCC event, also known as loss of coolant accident (LOCA), there is a breach in the pressure boundary of the system, which loses the capability to retain the coolant. This event causes air ingress into the lower plenum where it slowly diffuses into the core and oxidizes with the fuel accelerating core heating and releasing fission products (Reyes et al. 2010, Takeda 2010, McVay et al. 2015). As there is no heat sink for the core, the primary heat removal is through radiation, and the core may reach the failure temperature of 1600 ℃. While in a PCC, also known as loss of forced cooling accident (LOFA), there is no breach in the pressure boundary of coolant helium. This LOFA event is initiated due to a failure of pumps or break in inlet/outlet ducts (Martineau et al. 2010). Once a PCC event is initiated, forced coolant circulation system is lost, although the remaining heat is released as a result of radioactive decay (decay heat) that gives rise to temperatures variations within the core. Overtime, the resulting buoyancy forces would overcome the initial inertial forces, reversing the circulation of the coolant up through the inner (more heated) core channels into the upper plenum, and downwards through the outer (less heated) periphery core channels attached to the core barrel and the annular space between the reflector and the

core. Natural circulation is considered the cornerstone of the HTGRs' passive safety design that removes sufficient heat from the core so the core will not reach the failure temperature of the fuel, but may cause thermal stresses on the internal support structures in the upper plenum (McVay et al. 2015). High concern is directed to the cooling systems used in case of accidents in order to remove this decay heat, especially after the Fukushima Daiichi nuclear power plant accident in 2011.

Previous studies provided a preliminary assessment of these two possible versions of NGNP (Southworth et al. 2003, Southworth et al. 2004) and proved that both designs will meet the three basic requirements that have been set for the NGNP: a coolant outlet temperature of 1000 ℃, passive safety, and a total power output consistent with that expected for commercial high-temperature gas-cooled reactors. For a prismatic block design, two modifications of the GT-MHR are needed to obtain the desired conditions in prismatic VHTR of 1000 ℃ outlet temperature: reducing the bypass flow and better controlling the inlet coolant flow distribution to the core (Southworth et al. 2004).

1.4. LITERATURE REVIEW AND MOTIVATION

Previous related studies in the open literature can be divided into two categories: (1) natural circulation/convection studies concerned with representative geometries of PMRs, and (2) other studies that focus on natural circulation/convection inside vertical heated channels. For the first category, many experimental and computational studies in the open literature analyzed some of the phenomena that accompanied HTGRs, such as bypass and cross flow phenomena in the core (Kim et al. 2011, Yoon et al. 2011, Lee et al. 2014, Lee et al. 2015), mixing and flow visualization in the upper plenum during normal and accident

scenarios (Sabharwall et al. 2007, Jackson et al. 2009, Tung et al. 2011, McVay et al. 2015), and particle image velocimetry (PIV) based flow visualization and mixing in the lower plenum during normal and accident scenarios (McLlroy et al. 2009, Rodriguez et al. 2010, Gradecka et al. 2016). On the other hand, investigating buoyancy-driven flow inside vertical heated channels started as early as 1942 by the innovative work of convective heat transfer phenomena conducted by Elenbaas (1942). Since this initiating work, there have been a number of investigations using various analytical, numerical, and experimental techniques for different heating and geometrical conditions. Laminar natural convection flow in heated channels has been subjected to extensive investigations for both symmetrically and asymmetrically heating (Aung 1972, Aung et al. 1972, Dyer 1975, Martynenko et al. 1984, Sparrow et al. 1985, Cheng et al. 1988, Fujii et al. 1988). Later on, concern was directed to turbulent natural convection in vertical heated channels (Miyamoto et al. 1986) and consequently several related works were published (Fedorov et al. 1997, Habib et al. 2002, Badr et al. 2006, Yilmaz et al. 2007, Yilmaz et al. 2007). Other natural convection-associated incidents including flow destabilization and transient development (Jaluria et al. 1974, Bejan et al. 1990, Lau et al. 2012, Sanvicente et al. 2013), and flow reversals (Sparrow et al. 1984, Kihm et al. 1995, Fu et al. 2016) were considered. However, it is reported that such studies in simple geometries cannot be extended and applied to complex nuclear systems (Celataa et al. 1998) and only a single ongoing study related to P2P natural circulation heat transfer during DCC accidents is being conducted in an integral test facility with a representative geometry of PMRs (named High Temperature Test Facility "HTTF") at Oregon State University (OSU). It is concluded that limited experimental studies on natural circulation phenomenon in geometries mimicking complex

nuclear systems have been reported in the open literature. Additionally, limited measurement techniques for natural convection have been employed in general and with gas-cooled systems in particular.

Therefore, there is a need for establishing scaled-down separate effects experiments for studying thermal hydraulic behavior occurring within a component or particular region of PMRs, such as P2P gas dynamics during natural circulation. Designing and constructing such a test facility is a challenging task that is executed in a state-of-the-art manner by multiphase Reactors Engineering and Applications Laboratory (mReal) at Missouri S&T. This facility was designed with a representative geometry of PMRs for experimental investigations of plenum-to-plenum (P2P) natural circulation thermal hydraulics to overcome the previously mentioned data gap and to advance the knowledge and understanding of natural circulation phenomenon in advanced nuclear systems.

1.5. OBJECTIVES AND TASKS

The main aim of this work is to experimentally examine intra-core natural circulation phenomena in a scaled separate-and-mixed effects experimental setup of prismatic blocks that simulate HTTF core and the two plena during natural circulation by implementing sophisticated measurement techniques such as the hot wire anemometry (HWA), flush-mounted micro-foil sensors, and thermocouples that will provide local time-averaged measurements of coolant gas temperature and velocity fields at different locations along the core channels. This work will complement the ongoing experimental work at the High-Temperature Test Facility (HTTF), which aims to provide knowledge about in-vessel thermal-hydraulics behavior of PMR.

The main objectives of this study can be summarized as follows:

a. To develop a scaled separate-and-mixed effects experimental setup that can be operated under different intensities of natural circulation mimicking the core and the two plena of HTTF.
b. To advance and address experimentally the gaps in scientific and engineering knowledge and understanding of the intra-core natural circulation phenomenon in the PMR core by integrating advanced sophisticated measurement techniques, for the first time in such a study, as a separate-effects experiments by using each measurement technique separately or mixed-effects experiments by employing these measurement techniques simultaneously at various locations along the core channels.
c. To provide experimental benchmark data that is much needed and is missing in the literature for verification and validation of computational fluid dynamics (CFD) codes that are being used to analyze gas-cooled reactor thermal-hydraulics behavior, system models of the setup, to benchmark any system specific correlations and to perform safety analyses and assessment.

Proposed Tasks: This work will experimentally investigate intra-core natural circulation that occurs after LOFA by developing scaled experimental facility mimicking PMR natural circulation operation. Since the strength of the natural convection and its heat removal effectiveness strongly depends on the system geometry, designing an experimental setup mimicking the relevant physical conditions is an important and very challenging task. The following tasks represent the detailed benchmark experimental

investigations that are very much needed to address the objectives outlined above and to overcome the lack of knowledge available in the literature about the proposed topics.

Task 1: Designing a separate-and-mixed effects experimental test facility corresponding to the HTTF. In this task, the geometrical specifications of the developed facility (named *plenum-to-plenum facility "P2PF"*) is determined based on the experience gained from designing the developing the HTTF. It is worth mentioning the HTTF was designed with reference to the modular high-temperature gas-cooled reactors (MHTGR) by implementing the well-established hierarchical two-tiered scaling (H2TS) methodology from which the key dimensionless groups characterizing intra-core natural circulation phenomenon have been deduced and utilized in this study.

Task 2: Developing and testing the experimental setup. The preliminary design of the experimental setup is tested and refined by computational fluid dynamics (CFD) simulations and preliminary experiments in order to determine the design and operational parameters modifications needed to have the final design specifications that guarantee obtaining reliable and repeatable high-quality data.

Task 3: Integrating the advanced sophisticated measurement techniques in a novel way to be used either separately of simultaneously at different axial locations along the core channels. As mentioned earlier, local time-averaged thermal and velocity measurements are characterized by implementing advanced sophisticated measurement techniques (i.e., hot wire anemometry, flush-mounted micro-foil sensors, and thermocouples). Integrating these measurement techniques simultaneously requires special design of the core channel and other supplementary mechanical parts to obtain measurements at different axial and radial positions along the channels.

Task 4: Executing experimental investigations, carrying out experiments, acquiring data, performing analyses. Separate-and-mixed effects experiments are carried out to investigate the effect of natural circulation intensity on coolant steady state gas thermal and velocity fields along the core channels. Data acquisition, processing, and analysis are conducted to generate meaningful results.

1.6. ORGANIZATION OF DISSERTATION

The P2PF design and natural circulation intensity effect on gas thermal and velocity fields are examined and documented through the following papers:

I. Design and development of an experimental test facility with a representative geometry of prismatic block modular reactor core.
    - This paper provides a brief discussion of the reported HTGRs scaling methodology. The detailed design specifications of the P2PF that is designed, developed, and tested by multiphase Reactors and engineering laboratory (mReal) at Missouri S&T, and how the setup was designed, constructed, and refined with the guidance of the preliminary experiments and computational fluid dynamics (CFD) simulations (i.e., STAR-CCM+). The development, implementation, and integration of advanced sophisticated measurement techniques have also been presented.

II. Investigation of natural circulation in a separate effects facility of two channels representing prismatic modular reactors (PMRs) core.
    - This paper concerns with investigating how the cooled portions of the reactor affect gas temperature and velocity distribution along the channel

representing the heated portions of the PMRs core. Also, this manuscript provides a detailed discussion of the working principles of the HWA measurement techniques and corrections implemented to the obtained signals.

III. Buoyancy-driven gas flow within plenum-to-plenum facility down-comer channel.

- This paper deals with the effect of cooling configurations and intensity on flow fields inside the cooled (down-comer) channel.

IV. Natural convection flow fields within plenum-to-plenum facility heated channel.

- This paper analyze the effect of heating intensity on naturally driven gas flow fields.

PAPER

I. DESIGN AND DEVELOPMENT OF AN EXPERIMENTAL TEST FACILITY WITH A REPRESENTATIVE GEOMETRY OF PRISMATIC MODULAR REACTOR CORE

ABSTRACT

There is a need for designing and conducting new flexible separate-and-mixed effects experiments in order to overcome the lack of thermal hydraulics benchmark data of natural convection passive safety system for validating commercial computational fluid dynamics (CFD) codes. To provide consistent and complementary data sets, these experiments should be scaled and designed corresponding to the existing integral test. Therefore, multiphase reactors engineering and applications laboratory (mReal) at Missouri S&T University cooperated with Oregon State University (OSU) and University of Illinois to design, develop a plenum-to-plenum facility (P2PF) with the experience and knowledge gained from designing the high temperature test facility (OSU-HTTF) for experimental investigations of plenum-to-plenum (P2P) thermal hydraulics phenomena under different natural convection/circulation intensities. The current stage “phase-I” of P2PF was designed with only two channels to represent temperature gradients existing, as a result of decay heat transfer, within the prismatic block modular reactor (PBMR) core after the loss of flow accidents (LOFA). One channel represents a coolant flow channel from the innermost hexagonal fuel block of the core which is subjected to more heating. The other channel is representing a coolant flow one from peripheral hexagonal fuel block of the assembly that lies in less heated regions. Preface CFD simulations and preliminary experimental tests were conducted to determine the operational-and-design modifications needed to refine the proposed preliminary design to ensure data repeatability and proper

control of natural circulation intensities. The refined/final design is innovative and flexible to be advanced and upgraded to a multichannel core for future investigations. Advanced and sophisticated measurement techniques for heat transfer and gas dynamics characterization have been defined and integrated in a novel way within the P2PF for coupled investigations of thermal and velocity flow fields. These experimental investigations would complement the experiments that have been or can be, conducted at HTTF and/or other suitable integral test facilities. This study discusses the detailed design and construction chronology of the P2PF, novel implementation and integration of heat transfer and gas dynamics measurement techniques, and a brief explanation of ongoing experimental studies that have been, or currently being, conducted within the P2PF. These studies demonstrate the innovative design and successful development and construction of the P2PF and provide high fidelity benchmark data that are missing in the open literature and crucial for validating CFD codes.

1. INTRODUCTION

The Next Generation Nuclear Plants (NGNPs) are under development to enhance safety, security, sustainability, and competitiveness over previous generations of nuclear systems. The U.S. Department of Energy (DOE) is exploring the potential for high-temperature gas-cooled reactors (HTGRs) which were designated to be the basis of the NGNPs (Beeny et al. 2015). There are two proposed designs for HTGRs; the pebble bed modular reactor (PBMR) and the prismatic block modular reactor (PBMR). In the PBMR, safety is achieved through a combination of design choices and inherent characteristics. One of the safety characteristics involves using helium as a coolant gas because it is single

phase, inert, and has no fission reactivity effects. As well, the graphite moderator, which represents two-thirds of the core, provides high heat capacity, slow thermal response, and structural stability at very high temperatures. In addition, TRISO coated nuclear fuel particles retain fission products at temperatures much higher than the normal operation and postulated accident conditions; and the annular low power density core in the steel reactor vessel is surrounded by a reactor cavity cooling system (RCCS). Enhanced passive safety systems are major design criteria for NGNPs, to ensure inherent safety features and designs capable of removing decay heat passively in case of accidents and off-normal conditions. This should lead to no core damage risk and consequently no release of radioactive materials that would necessitate evacuation of the surrounding areas. The use of passive systems can eliminate the costs associated with the installation, maintenance, and operation of active systems that require multiple pumps with independent and redundant electric power supplies (LaBar et al. 2003, Doug Chapin 2004, LaBar et al. 2004, Sato et al. 2010, Choi et al. 2011).

The main components of the PBMR are shown in Figure 1(a). During normal operation, coolant gas enters the PBMR from the bottom, flows to the upper plenum through the inlet riser holes in the permanent side reflectors, then flows downwards through the core (i.e., coolant channels) and finally exits through the lower plenum, Figure 1(b). In case of loss of flow accidents (LOFA), radial and axial temperatures gradient existing within the core as a result of the decay heat causes coolant gas radial and axial density differences. Overtime, the resulting buoyancy forces would overcome the initial inertial forces, reversing the circulation of the coolant up through the inner (more heated) core channels into the upper plenum, and downwards through the outer (less heated) periphery

core channels attached to the core barrel. Natural circulation is considered the corner stone of the HTGRs' passive safety design that is capable of removing sufficient heat from the core to avoid reaching any unsafe temperatures. However, this circulation may also cause thermal stresses on the internal support structures in the upper plenum (King 2012, Basu et al. 2014, McVay et al. 2015). Plenum-to-plenum (P2P) natural circulation and the associated thermal hydraulics phenomena must be accurately characterized as the first step toward reliable safety analysis and design of HTGRs. Various significant thermal hydraulics `phenomena under normal as well as the off-normal operation of HTGRs, listed in Table 1, which must be studied in details for any safety analysis of the system.

Many experimental and computational studies in the open literature analyzed some of the phenomena that accompanied HTGRs such as bypass and cross flow phenomena in the core (Kim et al. 2011, Yoon et al. 2011, Lee et al. 2014, Lee et al. 2015), mixing and flow visualization in the upper plenum during normal and accident scenarios (Sabharwall et al. 2007, Jackson et al. 2009, Tung et al. 2011, McVay et al. 2015), and particle image velocimetry (PIV) based flow visualization and mixing in the lower plenum during normal and accident scenarios (McLlroy Jr et al. 2009, Rodriguez et al. 2010, Gradecka et al. 2016). These computational simulations must be validated against benchmark data before putting trust in the predictions and using them for safety and operational analysis. However, a systematic validation based on experimental benchmark data of computational fluid dynamics (CFD) codes have not yet been conducted in the open literature as limited measurement techniques have been employed in general and with gas-cooled systems in particular, thus limiting the use of these codes for reliable performance and safety analysis of HTGRs. Therefore, there is a need to design and develop separate-and-mixed effects

experiments for studying in a mechanistic approach the thermal hydraulics behavior occurring within a component or a particular region of HTGRs such as P2P natural convection heat transfer and gas dynamics. In addition, there is a need for implementing advanced sophisticated measurement techniques to obtain such benchmark data from a scaled down test sections for systematic validation of commercial CFD codes (Schultz et al. 2010, Johnson et al. 2011, Lee et al. 2014, McVay et al. 2015).

Accordingly, this work provides a brief discussion of the reported HTGR scaling methodology for scaling down complex advanced reactors such as PBMR. The detailed design specifications of the newly separate-and-mixed effects experimental test facility (named plenum-to-plenum facility (P2PF)) developed at multiphase reactors and engineering laboratory (mReal) at Missouri University of Science and Technology (Missouri S&T), and how the setup was designed, constructed and refined with the guidance of the preliminary experiments and computational fluid dynamics (CFD) simulations (i.e., STAR-CCM+) (Kao et al. 2015, Kao et al. 2015). The development, implementation, and integration of advanced sophisticated measurement techniques have been also presented. These measurements techniques have been integrated in a novel way for the first time in this study in order to simultaneously provide benchmark data of heat transfer and gas dynamics within the P2PF under different adjustable intensities of natural circulation.

2. SCALING METHODOLOGY

Several scaling approaches were reported for providing scaling relationships and similarity criteria upon which data from different facilities are compared together.

Following these approaches yields characteristic dimensionless groups that can be used as the basis for designing and conducting experiments on small scale and less expensive facilities. For instance, the scaling laws for modeling nuclear reactor systems started to appear as early as 1979 (Nahavandi). Ishii and Kataoka (1984) derived scaling criteria for thermal hydraulics under single and two phases natural circulation loops. Reviews of thermal hydraulics scaling criteria have been presented by Kiang (1984), Vijayan (1994), Wulff (1996), and D'Auria et al. (2010). Recently, Reyes and co-workers (2010) applied hierarchical two-tiered scaling (H2TS) methodology for the high-temperature test facility (HTTF), for PBMR, at Oregon State University (OSU) to ensure that the scaling objectives are met in an organized and clearly defined manner.

The H2TS methodology is fully described in the United States Nuclear Regulatory Commission's (NRC) Severe Accident Research Program's (SARP) presented in Appendix D of NUREG/CR-5809 (Zuber 1991). It has been successfully applied to design scaled down test facilities for light water reactors (LWRs) and gas-cooled reactors (GCRs) (Reyes Jr et al. 1998, Reyes Jr et al. 2003, Reyes et al. 2010, Schultz et al. 2010, CAl 2013). Since exact similarity cannot be achieved between test facilities and prototypes because of the differences in geometric scales and fluid properties (Kline 1965), optimization should be applied in designing scaled-down facilities and quantification of scaling distortions should be conducted to generate experimental data that are related and relevant to a full-scale prototype. Optimization means quantifying the most important process and/or phenomena to be simulated in the experimental facility with low scaling distortions from the full-scaled unit, regardless of other phenomena. This optimization definition is consistent with the H2TS analysis method basic elements, shown in Table 2.

The H2TS methodology's first element consists of subdividing the plant into a hierarchy of systems. Each system is subdivided into interacting subsystems which could be further sectioned into interacting constituents (materials) which are further partitioned into interacting phases (liquid, vapor, or solid). Each phase can be categorized by one or more geometrical configurations, and each configuration can be described by three field equations (mass, energy, and momentum conservation equations). This element has been applied to HTGRs yielding the hierarchy shown in Table 3. The second element consists of identifying the scaling level (i.e., phenomena to be investigated) at which similarity criteria should be developed. The third element consists of performing a top-down (system) scaling analysis to address the effects on a system caused by the constituents' interaction. The fourth element is the bottom-up scaling analysis in which similarity criteria are developed for specific processes of importance.

The specific objective of the H2TS methodology is to set up characteristic time ratios for transfer processes of interest as follows:

i. Write control volume balance equation for each constituent (k) of the conserved property (Ψ).

$$\frac{d\, V_k \Psi_k}{dt} = \Delta\left[Q_k \Psi_k\right] \pm \sum \left[j_{kn} A_{kn}\right] + S_k \qquad (1)$$

In this equation, (Ψ_k) is the conserved property such as mass (ρ), momentum (ρu), and energy (e) per unit volume. V_k represents the control volume and Q_k the volumetric flow rate. $j_{kn}A_{kn}$ is the transport process transfer term for phenomena where j_{kn} is the flux of the conserved property transferred from constituent "k" to constituent "n" across transfer area A_{kn}. S_k accounts for the distributed sources (such as body forces) or sinks on the control volume. The first term on the right-

hand side of equation (1) shows the convective flux of the conserved property and can be described using the following equation.

$$\Delta[Q_k \Psi_k] = [Q_k \Psi_k]_{in} - [Q_k \Psi_k]_{out} \quad (2)$$

ii. Convert the control volume balance equation (1) into a non-dimensional form by using the non-dimensional properties in terms of the initial and boundary conditions of the system.

iii. Substitute the non-dimensional properties into equation (1) to obtain the non-dimensional/normalized form of the control volume balance equation.

iv. Deduce the dimensionless groups ($\Pi - \text{groups}$) and characteristic time ratios from the normalized form of the conservation equation.

As mentioned earlier, the ideal goal of preserving these developed characteristic dimensionless groups ($\Pi - \text{groups}$) between the reference model and scaled down porotype cannot be achieved because of the complexity of nuclear systems. Hence, a distortion factor (DF) is to be determined (Equation 2). The DF is a quantification of the fractional difference in the amount of conserved property transferred through the evolution of a specific process in the prototype with that property value in the model during their respective residence times is defined by the following equation (Woods et al. 2015);

$$DF = \frac{[\pi]_P - [\pi]_M}{[\pi]_p} \quad (3)$$

The experimental results of the scaled-down prototype can then be scaled up with due consideration for the distortion factor to predict the behavior of the full-scale reference model. The previous procedures have been applied and a set of characteristic dimensionless groups ($\Pi - \text{groups}$) for normal operations (i.e., forced convection) and different accident scenarios in HTGRs have been developed for designing the integral high temperature test

facility (HTTF) at Oregon State university (OSU) as reported and described in detail in the literature (Reyes et al. 2010, Schultz et al. 2010, Woods et al. 2015). Examples of these reported characteristic groups concerning thermal hydraulic natural circulation during pressurized conduction cooldown (PCC) accident scenario are listed in Table 4, along with other dimensionless groups, listed in Table 5 that is obtained by the conventional Buckingham-π theory for general characterization of natural convection.

As shown in Table 4, similarity criteria are expressed in terms of ratios of model to prototype and design choices must be assumed to achieve closure in the design process. Achieving kinematic similarity, preserving friction and form loss between the HTTF and the modular high-temperature gas-cooled reactor (MHTGR) design choices were imposed. Substituting these choices in the scaling criteria ratios, a sample of them is shown in Table 4, yields all of the scale ratios and dimensions needed for the design of the HTTF. A list of the key dimensions of the HTTF is given in Table 6 and detailed description of the facility can be found elsewhere (Woods et al. 2015). From these dimensions, it is shown that the HTTF is ¼ axially and ¼ radially, which equates to $^1/_{16}$ area scaling and $^1/_{64}$ volumetric scaling from the MHTGR. Also, it can be operated at $^1/_8$ of the total pressure of the MHTGR with full temperature loading. The temperature similitude is achieved between the MHTGR and the HTTF by replacing the prismatic graphite blocks filling the core of the MHTGR by ceramic blocks that is employed in the HTTF. Since the HTTF contains no nuclear material, it is electrically heated by inserting electrical heaters rods in these ceramic blocks. The HTTF was designed to operate as both separate-and-integrated effects test facility. It was designed specifically to simulate scaled coolant flow and heat transfer in HTGRs during air ingress event that occurs after a depressurized condition cooldown

(DCC) accident scenario. To some extent, it can simulate the pressurized conduction cooldown (PCC) accident scenario and normal operations (King 2012, Gradecka et al. 2016). Despite the reported scaling distortions between HTTF and MHTGR that is attributed to the complexity of the phenomena encountered in the HTGRs, the HTTF has shown a strong similarity and relevance to the MHTGR. As a consequence of considering the HTTF integral facility as a long-term investment, there is vital and highly desirable for designing and constructing a smaller and less expensive separate effects test facilities to complement the integral tests conducted within HTTF (Woods et al. 2015). Therefore, mReal research team at Missouri S&T cooperated with Oregon State University and the University of Illinois in designing, developing, and successfully constructing a plenum-to-plenum facility (P2PF) with a representative geometry of prismatic block modular reactors (PBMR). A detailed description of this experimental test facility design and construction chronology is presented in detail in the following section.

3. GEOMETRIC DESCRIPTION OF THE MISSOURI S&T A PLENUM-TO-PLENUM FACILITY (P2PF)

3.1. MISSOURI S&T – PRELIMINARY DESIGN OF TWO CORE CHANNELS "PHASE-I"

The mReal research team at Missouri S&T adopted the same geometrical scaling ratio utilized by OSU in order to design, develop, and test the P2PF with a representative geometry of PBMR. A list of key dimensions of the P2PF with reference to the HTTF is listed in Table 6. This facility capable of representing thermal-fluid behavior that occurs within a component or region of the prismatic modular reactor during a PCC accident scenario and can fulfill the previously mentioned insufficiency of the benchmark data for validating CFD commercial codes.

The P2PF is made of a 403 stainless steel alloy, chosen for its high thermal conductivity that approaches 16.2 W/(m.K), for minimizing temperature measurements amplitude oscillations (Misale et al. 1987). Stainless steel also provides the capability for conducting high temperature and pressure experiments approaching the HTTF conditions (Said et al. 2017). This facility consists of the main PBMR features/components: (1) the lower plenum, (2) the upper plenum, and (3) a reactor core coolant channels. A physical picture and a schematic diagram of P2PF preliminary design are shown in Figure 2. As an introductory remark, the current stage "phase-I" of P2PF was designed with two channels and sufficiently flexible to be advanced and upgraded to a multichannel core for future investigations.

The lower plenum is a ¼ scaled down (i.e., axially and radially) with reference to the HTTF. It contains five openings; three of $^{3}/_{8}$ NPT inches ID and two of $1\,^{5}/_{8}$ NPT inches ID. One of the two larger openings is used as inlet/outlet of the coolant fluid into/out of the reactor and the other opening is used for installing a pressure gauge to monitor the pressure measurement inside the facility. The three other lead-ins are kept for implementing the measurement techniques. A physical picture of the lower plenum is shown in Figure 3.

The upper plenum, shown in Figure 4, contains four $^{3}/_{8}$ NPT inches ID openings. As for the lower plenum, a pressure gauge is inserted in one of these holes to get a direct pressure reading inside the facility. The other openings are kept to be used for implementing measurement techniques for further investigations of gas dynamics, plumes mixing, and stratification phenomena in the upper plenum. Both plena are connected to the

channels via stainless steel grid plates with O-ring flanges in order to prevent leakage from the unit.

The facility core was designed in a similar way to the OSU-HTTF core (hexagonal blocks with flow channels representing the central and periphery channels). The P2PF scaled down prismatic core was designed to accommodate 5 vertical layers of prismatic blocks compared to 10 vertical prismatic layers used in the HTTF (each block is 7.87 inches ~20 cm of height), as shown in Figure 5, while channels diameter is kept the same as HTTF. These blocks are accommodated in 11.78 inches diameter column accommodating one hexagonal block is in the center and six blocks are surrounding it as shown in Figure 6(a). Note that, the 15 inches diameter shown in Figure 4 accounts for the core diameter (i.e., 11.78 inches) and the annular space between the core and vessel outer barrel to allow further consideration of this annular space as a potential coolant flow path in future investigations. For experimental simplicity, the current phase of the facility "phase-I" was designed with only two channels: one to represent a coolant channel from an innermost hexagonal block of the core which is subjected to more heating after LOFA. The other channel is representing a coolant one from a peripheral hexagonal block of the assembly that lies in less heated regions (Sabharwall et al. 2007). Both channels locations are shown in Figure 6(b). Once experimental investigations of natural circulation gas dynamics and heat transfer are finalized within the current design phase, it can be extended and upgraded with multichannel core facility for comprehensive P2P natural circulation investigations and also to complement the integral tests conducted at OSU-HTTF.

The P2PF was designed to carry out P2P natural circulation investigations and assess its capability of removing decay heat during accident scenarios and off-normal conditions.

In the current study natural circulation is induced through the electrically heating innermost channel (mimicking the riser in natural circulation loop) by a configuration similar to the arrangement used by McVay et al. (McVay et al. 2015) investigations of plumes mixing in the upper plenum. The heated channel is divided into four sections, and each section is independently heated by electric heater wrapped around the channel, as shown in Figure 7. Each heater is connected to a separate PID temperature controller, shown in Figure 8, to control outer channel surface temperature. This heating configuration allows investigating the effect of varying heating intensities on flow behavior within the facility.

Generally, reaching steady state conditions within natural circulation loops necessitates using an external heat exchanger to remove the heat generated in the heat source region. Hence, the upper plenum was designed with an external cooling jacket/shell surrounding it and the outer channel (mimicking the down-comer channel in natural circulation loop) was surrounded with high thermal conductivity copper tube (400 W/(m.K), 0.138 inch ID and 0.03 inch thickness) acting as a helical coil heat exchanger as shown in Figure 9. During experiments, chilled water is continuously circulated form an external chiller (Applied Thermal Control Ltd., K4 chiller), to the upper plenum shell through inlet/outlet hoses. In addition, bypassed chilled water stream from the upper plenum hoses is allowed to flow through the helical copper coil heat exchanger surrounding the channel. To ensure uniform temperature distribution and proper thermal contact between the channel and copper tube, high thermal conductivity paste (OT-201-16, Omega Engineering, INC.) was used between the chilled water copper tubes and the cooled down-comer channel as shown in Figure 9. Chilled water temperature can be varied and controlled by using the temperature controller built in the chiller and characterized by

±0.1℃ temperature stability. This enables further investigations of the effect of cooling the upper plenum and channel together and separately on natural circulation thermal hydraulics within the facility.

3.2. CHANNEL DESIGN CHRONOLOGY

3.2.1. Preliminary Proposed Channel Design. The initial proposed design of the channels based on dividing the channel into two sections: a long and a short one as shown in Figure 10. Both ends of the short channel were fitted with connection blocks (same inner diameter of the channel, OD = 2.36 inch (~6 cm), and height of 0.98 inches (~2.5 cm)), as shown in Figure 11, is was custom designed in a novel way to implement and integrate in a novel way advanced measurement techniques. Locally measurements characterizing flow fields at different axial positions along both channels is planned to be obtained by flipping the channel according to the two configurations shown in

Figure 12. Therefore, preliminary experiments are needed to assess this proposed design and analyze flipping channel effect on data reproducibility. From experimental feasibility viewpoint, these experiments were carried out by monitoring only centerline coolant fluid temperatures at different axial positions along the channels. These experiments were carried out at high pressure (100 psi) approaching the HTTF operating conditions and compressed dehumidified air was used as the working coolant fluid. Five preliminary experiments under different conditions were considered in this analysis and listed in Table 7.

3.2.2. Preliminary Experiments: Procedures and Findings. For each experiment, the dehumidified air was first compressed inside the facility until the desired pressure value

was reached before turning on the heaters and the chiller and establishing natural circulation flow. Since steady state time is a function of the heat input and facility geometrical specifications (Hess et al. 1979), air temperatures along both channels were monitored until no temporal change observed and is this defined to be the steady state time (Rodríguez-Sevillano et al. 2011). In these experiments, it is found that the system needs at least 4 hours to reach steady state conditions after which data can be collected. Axial temperature measurements were obtained by using thermocouples (T-type of 0.06 inches diameter) at six different axial locations along each channel. The axial positions are represented by the dimensionless geometrical parameter (z/L = 0.04, 0.22, 0.4, 0.6, 0.78, 0.96) where z/L = 0.0 refers to the bottom end of the channel near the lower plenum and z/L = 1 is at the top end of the channel connected to the upper plenum. In order to analyze the effect of channel flipping on data reproducibly, experiments were repeated under the same conditions for both ‘a’ and ‘b’ channel configurations (Figure 12).

Axial air temperature distribution obtained for configuration (a), where the short channel section is located at the top and connected to the upper plenum, as shown in

Figure 12(a). Results show temperature variation trends similar to previous findings (Mohammed et al. 2007, Sanvicente et al. 2013, Tkachenko et al. 2016). Temperature is found to monotonically increase as air flows upward inside the heated channel (Figure 13(a)). However, there is an observable inflection point in the temperature distribution at $z/L \approx 0.8$ near the top end of the heated channel. This change in temperature is attributed to the end losses effect (Lau et al. 2012) that is represented in the P2PF by conjugate heat transfer between the air, stainless steel material of the channel, and heat conduction through the top stainless steel flange connecting the channel to the plena (Kao et al. 2015); and also

attributed to the flow reversal phenomenon reported in the literature (Kihm et al. 1995, Li et al. 2013, Fu et al. 2016, Said et al. 2017) along with the possibility of the interaction with plumes mixed in the plena with jet flow exiting the heated channel. This mixing phenomenon is revealed by preliminary computational simulations carried out for this test facility (Kao et al. 2015) and other computational studies (Guillen et al. 2007, McVay et al. 2015). Figure 13(b) shows that air temperature continuously decreases as it flows downwards inside the down-comer channel. Insignificant temperature reduction is found along the cooled channel implies that the majority of heat supplied is removed through the upper plenum.

The effect of flipping the channel on data reproducibility was analyzed by repeating the same conditions experiments for configuration ‘b’. Sample results comparing obtained temperature measurements for same experiments for both configurations shown in Figure 14 and 15. The discrepancy observed is found to be maximum at both ends (± 30% temperature difference) where the designed connection block exists, marked earlier as an orange box in

Figure 12. Also, the large size of the connection block relative to the channel (same inner diameter of the channel, outer diameter (OD) of the block and the channel are 2.36 and 0.94 inches, respectively and block height of 0.98 inch) provides larger resistance to heat transfer than the channel and thus affecting uniformity of heat supplied distribution along the channel. Further assessment of this proposed design was carried out via preliminary computational studies conducted in the University of Illinois for this preliminary phase of P2PF (Kao et al. 2015). There are discrepancies reported between experimental and computational results as a result of uncertainties associated with

achieving uniform constant surface temperature boundary conditions experimentally in such systems. Hence, computational fluid dynamics (CFD) approaches and closures cannot accurately model this boundary condition. These preliminary experimental and computational findings highlight the modifications needed to control supplied heating intensity and to ensure obtaining reliable and repeatable measurements that is currently missing and much needed for validating commercial CFD codes. These modifications are discussed in detail in the subsequent section.

3.2.3. Modifications and the Final Design. Preliminary testing of the facility design reveals the needed modifications to overcome the technical difficulties confronting obtaining repeatable and accurate experimental measurements that are vital for validating the CFD codes. These modifications can be classified as (1) operational parameters and (2) design parameters. Operational parameters involve the parameters by which experimental conditions can be controlled (i.e., heating intensity, etc.). Design parameters indicate the geometrical specifications of the facility (i.e., channel design and dimensions, etc.).

- Operational parameters

Preliminary results highlight the need of changing the heat supplied power controlled to be expressed in terms of flux surface boundary conditions instead of outer channel surface temperature. This modification was conducted by connecting each electrical heater to a Variac power controlling system (BT-V, Variac, 0V to 130V Adjustable transformer with a digital voltage reader or 0.2% accuracy), shown in Figure 16, instead of the proportional–integral–derivative (PID) temperature controller system mentioned earlier. This configuration of power regulation also enables variable axial heating boundary conditions (i.e., isoflux and non-isoflux heated wall channel) that can be simulated by CFD

codes and facilitates conducting investigations of the effect of heat supplied on heat transfer and gas dynamics.

- Design parameters

Preliminary experimental findings have shown that flipping the channel to obtain velocity and thermal measurements at different axial positions along both channels will adversely impact data repeatability. Also, the size of connection blocks is larger than the channel and thus heat transfer resistance along the channel in non-uniform and this could affect heat supplied distribution along the channel. Therefore, channel design was adjusted to account for these technical difficulties by dividing the channel into smaller sections (Figure 17) instead of the initial design of two sections (i.e., short and long one). The ends of these smaller sections are equipped with smaller connection blocks have the same inner-and-outer diameter of the channel to avoid non-uniform heat transfer resistance along the channel. Six of these connection blocks were distributed at equal distances along the heated channel. For the down-comer channel, axial measurements are enabled through using three connection blocks. This smaller number of axial positions to be considered along the down-comer channel is due to the current preliminary experimental and computational (Kao et al. 2015, Kao et al. 2015) findings that the majority of the heat supplied is removed through the upper plenum and insignificant air coolant temperature variations exist along the channel. This new design of the connection blocks enables obtaining axial measurements along both channels with no need to flip each.

3.2.4. Measurement techniques implementation. The objective of designing the P2PF is to experimentally investigate natural convection heat transfer and gas dynamics in a facility with a representative geometry of prismatic modular reactor core and provide

benchmark data for validating CFD codes. For characterizing heat transfer, advanced integrated fast response heat transfer technique has been developed and successfully implemented in various multiphase reactors by mReal research team (Wu et al. 2007, Abdulmohsin et al. 2011, Abdulmohsin et al. 2015). It consists of (1) heat flux foil sensors (0.25 x 0.7 x 0.003 inches) flush mounted on the channel inner wall in a noninvasive way to the flow and (2) T-type thermocouples of 0.06 inches diameter. The heat flux foil sensors provide direct measurements of local instantaneous and time-averaged wall temperature $\left(T_{s_i}\right)$ and heat flux $\left(q_i\right)$ transferred between the inner channel wall and the flowing fluid simultaneously. T-type thermocouples have been selected due to its stability, accuracy ($\pm 1℃$), and small size that minimizes flow disturbances and used to obtain local temperature measurement of flowing fluid $\left(T_{b_i}\right)$. Afterwards, local time-averaged heat transfer coefficient (h) values are calculated by using following equation:

$$h = \frac{1}{n} \sum_{i=1}^{n} \frac{q_i}{T_{s_i} - T_{b_i}} \tag{4}$$

where n is the number of obtained time series experimental data points.

For velocity field characterization, DANTEC constant temperature anemometer (CTA) has been selected for its capability of providing local information of small and fast flow fluctuations. While the technique is invasive, due to its small size, it could cause minimum flow disturbances. The CTA is based on the principle that when a wire is heated electrically, to maintain its temperature constant, the voltage supplied to keep the wire temperature constant is a direct measure of the fluid velocity. It has been reported that the anemometer was successfully implemented for characterizing bypass phenomena in a

pebble bed reactor (Amini et al. 2014) and for detecting natural convection laminar-to-turbulent flow regimes transition (Rodríguez-Sevillano et al. 2011).

These measurement techniques have been implemented and integrated simultaneously via the novel design of the connection blocks (Figure 18). The connection blocks contain three openings at the same cross section: two small ones ($^1/_8$ NPT inch ID) and another larger one ($^5/_8$ NPT inch ID). The two small openings are used to introduce the foil sensor to be flush mounted on the inner wall surface of the channel and the other small one for inserting a T-type thermocouple directly in front of the foil sensor. While the CTA sensor introduced through the lager opening. For comprehensive investigations of flow field inside the facility, highly accurate radial adjusters were designed for the T-type thermocouple and the anemometer (Figure 19). This allows quantify flow temperatures and velocities from the inner wall to the centerline of the channel by 1 mm radial increment.

4. SUMMARIZED PRESENTATION OF ONGOING HEAT TRANSFER AND GAS DYNAMICS INVESTIGATIONS

In this section, summary of the ongoing heat transfer and gas dynamics investigations that demonstrate the success of the final design of the P2PF are presented. Said et al. (2017) investigated natural convection heat transfer in both channels of the P2PF by using the advanced sophisticated heat transfer measurement technique. Natural circulation intensity has been varied in this study by controlling the outer surface temperature of the upper plenum and the down-comer channel via the built-in temperature controller in the chiller (K4 chiller) while the heat supplied kept fixed. A detailed explanation of air coolant gas thermal fields along both channels has been presented. Implementation of the flush mounted heat flux foil sensors in the way mentioned earlier leads to a significant

characterization of heat transfer reversal near the top section (channel exit) of the heated channel. Time-averaged heat transfer results have been presented in terms of local heat transfer coefficients and Nusslet number (Nu) dimensionless group and compared the results with related existing correlations in the open literature. Further experimental studies addressing the effect of pressure and isoflux heating intensities supplied to the riser channel on heat transfer natural convection within the P2PF (Said et al. Under review, Said et al. Under review) have been conducted. These experiments were conducted by using helium as the working gas as it is the coolant fluid used in existing PBMR. An introductory investigation of coupled thermal and velocity natural convection air flow fields along the heated channel has been presented (Taha et al. Under review) by integrating the CTA and the T-type thermocouples in a novel way to advance visualizing and understanding of flow behavior inside the heated channel. Similarly, natural circulation intensity has been controlled in this study by varying the upper plenum and down-comer channel outer surface temperatures. Outlined time-and-frequency domain analysis emphasize the proper sampling frequencies and intervals used to obtain statistically-stationary time series measurements. This study, for the first time, investigates how the less heated regions in the PBMR core affect flow behavior in the central more heated core channels. Flow behavior along the down-comer (cooled) channel of the P2PF have been investigated as well (Taha et al. Under review) at different chilled water temperatures. Analysis of time series velocity and temperature measurements stability and repeatability have been reported and underline the delicate nature of natural convection phenomenon and high dependency of steady state time on experimental conditions (i.e., cooling configuration, heating intensity) and the geometrical dimensions and arrangement of natural circulation loops.

This summarized presentation of part of the ongoing experimental investigation of natural convection heat transfer and gas dynamics highly demonstrate the innovative design and successful construction, development, and testing of the P2PF with a representative geometry of PBMR. Ongoing investigations are currently being carried out within the P2PF to advance knowledge and understanding of natural convection phenomenon and its capability as a passive safety system. The provided high fidelity benchmark data from these studies are necessitous for validating CFD codes.

5. REMARKS

Multiphase reactors engineering and applications laboratory (mReal) research team at Missouri S&T cooperated with Oregon State University and University of Illinois to design, develop a separate-and-mixed effects facility (P2PF) with the experience and knowledge gained from designing the high temperature test facility (OSU-HTTF). The facility was designed with a representative geometry of the PBMR main features/components (1) core channels, (2) upper plenum, and (3) lower plenum. The current stage "phase-I" of P2PF was designed with two channels: one to represent a coolant channel from inner most hexagonal block of the core which is subjected to more heating after loss of flow accidents (LOFA). The other channel representing a coolant flow one from peripheral hexagonal block of the assembly that lies in less heated regions. The design is innovative and flexible to be advanced and upgraded to a multichannel core for future investigations. Measurement techniques for heat transfer and gas dynamics characterization have been defined and integrated simultaneously in a novel way within the P2PF to enable coupled investigations of thermal and velocity fields with minimum

flow disturbances. Additionally, this newly developed facility would complement the experiments that have been, or can be, conducted at HTTF and/or other suitable integral test facilities. Ongoing and future investigations of gas dynamics and heat transfer within the P2PF provides high fidelity benchmark data that are missing in the open literature and crucial for validating CFD codes.

Table 1. Thermal-hydraulic phenomena in prismatic high-temperature gas-cooled reactors

Normal Operation	
- Coolant flow and temperature distribution through reactor core channels ("hot channel factors") - Mixing of hot jets in the reactor core lower plenum ("hot streaking")	
Loss of flow accident (LOFA or "pressurized cooldown")	Plenum-to-Plenum (P2P) experiments
- Mixing of hot plumes in the reactor core upper plenum - Coolant flow and temperature distributions through reactor core channels (natural circulation) - Rejection of heat by natural convection and thermal radiation at the vessel outer surface; RCCS	
Loss of coolant accident (LOCA or "depressurized cooldown")	
- Prediction of reactor core depressurized cooldown – conduction and thermal radiation - Rejection of heat by natural convection and thermal radiation at the vessel outer surface; RCCS	

Table 2. Hierarchical two-tiered scaling analysis (H2TS) components (Zuber 1991)

Element 1 *System Decomposition*	**Element 2** *Scale Identification*	**Element 3** *Top-Down/system Scaling Analysis*	**Element 4** *Bottom-up/Process Scaling Analysis*
Provide: System hierarchy	**Provide hierarchy for:** Volumetric Concentrations Area concentrations Process time scales	**Provide:** Conservations equations	**Performs:** Detailed scaling analysis for important processes
Identify characteristics: Concentrations Geometries Processes		**Derive:** Scaling groups and characteristic time ratios	**Derive and validate:** Scaling groups
		Identify: Important processes to be addressed in bottom-up processes scaling analyses	

Table 3. VHTR system breakdown and hierarchy (Woods et al. 2015)

System	High-Temperature Gas Reactors (HTGRs)			
Subsystem	Reactor coolant system			
Constituents	Helium	Helium/Air	Helium/Air	Reactor vessel
Geometrical configurations	• Volume • Break size	• Elevation • Lengths	• Elevation • Lengths	• External surface area • Graphite reflector
Fields	▪ Mass ▪ Energy	▪ Mass ▪ Momentum ▪ Energy ▪ Gas concentration	▪ Mass ▪ Momentum ▪ Energy ▪ Gas concentration	▪ Energy
Process to be scaled	Primary system blowdown	Air ingress	Gas natural circulation	Radiation heat transfer and core heat conduction

Table 4. Examples of characteristic ratios dimensionless groups (Woods et al. 2015)

Π – groups	**Equation**
PCC natural circulation Richardson number ratio $(\pi_{RI,PCC})_R$	$\left[\frac{g\left(\rho_{avg,C} - \rho_{avg,H}\right)_0 L_{TC}}{\rho_{avg,core,0} W_{avg,core,0}^2}\right]_R$
PCC natural circulation Peclet number ratio $(\pi_{Pe,PCC})_R$	$\left[\frac{\rho_{avg,core,0}\left(C_{p,avg,core}\right)_0 W_{avg,core,0} L_{TC}}{k_{avg,core,0}}\right]_R$
PCC natural circulation time scale ratio $(t_{PCC})_R$	$\left[\frac{L_{TC}}{W_{avg,core,0}}\right]_R$

Table 5. Dimensionless groups characterizing natural convection phenomenon inside vertical channels

Dimensionless group	**Equation**
Prandtl number (Pr)	$\mathrm{Pr} = \frac{\mu C_p}{k}$
Grashof number (Gr)	$\mathrm{Gr} = \frac{\ell^3 g \rho^2 \beta \Delta T}{\mu^2}$
Nusselt number (Nu)	$\mathrm{Nu} = \frac{h \ell}{k}$
Channel length / Channel diameter	$L/d_{channel}$
Channel pitch / Channel diameter	$P/d_{channel}$
Upper plenum length / Channel diameter	$L_{up}/d_{channel}$
Lower plenum length / Channel diameter	$L_{lp}/d_{channel}$

Table 6. Dimension of scaled-down DCF with reference to HTTF

Parameter	Current Facility	OSU-HTTF
Tube diameter (inch)	0.625	0.625
Tube length (inch)	Five layers of vertical prismatic blocks (each of 7.87 inches and total of 39.37 inches)	Ten layers of vertical prismatic blocks (total of 92.92 inches)
Upper plenum height (inch)	9.41	37. 64
Core diameter (inch)	15	60
Number of channels	Two channels (one up-ward and other down-ward)	516 coolant channel 210 Heater rod 6 inner gap channel 36 outer gap channel

Table 7. Preliminary experiments conditions

Experiment number	Heating intensity as heated channel outer wall surface temperature
1)	50 ℃ wall temperature±2℃
2)	75 ℃ wall temperature ±2℃
3)	100 ℃ wall temperature ±2℃
4)	150 ℃ wall temperature±2℃
5)	200 ℃ wall temperature ±2℃
	Upper plenum and down-comer channel
Experiments 1 - 5	Chilled water temperature (outer surface temperature of upper plenum and down-comer channel) is kept fixed at 22℃
	Lower plenum
Experiments 1 - 5	Kept adiabatic for all experiments
The facility (channels and plena) are thermally insulated by 2 inch thermal ceramic fiber (thermal conductivity of 0.07 W/(m.k)) to minimize heat losses to surrounding	

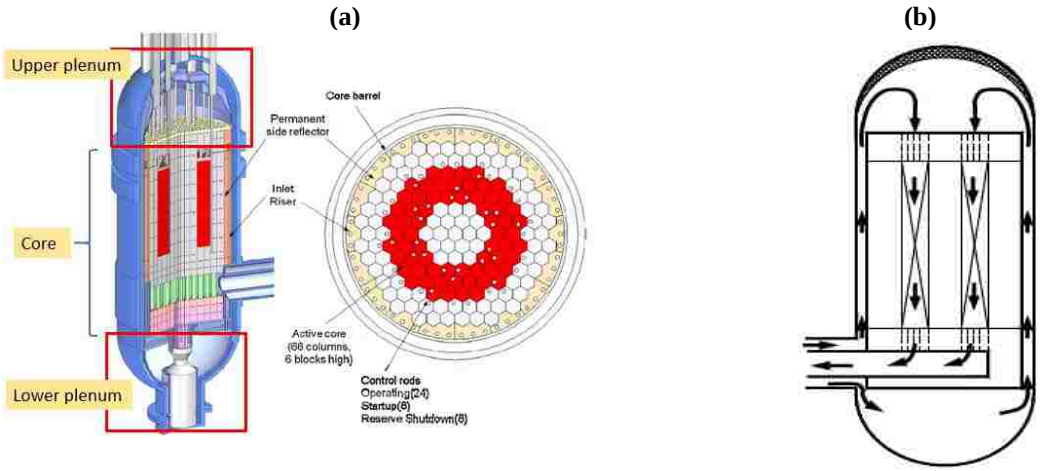

Figure 1. Schematic diagram of (a) the PBMR main components and (b) Gas coolant flow path during normal conditions (Kim et al. 2010)

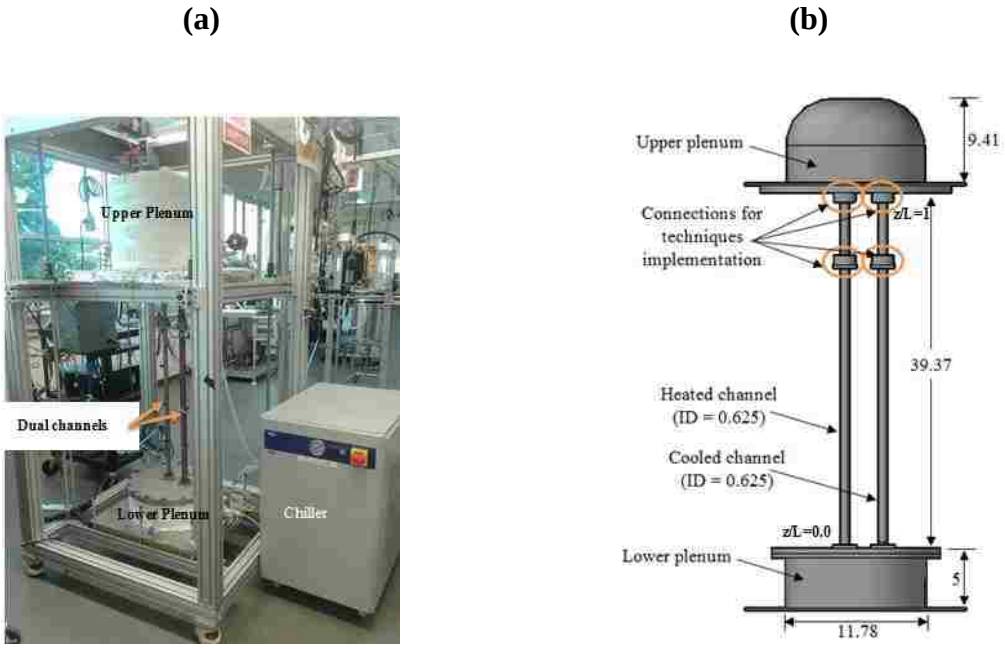

Figure 2. (a) Picture of P2PF preliminary design, (b) Schematic diagram of P2PF preliminary design (all dimensions in inches)

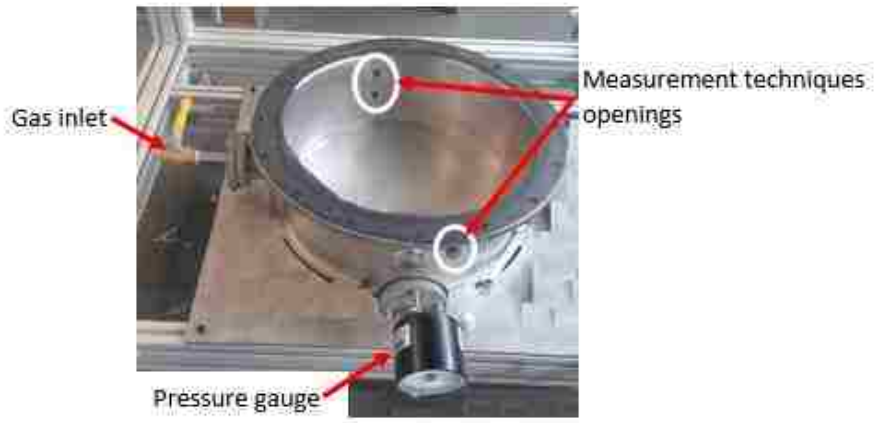

Figure 3. Picture of the lower plenum

(a)

(b)

Figure 4. (a, b) Pictorial representation of the upper plenum before and after insulation

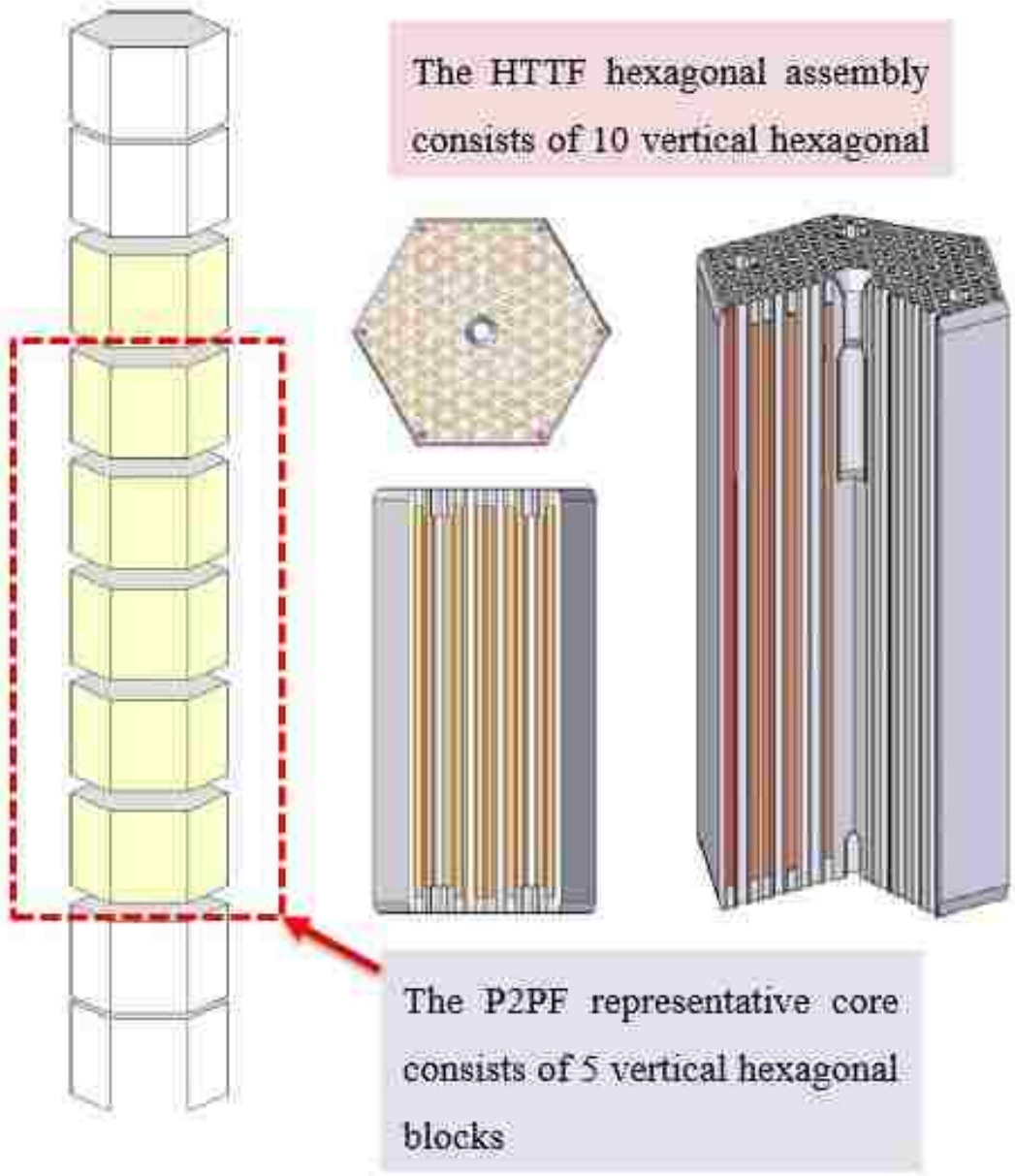

Figure 5. Schematic diagram of the vertical hexagonal blocks assemblies forming the core

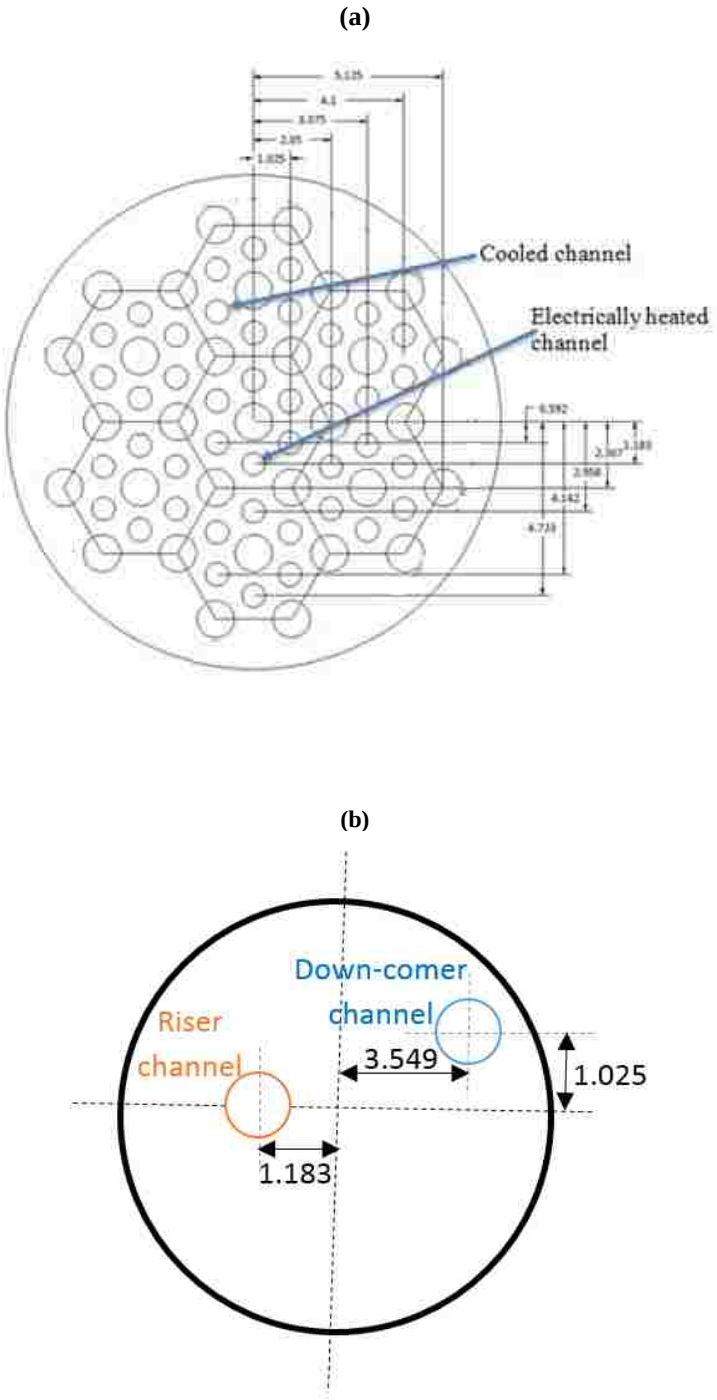

Figure 6. Schematic diagram of hexagonal fuel blocks representing Missouri S&T-P2PF core (a) showing representative fuel channels (larger channels) and coolant channels (smaller ones) and (b) phase-I two channels location

Figure 7. Electrical heaters wrapped around the heated channel

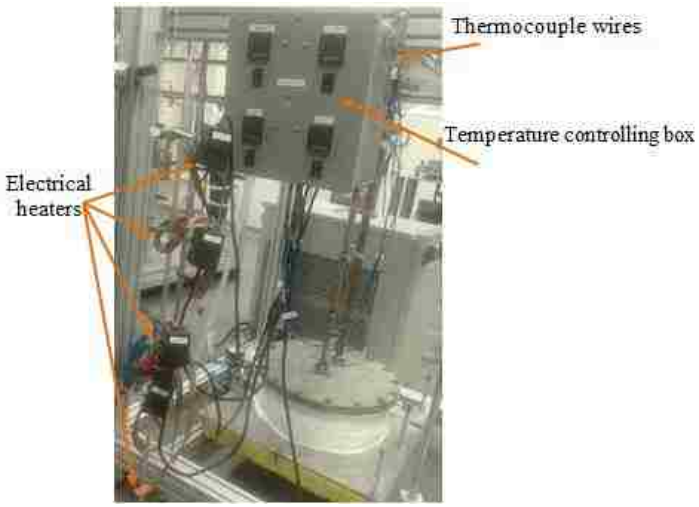

Figure 8. PID temperature controller system

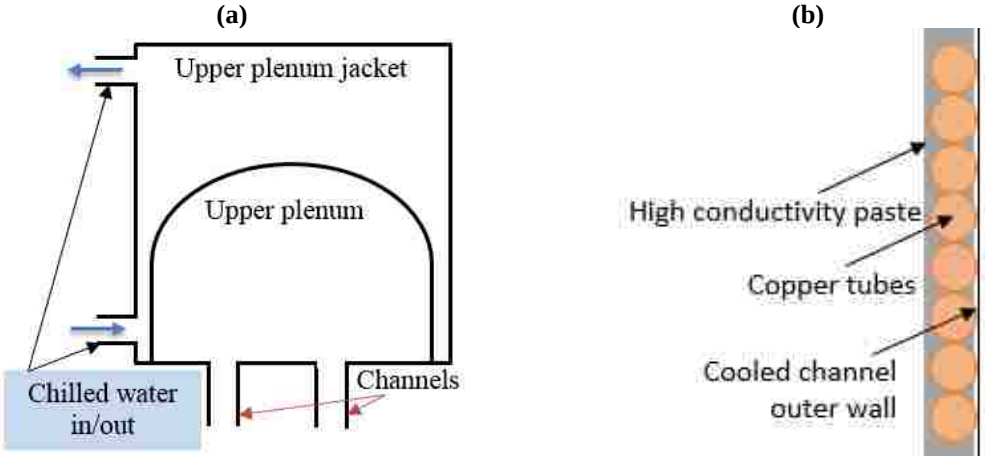

Figure 9. Schematic diagram of (a) upper plenum with the cooling jacket and (b) Copper helical coil heat exchanger with high conductivity paste.

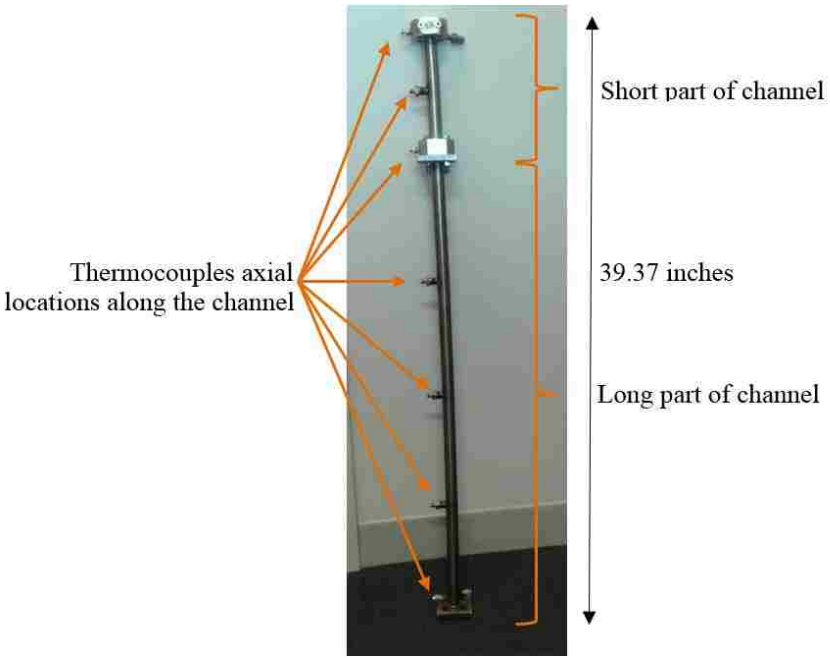

Figure 10. The channel consists of two parts with different lengths

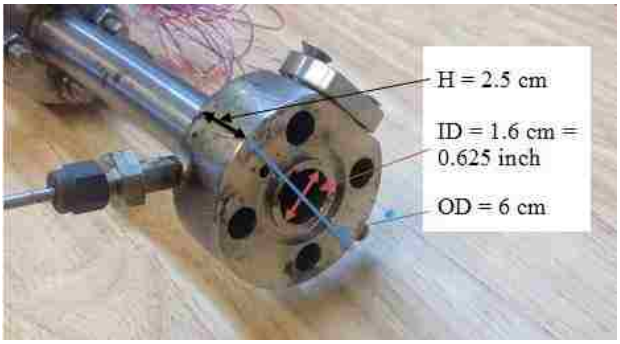

Figure 11. Connection blocks preliminary design

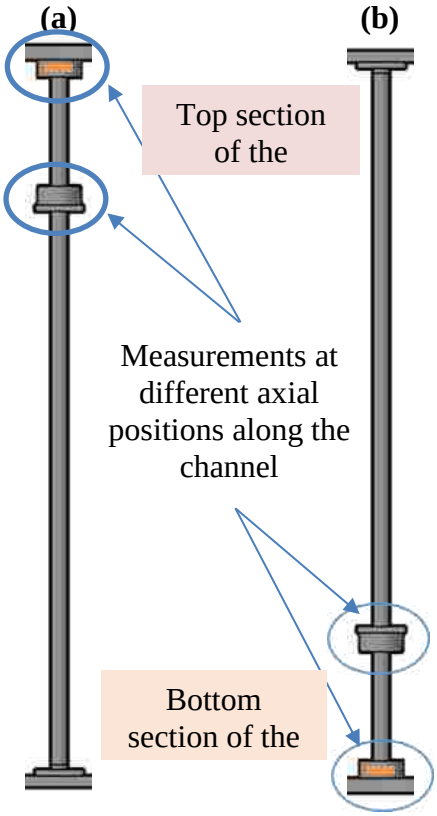

Figure 12. The proposed configurations for the channels to determine axial temperature variation

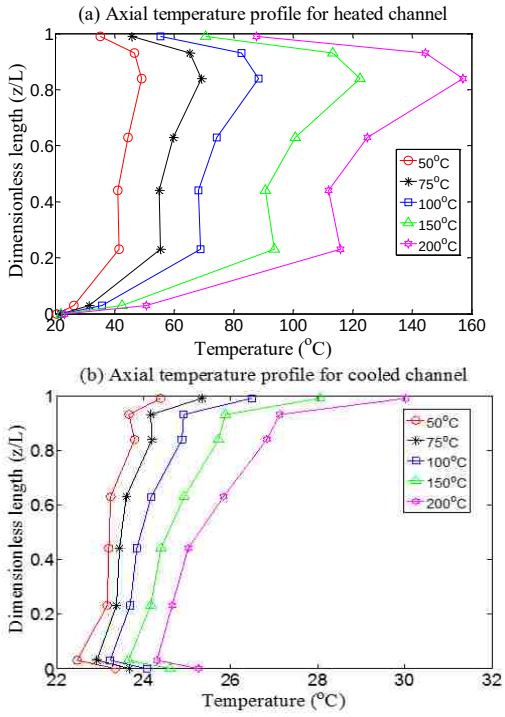

Figure 13. Axial temperature profile obtained for (a) heated channel, (b) cooled channel

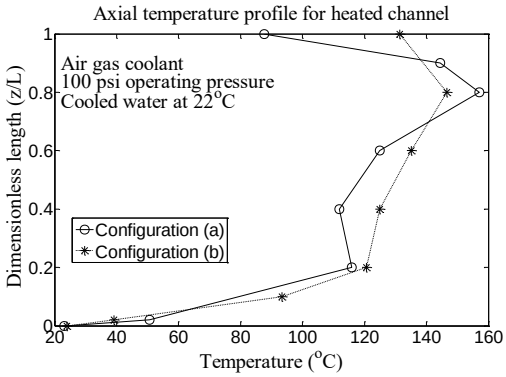

Figure 14. Sample results comparing axial temperature profile for 'a' and 'b' configurations under the same experimental conditions (Experiment 5)

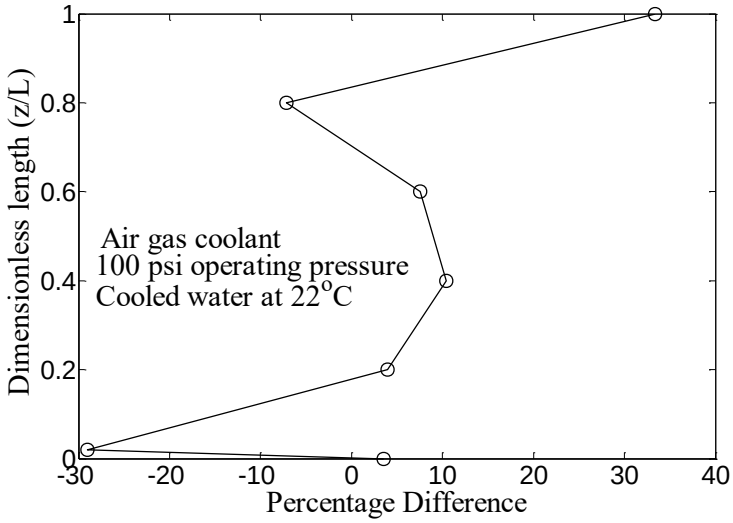

Figure 15. Discrepancies between temperature data obtained for configurations (a) and (b)

Figure 16. Variac power controlling system (BT-V)

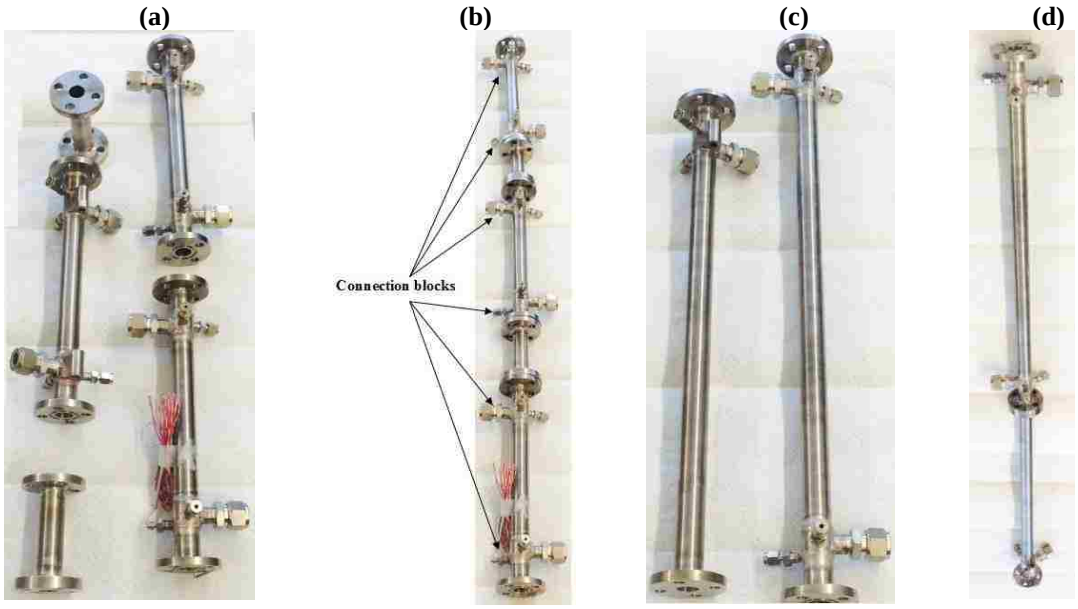

Figure 17. Core channels with new design of connection blocks (a, b) heated channel and (c, d) cooled channel

Figure 18. (a) Physical picture and (b) Schematic diagram of the novel integration of heat transfer and gas velocity measurement techniques within the connection blocks

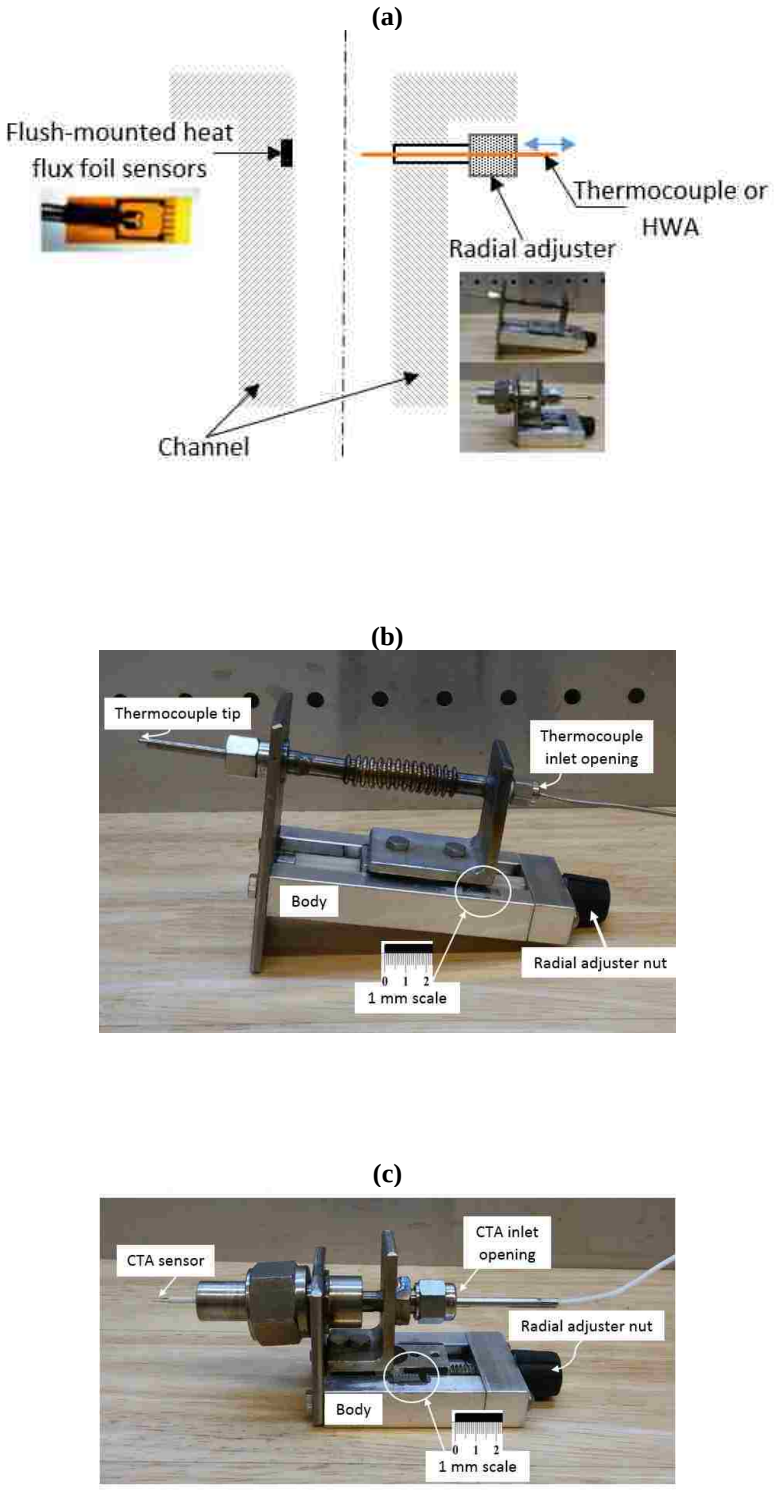

Figure 19. (a) Schematic diagram showing the radial adjuster function (b, and c) Physical pictures of the radial adjusters of thermocouple and CTA, respectively

NOMENCLATURE

Symbol	
A	Transfer area
C_p	Heat capacity
d	diameter
g	Gravitational acceleration [m/s^2]
h	Heat transfer coefficient [$W/(m^2.k)$]
j	Flux transferred of the conserved property
k	Thermal conductivity [W/(m.k)]
ℓ	Characteristic length
L	Length [m]
n	Number of experimental data points
P	Channel pitch
q	Heat flux
Q	Volumetric flow rate [m^3/s]
S	Distributed sources (such as body forces or sinks) acting on the control volume
t	Natural circulation time [s]
T	temperature
ΔT	Temperature difference between channels
V	Control volume
w	Gas molar velocity [m/s]

Dimensionless groups

Ri	Richardson number
Pe	Peclet number
Nu	Nusselt number
Gr	Grashof number

Greek letters

Π	Dimensionless characteristic group
Ψ	Conserved property
ρ	Density [kg/m^3]
μ	Dynamic viscosity [$N.s/m^2$]
β	Thermal expansion coefficient [1/K]

Subscripts

k,n	Refers to constituents
p	Prototype
M	Model
R	Ratio between model and prototype
0	Reference (either initial or maximum)
TC	Thermal center
C	Cool gas
H	Upper plume or horizontal or hot gas leaving core

avg	Average
channel	Channel
up	Upper plenum
lp	Lower plenum

List of abbreviations

DCF	Dual channel facility
MCF	Multichannel facility
HTGRs	High temperature gas-cooled reactors
CFD	Computational fluid dynamics
HTTF	High temperature test facility
OSU	Oregon state university
LOFA	Loss of forced flow accidents
RCCS	Reactor cavity cooling system
HWA	Hot wire anemometry
NGNPs	Next generation nuclear plants
DOE	U.S. department of energy
PBMR	Pebble bed modular reactor
PMR	Prismatic modular reactor
P2P	Plenum-to-plenum
LOCA	Loss of coolant accidents
H2TS	Hierarchical two-tiered scaling
NRC	Nuclear regulatory commission

SARP	Severe accident research program
LWRs	Light water reactors
GCRs	Gas-cooled reactors
DF	Distortion factor
PCC	Pressurized conduction cooldown
MHTGR	Modular high-temperature gas-cooled reactor
DCC	Depressurized conduction cooldown
NPT	National pipe thread
CTA	Constant temperature anemometry
PIV	Particle image velocimetry
ID	Internal/inside diameter
OD	Outside diameter

REFERENCS

Abdulmohsin, R. and A.-D. M. H. (2015). "Characteristics of convective heat transport in a packedpebble-bed reactor." Nuclear Engineering and Design 284(1): 143–152.

Abdulmohsin, R. S., B. A. Abid and M. H. Al-Dahhan (2011). "Heat transfer study in a pilot-plant scale bubble column." Chemical Engineering Research and Design 89(1): 78-84.

Amini, N. and Y. A. Hassan (2014). "Experimental study of bypass flow in near wall gaps of a pebble bed reactor using hot wire anemometry technique." Annals of Nuclear Energy 65: 60-71.

Basu, D. N., S. Bhattacharyya and P. K. Das (2014). "A review of modern advances in analyses and applications of single-phase natural circulation loop in nuclear thermal hydraulics." Nuclear Engineering and Design 280(0): 326-348.

Beeny, B. and K. Vierow (2015). "Gas-cooled reactor thermal hydraulic analyses with MELCOR." Progress in Nuclear Energy 85: 404-414.

CAl, X. (2013). Scaling assessment for the integral effect tests (1)-closed loop natural circulation. 21st International Conference on Nuclear Engineering. Chengdu, China.

Choi, J.-H., J. Cleveland and N. Aksan (2011). "Improvement in understanding of natural circulation phenomena in water cooled nuclear power plants." Nuclear Engineering and Design 241(11): 4504-4514.

Doug Chapin, S. K., and Jim Nestell (2004). The very hight temperature reactor: A technical summary, MPr Associates, Inc.

F. D'Auria, a. G. M. G. (2010). "Scaling in nuclear reactor system thermal-hydraulics." Nuclear Engineering and Design 240: 3267–3293.

Fu, W. S., W. S. Chao, T. E. Peng and C. G. Li (2016). "Flow downward penetration of vertical parallel plates natural convection with an asymmetrically heated wall." International Communications in Heat and Mass Transfer 74: 55-62.

Gradecka, M. J. and B. G. Woods (2016). "Development of thermal mixing enhancement method for lower plenum of the High Temperature Test Facility." Nuclear Engineering and Design 305: 81-103.

Guillen, D. P. and H. M. McIlroy Jr (2007). Preliminary study of turbulent flow in the lower plenum of a gas-cooled reactor. Proceedings - 12th International Topical Meeting on Nuclear Reactor Thermal Hydraulics, NURETH-12.

Hess, C. F. and C. W. Miller (1979). "Natural convection in a vertical cylinder subject to constant heat flux." International Journal of Heat and Mass Transfer 22(3): 421-430.

Jackson, R. B., E. Smith and B. G. Woods (2009). FLUENT modeling for heat transfer in upper plenum of VHTR. Transactions of the American Nuclear Society.

Johnson, R. W., H. M. McIlroy, R. C. Johnson and D. P. Christensen (2011). "Undesirable flow behavior in a proposed validation data set." Nuclear Engineering and Design 241(12): 4682-4690.

Kao, M. T., P. Jain, S. Usman, I. A. Said, M. M. Taha, M. H. Al-Dahhan and Rizwan-Uddin (2015). Investigation of plenum-to-plenum heat transfer and gas dynamics under natural circulation in a scaled-down dual channel module mimicking prismatic VHTR core using CFD. International Topical Meeting on Nuclear Reactor Thermal Hydraulics 2015, NURETH 2015, American Nuclear Society.

Kao, M. T., P. Jain, S. Usman, I. A. Said, M. M. Taha, M. H. Al-Dahhan and U. Rizwan (2015). Study of Plenum to Plenum (P2P) natural cireulation phenomena in a dual channel scaled module of very high temperature reactor design by using CFD. Nuclear Engineering Division 2015 - Core Programming Area at the 2015 AIChE Annual Meeting.

Kiang, R. L. (1984). "Scaling Criteria for Nuclear Reactor Thermal Hydraulics." Nuclear Science and Engineering 89: 207-216.

Kihm, K. D., J. H. Kim and L. S. Fletcher (1995). "Onset of flow reversal and penetration lengths of natural convective flow between isothermal vertical walls." Journal of Heat Transfer 117(3): 776-779.

Kim, M.-H. and H.-S. Lim (2011). "Evaluation of the influence of bypass flow gap distribution on the core hot spot in a prismatic VHTR core." Nuclear Engineering and Design 241(8): 3076-3085.

Kim, M. H., N. I. Tak and H. S. Lim (2010). "Thermal-fluid assessment of the design options for reactor vessel cooling in a prismatic core VHTR." Annals of Nuclear Energy 37(12): 1774-1782.

King, B. M. (2012). Natural Circulation Scaling of a Pressurized Conduction Cooldown Event in the Upper Plenum of the Modular High Temperature Gas Reactor. Master, Oregon State University.

Kline, S. J. (1965). Similtude and approximation theory. New York, McGraw-Hill.

LaBar, M. P., A. S. Shenoy, W. A. Simon and E. M. Campbell (2003). "The Gas Turbine-Modular Helium Reactor." Nuclear News 46(11): 28-37.

LaBar, M. P., A. S. Shenoy, W. A. Simon and E. M. Campbell (2004). "Introducing the GT-MHR." Nuclear Engineering International 49(596): 18-23.

Lau, G. E., V. Timchenko, C. Ménézo, S. Giroux-Julien, M. Fossa, E. Sanvicente, J. Reizes and G. H. Yeoh (2012). "Numerical and experimental investigation of unsteady natural convection in a vertical open-ended channel." Computational Thermal Sciences 4(5): 443-456.

Lee, J. H., S. J. Yoon, H. K. Cho, M. Jae and G. C. Park (2015). "Experimental investigation and CFD analysis on cross flow in the core of PMR200." Annals of Nuclear Energy 83: 422-435.

Lee, J. H., S. J. Yoon, E. S. Kim and G. C. Park (2014). "CFD analysis and assessment for cross-flow phenomena in VHTR prismatic core." Heat Transfer Engineering 35(11-12): 1152-1160.

Li, R., M. Bousetta, E. Chénier and G. Lauriat (2013). "Effect of surface radiation on natural convective flows and onset of flow reversal in asymmetrically heated vertical channels." International Journal of Thermal Sciences 65: 9-27.

M. Ishii, a. I. K. (1984). "Scaling laws for thermal-hydraulic system under single phase and two-phase natural circulation." Nuclear Engineering and Design 81(3): 411–425.

McLlroy Jr, H. M., D. M. McEligot and R. J. Pink (2009). Idaho national laboratory experimental program to measure the flow phenomena in a scaled model of a prismatic gas-cooled reactor lower plenum for validation of CFD codes. 2008 Proceedings of the 4th International Topical Meeting on High Temperature Reactor Technology, HTR 2008.

McVay, K. L., J.-H. Park, S. Lee, Y. A. Hassan and N. K. Anand (2015). "Preliminary tests of particle image velocimetry for the upper plenum of a scaled model of a very high temperature gas cooled reactor." Progress in Nuclear Energy 83: 305-317.

Misale, M. and L. Tagliafico (1987). "Transient and stability of single-phase natural circulation loops." Heat and Technology 5(1-2): 101-116.

Mohammed, H. A. and Y. K. Salman (2007). "Laminar air flow free convective heat transfer inside a vertical circular pipe with different inlet configurations." Thermal Science 11(1): 43-63.

Nahavandi, A. N. (1979). "Scaling laws for modling nuclear reactor systems." Nuclear Engineering and Design 72: 75-83.

Reyes, J. N., J. T. Groome, B. G. Woods, B. Jackson and T. D. Marshall (2010). "Scaling analysis for the high temperature Gas Reactor Test Section (GRTS)." Nuclear Engineering and Design 240(2): 397-404.

Reyes Jr, J. N. and L. Hochreiter (1998). "Scaling analysis for the OSU AP600 test facility (APEX)." Nuclear Engineering and Design 186(1–2): 53-109.

Reyes Jr, J. N. and Q. Wu (2003). AP1000 testing and analysis program at Oregon State University. 2003 International Congress on Advances in Nuclear Power Plants - Proceedings of ICAPP 2003.

Rodríguez-Sevillano, A., I. Pérez-Grande and J. Meseguer (2011). "On the onset of turbulence in natural convection on inclined plates." Experimental Thermal and Fluid Science 35(1): 68-72.

Rodriguez, S. B. and M. S. El-Genk (2010). On enhancing VHTR lower plenum heat transfer and mixing via swirling jets. International Congress on Advances in Nuclear Power Plants 2010, ICAPP 2010.

Sabharwall, P., T. Marshall, K. Weaver and H. Gougar (2007). CFD Analysis for Flow Behavior Characteristics in the Upper Plenum during low flow/low pressure transients for the Gas Cooled Fast Reactor (GCFR), Idaho National Laboratory (INL).

Said, I. A., M. M. Taha, Rizwan-Uddin, U. Shoaib and M. H. Al-Dahhan (Under review). "Experimental study of the effect of helium pressure on the natural convection heat transfer in prismatic dual-channel circulation loop." International Journal of Thermal Sciences.

Said, I. A., M. M. Taha, U. Shoaib and M. H. Al-Dahhan (Under review). "Experimental investigation of the helium natural circulation heat transfer in two channels facility using varying riser channel heat fluxes." Experimental Thermal and Fluid Sciences.

Said, I. A., M. M. Taha, U. Shoaib, B. G. Woods and M. H. Al-Dahhan (2017). "Investigation of Natural Convection Heat Transfer in a Unique Scaled-Down Dual-Channel Facility." AICHE Journal 63(1): 387-396.

Sanvicente, E., S. Giroux-Julien, C. Ménézo and H. Bouia (2013). "Transitional natural convection flow and heat transfer in an open channel." International Journal of Thermal Sciences 63: 87-104.

Sato, H., R. Johnson and R. Schultz (2010). "Computational fluid dynamic analysis of core bypass flow phenomena in a prismatic VHTR." Annals of Nuclear Energy 37(9): 1172-1185.

Schultz, R. R., P. D. Bayless, R. W. Johnson, G. E. McCreery, W. Taitano and J. R. Wolf (2010). Studies Related to the Oregon State University High Temperature Test Facility: Scaling, the Validation Matrix, and Similarities to the Modular High Temperature Gas-Cooled Reactor, Idaho National Lab

Taha, M. M., I. A. Said, U. Shoaib and M. H. Al-Dahhan (Under review). "Buoyancy-driven air flow within plenum-to-plenum facility down-comer channel." Experiments in Fluids.

Taha, M. M., I. A. Said, U. Shoaib and M. H. Al-Dahhan (Under review). "Investigation of natural circulation in a separate effects facility of two channels representing prismatic modular reactors (PMRs) core." International Journal of Thermal Sciences.

Tkachenko, O. A., V. Timchenko, S. Giroux-Julien, C. Menezo, G. H. Yeoh, J. A. Reizes, E. Sanvicente and M. Fossa (2016). "Numerical and experimental investigation of unsteady natural convection in a non-uniformly heated vertical open-ended channel." International Journal of Thermal Sciences 99: 9-25.

Tung, Y. H. and R. W. Johnson (2011). CFD calculations of natural circulation in a high temperature gas reactor following pressurized circulator shutdown. ASME 2011 International Mechanical Engineering Congress and Exposition, IMECE 2011.

Vijayan, P. K. and H. Austregesilo (1994). "Scaling laws for single-phase natural circulation loops." Nuclear Engineering and Design 152(1-3): 331-347.

Woods, B. G., R. B. Jackson, B. L. Nelson, S. R. Cadell and J. N. Reyes (2015). Scaling Analysis for the Very High Temperature Reactor Test Facility at Oregon State University. OSU-HTTF-000000-TECH-001-R0, Oregon State University.

Wu, C., M. H. Al-Dahhan and A. Prakash (2007). "Heat transfer coefficients in a high-pressure bubble column." Chemical Engineering Science 62(1-2): 140-147.

Wulff, W. (1996). "Scaling of thermohydraulic systems." Nuclear Engineering and Design 163: 359-395.

Yoon, S. U. J., C. Y. Jin, M. H. Kim and G. C. Park (2011). "Experimental and computational assessment of core bypass flow in block-type very high temperature reactor." Nuclear Technology 175(2): 419-434.

Zuber, N. (1991). An Integrated Structure and Scaling Methodology for Severe Accident Technical Issue Resolution. EG&G Idaho, NUREG:CR-5809 (Draft Report for Comment).

II. INVESTIGATION OF NATURAL CIRCULATION IN A SEPARATE EFFECTS FACILITY OF TWO CHANNELS REPRESENTING PRISMATIC MODULAR REACTOR CORE

ABSTRACT

In this study, the effect of cooling intensity, which is represented by chilled water temperature (i.e., for the upper plenum and cooled channel namely; 5, 15, 25, and 35 ℃), on air gas velocity and temperature inside the heated channel was investigated for the first time by implementing a hot wire anemometry (HWA) technique, micro-foil sensors and thermocouples in a scaled down separate effects test facility of two channel and two plena mimicking the prismatic modular reactor (PMR) core. Air temperature and velocity measurements were obtained at three axial locations along the channel (i.e., z/L = 0.04, 0.59, and 0.96). For each axial location, radial measurements were obtained from the inner wall (r/R = 1) to the centerline (r/R = 0.0) of the channel with increment of 1 mm. For all cooling intensities, it is found that both temperature and velocity increase as distance increase from the inlet to the mid-channel. At the outlet, however, a sudden drop in temperature and air velocity was observed. This sudden drop was reported previously and is attributed to end losses effect. Present study indicated this loss is because of flow reversal and the interaction between heated air exiting the top of the heated channel and the cooled air plumes of lower density in the upper plenum and due to conjugate heat conduction through the channels material itself and the cold upper plenum. Air velocity change was found to increase by 30% maximum with decreasing chilled water temperature from 35 to 5 ℃. On the other hand, air temperature is found to decrease by 6.4% near the outlet while no significant change was observed for downstream positions. These results

provide detailed velocity and temperature variation which can be useful for validating CFD codes.

1. INTRODUCTION

The Prismatic Modular Reactor (PMR) is a Generation IV reactor concept that are graphite-moderated, gas-cooled nuclear reactor and can conceptually have an outlet temperature of as high as 1000 °C. This high temperature enables applications such as process heat or hydrogen production via for example thermochemical sulfur–iodine cycle in addition to high efficiency electricity production. In order to absorb the heat generated during normal operations, gas coolant is forced to flow downwards through the reactor core coolant channels and then introduced to a steam generator. This forced circulation system is lost after shutdown or in case of a postulated loss of flow accidents (LOFA). However, the reactor continues to generate heat due to the decay of radioactive fission products. Indeed, this decay heat has to be removed to maintain fuel temperatures within safe limits. In view of this, the PMRs are designed to remove decay heat by natural circulation resulting from the different gas/coolant densities of relative cold and heated portions of the reactor core. Therefore, the gas coolant flow direction inside the reactor vessel is reversed and naturally rising inside the channels representing the heated portions of the core, acts as a riser, and downward flowing through the channels representing the cooled portions of the core and acts as the down-comer for this natural circulation loop (Kao et al. 2015, McVay et al. 2015).

Plenum-to-plenum (P2P) natural circulation flow measurements are recognized as one of the need-to-know process parameters alongside temperature measurements for PMR safety analysis and validation of computational fluid dynamics (CFD). Considerable

experimental and numerical studies have been reported concerning natural circulation flow and temperature distributions insides vertical heated channels (Aung et al. 1972, Tanda 1988, Habib et al. 2002, Hernández et al. 2005, Lau et al. 2012, Tkachenko et al. 2016). However, it is reported that such studies in simple geometries cannot be extended and applied to complex nuclear systems (Celataa et al. 1998). Extensive computational investigations studying thermal hydraulics of natural circulation in scaled down PMRs and other reactors have been reported in the open literature (Tak et al. 2008, Jackson et al. 2009, Kim et al. 2011, Shibahara et al. 2013, Lee et al. 2014). Additionally, there is an ongoing study related to plenum-to-plenum (P2P) natural circulation heat transfer during depressurized conduction cooldown (DCC) accidents at Oregon State University (OSU) integral test facility (named High Temperature Test Facility "HTTF") (Woods et al. 2015). In general, limited experimental studies on natural circulation phenomenon in geometries mimicking complex nuclear systems have been reported in the open literature and in addition limited measurement techniques for natural convection have been employed in general and with gas-cooled systems in particular. Therefore, there is a need for establishing a scaled down separate effects experiments for studying thermal hydraulic behavior occurring within a component or particular region of PMRs such as P2P gas dynamics during natural circulation.

To overcome previously mentioned data gap and to advance the knowledge and understanding of natural circulation phenomenon in nuclear systems, multiphase reactors engineering and applications laboratory (mReal) research team at Missouri S&T designed and developed separate effects scaled down test facility with reference to the high temperature test facility (HTTF) for experimental investigations of plenum-to-plenum

(P2P) natural circulation thermal hydraulics behavior. This work is aimed at investigating how the cooled portions of the reactor affects temperature and gas velocity distribution along the channel representing the heated portions of the prismatic VHTR core. For such measurements, advanced techniques such as temperature micro-foil sensors, moveable thermocouples, and hot wire anemometry (HWA) are implemented and integrated for the first time in such a study.

2. EXPERIMENTAL SETUP

The experimental apparatus, shown in Figure 1, is a scaled down separate effects facility made of stainless steel and capable of simulating post shutdown and accident scenarios thermal hydraulics phenomena in PMRs. It is mimicking the main components of PMRs: (1) reactor core coolant channels and (2) the two plena (i.e., upper and lower). The core channels are represented by two channels to mimic the heated and cooled portions of PMR core regions. Both channels have the same dimensions of 1 m (39.37 inch) height and 0.016 m (0.625 inch) ID (i.e., aspect ratio, L/D = 62.5). The scaled down prismatic core was designed to accommodate five layers of scaled down prismatic blocks used in the HTTF (each block is 7.87 inch ~20 cm of height) while channels diameter is kept the same as for the channel of the HTTF. The channel representing the heated regions of the core (i.e., riser) is electrically heated by four 1 inch by 24 inch heavily insulated Duo-Tape electrical heaters with maximum capacity of 312 watts at 120 V. Each heater is connected to BT-V Variac power controller to adjust and control the amount of heat supplied from each heater separately. This allowed experiments to be conducted under different heating intensities and axial flux shape (i.e., isoflux and non-isoflux). The natural circulation loop

cooled regions are mimicked by cooling the other channel (i.e., acts as down-comer) and the upper plenum by using chilled water provided from an external chiller (Applied Thermal Control Ltd, K4 chiller). This chilled water is introduced into copper tubes wrapping the channel and into a cooling jacket surrounding the upper plenum, simultaneously. The temperature of the chilled water can be varied by temperature controller with ±0.1℃ temperature stability built-in the chiller. In order to minimize environment interference and heat losses, the entire setup (i.e., core channels and the two plena) are heavily insulated by ceramic fiber insulation. Detailed explanation of the experimental setup can be found elsewhere (Said et al. 2017).

3. INSTRUMENTATION AND MEASUREMENT TECHNIQUES

In order to measure the temperature and flow characteristics, temperature sensors and flow velocity including a hot wire anemometry (HWA) techniques were integrated and processed simultaneously. These techniques and their measurements are discussed below.

3.1. TEMPERATURE MEASUREMENTS

Inner wall surface temperatures were recorded at six axial positions (z/L) along the heated channel by using micro-foil sensors. These sensors are flush mounted on the wall of the channel. Local temperatures of flowing air were measured by inserting T-type thermocouples (1.6 mm in diameter) at only three axial positions along the heated channel (i.e., z/L = 0.04, 0.59, and 0.96). These locations are selected, for the current study, to represent the three distinct regions characterizing flow field inside the vertical channel which are the inlet, where the entry effects are noticeable, the mid-channel and the

outlet/exit, where the complex flow reversal and mixing may be dominated (Hess et al. 1979). For each axial position, nine radial measurements were obtained from the inner wall (r/R = 1) to the centerline of the channel (r/R = 0.0) by using the adjuster shown in Figure 2. This adjuster was manufactured in a way which enables changing the radial position of the thermocouple (and also the HWA) by 0.001 m (1 mm) increments.

3.2. GAS VELOCITY MEASUREMENT

The hot wire anemometry (HWA) is a widely-used technique capable of measuring the smallest and fastest flow fluctuations at a point. It is characterized by high frequency response, high spatial and temporal resolution, good signal-to-noise ratio, and low cost. While the technique is invasive, due to its small size, it causes minimum flow disturbances. As shown in Figure 3, it can provide continuous analogue output signal which represents the velocity at the point of measurement in contrast to laser Doppler anemometry (LDA) or particle image velocimetry (PIV). While both LDA and PIV have several advantages including the non-invasive nature of the system, ability to simultaneously measure all three components of the velocity but the technique has inferior time resolution. On the other hand, the HWA sensor is very delicate and can easily break therefore it needs to be carefully handled. Additionally, it is negatively affected by flow problems such as contamination of fouling materials or impurities on the wire sensor. However, these difficulties can be minimized by incorporating a filtration system on the fluid inlet stream before impinging the wire sensor, cleaning the sensor with suitable solvents, and recalibration the wire sensor before each experiment, if possible (Bruun 1995).

The HWA wire sensor material must be selected to have the following desired properties:

1. High value of high temperature coefficient of resistance (increased sensitivity to velocity variations)
2. Electrical resistance (easily heated by electric current resulting in fast response)
3. Small size (for high spatial resolution)
4. High tensile strength (for durability)

A comparison of the common materials fulfilling these properties is shown in Table 1.

For economic reasons, most sensors wires are fabricated from tungsten and coated with layer of platinum to improve mechanical strength and resistance to oxidation with higher temperature coefficient of resistance $(0.0032/℃)$. The HWA wire is connected to the prongs (also called stems) that are supporting the HWA sensor by wire ends (named stubs) which are parts of the wire as shown in Figure 4. These stubs are made of gold or copper materials that results in better mechanical properties and reduce heat conduction losses to the prongs. The HWA wire is electrically heated by Joule effect using two systems of operation: (1) constant current mode and (2) constant temperature mode. The first mode is based on maintaining the current supplied to the heated wire at a fixed value and allowing wire temperature to be varied based on the flowing flow conditions. While in the second approach, current supplied to the wire is varied in a way to maintain the wire temperature constant.

3.2.1. Operating Principle and Governing Equation. The HWA operating principle is based on that the change in the electrically heated wire resistance (expressed as change in output voltage readings) is a function of the fluid flow conditions such as velocity or temperature. Thus, a relationship between the fluid velocities with the HWA

output voltage is needed to be established before using the HWA in experiments (Jensen 2004, Schena et al. 2015). This relationship is governed by the following equation:

$$\frac{dQ}{dt} = W - H \tag{1}$$

where:

W	Power generated by Joule heating ($W = I^2 R_w$)
I	Current supplied to the heated wire
R_w	Resistance coefficient of the wire sensor
Q	Thermal energy stored in the wire ($Q = C_w T_w$)
C_w	Wire heat capacity
T_w	Temperature of wire
H	Heat transferred to surrounding

Considering negligible heat losses by radiation and conduction to the wire prongs, in equilibrium conditions where the heat storage is zero, the Joule heating (W) becomes equal to the convective heat transfer to surrounding (H). Hence, the governing equation can be expressed as follows;

$$\frac{dQ}{dt} = 0.0 \quad \Rightarrow \quad W = H \tag{2}$$

$$I^2 R_w = h_w A (T_w - T_f) \tag{3}$$

where h_w is the heat transfer coefficient, A is the heat transfer area, and (T_w -T_f) is the temperature difference between the wire and the fluid.

If the flowing fluid conditions such as: velocity or temperature are changed, the convective heat transfer coefficient will change and new equilibrium conditions will be established for the wire. The heat transfer coefficient dependency on fluid velocity can be expressed as follows (Schena et al. 2015);

$$h_w = A + B(\rho v)^n \quad (4)$$

Also, the same equation can be rewritten in terms of HWA output voltage (E)

$$E = A + Bv^n \quad (5)$$

where ρ is the fluid density, v is the fluid velocity, A and B are calibration constants, and the coefficient n is usually taken to be ½ (King 1914). Since the HWA output voltage (E) has a nonlinear relation with the input fluid velocity (v), using King's law can cause large measurement errors. Hence, the HWA input-output relation is often represented by a fitted fourth order polynomial relationship (i.e., v (m/s)=a $E^4 \pm$b $E^3 \pm$c $E^2 \pm$d E $\pm$e) (Van Dijk et al. 2004) or different values of the coefficient n used in equation (5) (Özahi et al. 2010). In the current study, the polynomial relationship is found to give the highest coefficient of determination (R^2) for calibration data points as shown in Figure 5.

3.2.2. Calibration and Data Acquisition. In the current study, MiniCTA (Mini - constant temperature anemometry) system (54T42 model from Dantec Dynamics) was used. The MiniCTA is a single channel anemometer optimized for moderate speed airflow (up to 100 m/s) and low speed water flow measurements (up to 2 m/s). Additionally, an automatic calibrator was utilized for in situ air velocity calibration to ensure high accuracy at all times. The automatic calibrator is designed for air calibration at velocities from few cm/s up to > 300 m/s. The wire sensor is placed in a free jet with a flat low-turbulent velocity profile during calibration. The automatic calibrator is connected to a computer via USB and the calibration process is controlled from StreamWare Basic software package. The calibrator contains a set of control valves, pressure and temperature transducers and a settling chamber with an exchangeable exit nozzle. Four nozzles cover the entire velocity

range. In the current study, sensor calibration was conducted before each set of experiments to minimize measurement errors. All these components are shown in Figure 6.

3.2.3. Temperature Correction. The HWA has a disadvantage of misleading velocity measurements if it is calibrated at temperature (T_o) which is different from the flowing fluid temperature (T_f). There were many methods for deducing temperature corrections factor in the open literature (Bearman 1971, Lomas 1986, Bruun 1995, Ball et al. 1999). These correction methods were reviewed by Benjamin et al. (Benjamin et al. 2002) and found to be unsatisfactory. Hence, they made exploration of the theoretical basis for correction factors used to interpret the HWA output voltage readings and presented new correction method. This correction method has the following formula;

$$E_c = E_{Exp}\left[1 - 0.5\left\{\frac{(T_o - T_{Exp})}{(T_w - T_{Exp})}\right\}\right] \quad (6)$$

where E_c is the corrected voltage, E_{Exp} is the voltage during hot flow experiment, T_{Exp} is the flowing fluid temperature during the experiment, T_o is the calibration temperature, and T_w is the wire sensor temperature. Once the corrected voltage is calculated, it is used in the HWA polynomial output-input relationship (calibration equation) to obtain the corrected value of the fluid velocity. This correction method was tested and found to be valid to elevated temperatures up to 230 ℃ and at high velocities up to 14 m/s (Benjamin et al. 2002).

4. EXPERIMENTAL WORK AND CONDITIONS

The experiment is initiated by introducing dehumidified air gas into the setup until the desired pressure value is achieved. The experimental setup was manufactured and constructed to withstand high pressure values up to 100 psi. However, the current results

are reported for experiments conducted at atmospheric pressure. Afterwards, the electrical heaters and external chiller are switched on. Each electrical heater is adjusted separately to the desired heating intensity value. In the current study, two isoflux heating intensities are considered typically 860 (low heat supplied) and 2290 (high heat supplied) W/m^2 to simulate two reactor powers. Although the heaters can supply more heat but this can potentially damage the foil sensors utilized for measuring channel surface temperature. The external chiller high capacity causes inconsiderable change in the circulating chilled water temperature. Four chilled water temperatures are examined typically; 5 to 35 ℃ with 10 ℃ temperature increments. This temperature range is limited by the chiller capability. This potential of varying the heating and the cooling subjected to both channels enables investigating different degrees of radial temperature gradients that could exist within the prismatic core during accident scenarios and onset of natural circulation as a result of the non-uniformity of the heat supplied from the nuclear rods. The experiment is allowed sufficient time (i.e., 3 hours) to reach thermal steady state conditions before collecting data. This time varies based on the experimental conditions and emphasizes the delicate nature of natural circulation phenomenon (Papanicolaou et al. 2002, Lau et al. 2012, Tkachenko et al. 2016). In each experiment, surface measurements are collected simultaneously as foil sensors were flush mounted on the inner wall of the channel. On the other hand, local air temperature and air velocity measurements are collected for each axial position separately. Hence, each experiment is repeated three times with changing thermocouples and HWA sensor between the axial locations. For each axial location, experiment is repeated twice to ensure data reproducibility while radial measurements are collected from the inner wall

(r/R = 1) to the centerline (r/R = 0.0) of the channel. Time series temperature and velocity measurements were collected at frequencies of 0.05 and 0.1 KHz, respectively.

5. TIME SERIES DATA ANALYSIS

In the current study, the HWA 3000-time series output signals are obtained at frequency of 0.1 kHz with 0.01 seconds sampling interval for a total of 30 seconds sampling time. This time series data was analyzed to guarantee proper sampling frequency and time was implemented. In general, there are three methods for time series data analysis: (1) amplitude-domain, (2) frequency-domain, and (3) time-domain methods (Sklar 2001). The first method of analysis provides information about the amplitude distribution in the signal. Time series results, shown in Figure 7, were expressed in terms of mean velocity ($\bar{v}$) and standard deviation (also named root mean square, rms) (v_{rms}) according to the following formulas:

$$\bar{v} = \frac{1}{N}\sum_{k=0.0}^{k=N} v_k \tag{12}$$

$$v_{rms} = \left(\frac{1}{N-1}\sum_{k=0.0}^{k=N} (v_k - \bar{v})^2\right)^{0.5} \tag{13}$$

where N is total number of samples obtained during the sampling time and the index k refers to the sampling time.

These results reveal that the maximum standard deviation of 0.01 is obtained for the time series data which indicates that the data are not widely deviated from the mean value and reflect the intensity of the fluctuations which is related to the intensity of turbulence. The second method includes spectral analysis that characterizes the distribution of the

signal's energy in the frequency domain. This method refers to the proper sampling frequency that should be used in collecting data. The spectrum shown in Figure 8 reveals low-frequency peaks [40 Hz max]. According to Nyquist sampling criteria (Sklar 2001), the sampling frequency to be implemented should be at least twice the frequency at which peaks are observed to avoid interference between the signals. Thus, the sampling frequency was selected to be 0.1 kHz which is the minimum value provided by the HWA data acquisition system and satisfies these sampling criteria. The third method includes autocorrelation analysis in which signals are analyzed with respect to time in order to examine the sufficient time needed to collect time series measurements. In most CTA (constant temperature anemometers) application software with data reduction features, as the one used in the current study, the autocorrelation coefficient function is calculated and graphically displayed as shown in Figure 9. It is shown that the autocorrelation coefficient starts with the value 1 at time zero and drops down to zero after 20 seconds and then continues oscillating around zero. A reasonable estimate of sampling time is the time takes the coefficient to drop from unity to zero. This emphasize that selected 30 seconds sampling time is statistically sufficient to have real estimation of time-averaged value.

6. RESULTS AND DISCUSSIONS

The effects of the chilled water temperature (outer surface temperature of the upper plenum and cooled channel) on the temperature and velocity distributions at three different axial positions (z/L) along uniformly heated channel are explored experimentally. The results are presented in terms of heated channel inner wall temperature, local time-averaged air temperature and velocity at these three positions.

6.1. UNIFORMLY HEATED CHANNEL INNER WALL TEMPERATURE

Inner wall surface temperature is factorized with respect to air inlet temperature entering the heated channels (z/L = 0.0) and expressed in terms of the inner wall temperature (i.e., surface temperature, T_s) minus air inlet temperature to the channel (T_{inlet}) as shown in Figure 10. It is found that inner wall surface temperature (T_s) distribution is consistent qualitatively with previous findings (Lau et al. 2012, Sanvicente et al. 2013) as surface temperature increases from the minimum value at the leading edge (z/L = 0.0) to a maximum value at z/L = 0.8. However, the observed deviation in this quantity is attributed to varying experimental conditions between present study and the literature as a result of the dependency of surface temperature change on the amount of heat supplied. Although there is no continuity (data gaps axially) of T_s-T_{inlet} values obtained in the current study, previously reported trends (Lau et al. 2012, Sanvicente et al. 2013) can be observed and considered in the current study . In the inlet region (bottom part) of the channel (z/L < 0.3), the wall temperature rapidly increases and the maximum gradient is located at the leading edge of the channel. Between z/L ≅ 0.3 and z/L ≅ 0.8 the temperature is found to increase linearly at a lower rate. In the outlet region of the channel (top part, from z/L ≅ 0.8 to z/L ≅ 1), temperature is observed to decrease although this part of channel is subjected to heating. Presence of this inflection point was reported by several authors (Mohammed et al. 2007, Lau et al. 2012, Tkachenko et al. 2016). However, there is no agreement on the axial location where this inflection point will exist. The location of this point is varied as a result of the geometric channel parameters and experimental conditions, and this emphasizes the delicate nature of natural convection phenomenon. Existence of this inflection point was attributed to the heat losses at channel outlet (Mohammed et al. 2007,

Lau et al. 2012, Sanvicente et al. 2013, Tkachenko et al. 2016). These heat losses are represented in this study by heat conduction losses through stainless steel channel wall to the cooled upper plenum. Additionally, these end losses are accompanied with air plumes mixing and thermal stratification phenomena in the upper plenum. These phenomena were previously reported (Sabharwall et al. 2007, McVay et al. 2015) and are influencing the occurrence of flow reversal (flow and heat) of cooled air plumes from the upper plenum back into the upper part of the channel (Sparrow et al. 1984, Fu et al. 2016).

6.2. INSTANTANEOUS FLOW AND TEMPERATURE FIELDS IN THE UNIFORMLY HEATED CHANNEL

Figure 11 to 16 show the relevant results obtained for temperature and velocity radial distributions (from wall at r/R = 1 to the centerline of the channel at r/R = 0.0). For inlet (z/L = 0.04) and mid-channel (z/L = 0.59) axial positions, temperature distribution is found to have a maximum value at the inner wall of the heated channel (r/R = 1) followed by a temperature reduction towards the centerline of the channel (r/R = 0.0), Figure 11(b) and 12(b), respectively. It is observed that increasing the amount of heat supplied results in higher temperature gradient between the wall and the centerline of the channel as shown in Figure 14(b) and 15(b). By assuming non-slip flow conditions at the inner wall of the heated channel, local time-averaged velocity starts from zero at the inner wall (r/R = 1) and increases towards the centerline of the channel (r/R = 0.0) as shown in Figure 11(a) and 12(a). In case of high heating intensities, there is a noticeable velocity peak observed close to the channel inner wall, which moves further from the wall towards the centerline of the channel becomes almost constant as shown in Figure 14(a) and 15(a). The location and gradient of the velocity peak seems to be dependent on the axial location as well as the

intensity of heating. The velocity peak seems to be migrating towards the radial centerline of the channel as the location of measurement moves away from the inlet.

At channel outlet, it is found that temperature and velocity radial distribution is different from downstream (z/L) positions. Although temperature is dropped from the inner wall to the adjacent regions, it is followed by an increase as thermocouple moves towards the centerline of the channel. On the other hand, air velocity is starting at low values at the inner channel wall and increasing as the measurement point moves towards the channel centerline. Also, the time-averaged velocity values obtained near channel outlet are lower than those obtained for downstream (z/L) positions for both examined heating intensities. This different behavior is attributed to the previously mentioned end losses between the upper part of the channel and the cooled upper plenum. In addition, these end losses are accompanied with mixing of air plumes and thermal stratification phenomena in the upper plenum. These phenomena were previously reported (Sabharwall et al. 2007, McVay et al. 2015) and are influencing the occurrence of flow reversal (flow and heat) of cooled air plumes from the upper plenum back into the upper part of the channel. Flow reversal phenomenon was highlighted by several authors even for laminar flow (Sparrow et al. 1984, Kihm et al. 1995, Fu et al. 2016, Said et al. 2017). Occurrence of flow reversal causes the cooled plumes to move across the channel and lead to mixing between the rising hot air and the reversed cold air. These factors cause a reduction in both channel inner wall temperature and flowing air temperature and consequently a decrease in the air velocity.

6.3. EFFECT OF HEAT SUPPLIED ON AXIAL VELOCITY DISTRIBUTION INSIDE THE CHANNEL

During accident scenarios and onset of natural circulation, the core channels are subjected to various radial temperature gradients as a result of the non-uniformity of heat supplied from nuclear fuel rods. Axial distribution of air velocity is found to be significantly influenced by the amount of heat supplied to the riser channel (where air flows upward). For lower heating intensities, it is found that air velocity reaches highest values close to the channel entrance, Figure 11(a). While higher heating higher air velocities are achieved at the mid-channel, Figure 15(a). The observed increase in the air velocity at the inlet is attributed to the fact that the inlet is a sharp entry without chamfers, shown in Figure 17, that can lead to turbulence and boundary layer separation near the channel inlet (Sparrow et al. 1984, Kihm et al. 1995, Habib et al. 2002, Fu et al. 2016, Said et al. 2017). For low amount of heat supplied, axial air temperature rise is found to be small (i.e., 20 ℃ from inlet to mid-channel position). The capability of this small temperature rise in moving air naturally inside the channel is not exceeding the chimney effect near the inlet. On the other hand, subjecting the riser to higher heating causes a sufficient increase in air temperature along the channel (more than 100 ℃ from inlet to mid-channel positions) that exceeds the turbulence and recirculation occurs at the inlet. The effect of heat supplied requires further investigation with measurements at additional axial locations along the heated channel with more attention to the flow and temperature fields at the region near the outlet.

6.4. EFFECT OF CHILLED WATER TEMPERATURE ON AIR TEMPERATURE AND VELOCITY INSIDE THE CHANNEL

The previously mentioned radial temperature gradients that exist during accident scenarios are mimicked in the current study by varying the outer surface temperature of the experimental setup components (i.e., upper plenum and cooled channel) by controlling the chilled water temperature circulated between the external chiller and experimental setup. As mentioned earlier, four chilled water temperatures are examined typically; 5 to 35 ℃ with 10 ℃ temperature increment. Temperature and velocity radial distributions for the selected axial positions at different heating intensities for these chilled water temperatures are shown in Figure 11 and 16. These results reveal that same temperature and velocity radial distribution trends are obtained for all chilled water temperatures. Increasing chilled water temperature causes an increase in air temperature near the heated channel outlet Figure 13(b). While no significant variation is observed at inlet and mid-channel positions, Figure 11(b)-12(b),14(b)-15(b). Air temperature variation is amplified with increasing the amount of heat supplied to the riser channel Figure 16(b). The magnitude of air temperature change is assessed by calculating the ratio between the change in radially averaged air temperature and the averaged surface temperature obtained for the two limits of chilled water temperature (i.e., 35℃ (T1) and 5℃ (T2)) according to the following formula;

$$\%\ \text{Temperature change} = \frac{\overline{T_{f_{\iota,T1}}} - \overline{T_{f_{\iota,T2}}}}{\bar{T}_{s,i,T1T2}} * 100 \tag{7}$$

where radially averaged air temperature is calculated as follows

$$\overline{\mathrm{T_{f_{\iota,T}}}} = \frac{1}{\mathrm{n}} \sum_{\mathrm{j=0.0}}^{\mathrm{j=n}} \mathrm{T_{f_{ij,T}}} \tag{8}$$

$$T_{f_{ij,T}} = \frac{1}{N}\sum_{k=0.0}^{k=N} T_{f_{ijk,T}} \quad (9)$$

$$\overline{T}_{s,i,T1T2} = \frac{T_{s,i,T1} + T_{s,i,T2}}{2} \quad (10)$$

$$T_{s_{i,T}} = \frac{1}{N}\sum_{k=0.0}^{k=N} T_{s_{ik,T}} \quad (11)$$

where n is the total number of radial position from the wall to the centerline of the channel, N is total number of samples obtained during the sampling time, and i and j are indices refer to the axial and radial positions, respectively. The index k refers to the sampling time. While T refers to chilled water temperature (i.e., experiments operational condition of cooling intensity). $T_{f_{ij,T}}$ is the time-averaged fluid temperature (i.e., air temperature) and $\overline{T_{f_{i,T}}}$ is the radially-averaged air temperature for each axial position i. $T_{s,i,T1}$ and $T_{s,i,T2}$ indicates to inner wall surface temperature at axial position (i) for different chilled water temperatures (i.e., T1 and T2). $\overline{T}_{s,i,T1T2}$ represents the inner wall mean temperature for different chilled water temperatures and $T_{s_{i,T}}$ is the time-averaged inner wall surface temperature at axial position (i) for certain cooling intensity (T). By following these calculations, the maximum air temperature increase obtained by increasing chilled water temperature from 5 to 35 ℃ and is found to occur at channel outlet, as listed in Table 2.

On the other hand, it is found that air velocity values are inversely proportional to the chilled water temperature. This is attributed to that decreasing chilled water temperature at certain heating supplied will increase the driving force (i.e., density difference) between the two channels of the natural circulation loop. Hence, natural circulation intensity which is represented by air velocity in the heated channel will be increased. Air velocity acceleration is evaluated by comparing local time-averaged air velocities (ν) obtained at

each axial and radial position (i and j) for the two limits of chilled water temperature (i.e., 35℃ (T1) and 5℃ (T2)) with respect to the air velocity at 35 °C as follows.

$$\% \text{ velocity acceleration} = \frac{\nu_{ij,T1} - \nu_{ij,T2}}{\nu_{ij,T1}} * 100 \quad (12)$$

As listed in Table 3, the velocity acceleration is significantly changed by changing the chilled water temperature and increasing the amount of heat supplied especially near the channel outlet (z/L = 0.96). This observation implies the flow is sensitive to radial temperature gradients within the PMRs core channels.

7. REMARKS

The effect of degree of cooling (i.e., chilled water temperature) on air velocity and temperature fields in three distinct regions in the heated regions was investigated. These results provide for the first-time detailed velocity and temperature variation which can be used for validating CFD codes. The key findings can be summarized as follows:

- Radial temperature gradients that exist within the PMRs core during accident scenarios as a result of the non-uniformity of the heat supplied from the nuclear rods were mimicked experimentally in the current study by controlling the heating and cooling subjected to the experimental setup components (i.e., upper plenum and two channels).
- Inner wall surface temperature is found to increase from the leading edge of the channel to z/L = 0.8 where and inflection point is observed.
- The inflection is attributed to end losses, that are represented by conjugate heat conduction through the channels material itself and the cold upper plenum, and the

interaction between the hot air rising inside the heated channel and the upper plenum mixed cold air plumes near the channel outlet.

- For inlet and mid-channel positions, air temperature is found to decrease from the inner wall towards centerline of the channel. While air velocity starts from zero at channel wall and increases towards the channel centerline.
- There is a noticeable peak in the velocity value observed near the inner wall of the channel. The location and gradient of this peak seems to be dependent on the axial location and the amount of heat supplied.
- Air temperature and velocity were found to be highly sensitive to chilled water temperature (outer surface temperature of upper plenum and down-comer channel) change near the channel outlet.
- While the results presented here are good start, it seems additional studies are needed to further validate test results and findings.

The current results provide detailed velocity and temperature variations for two channels and tow plena scaled down test facility which can be useful for validating CFD codes.

Table 1. Comparison between the common materials used for fabricating the wire sensor

Material	**Properties**
Tungsten	• Mechanically strong • High temperature coefficient of resistance (0.004/℃) • Poor resistance to oxidation at high temperatures in many gases • Most popular
Platinum	• Good oxidation resistance • Good temperature coefficient of resistance (0.003/℃) • High cost

Table 2. Percent change of flowing air temperature (equation 7) between chilled water limits (35 ^{o}C (T1) and 5 ^{o}C (T2))

Axial position	**Low heating (860 w/m^2)**	**High heating (2290 w/m^2)**
Outlet (z/L = 0.96)	12.4%	6.4%
Mid-channel (z/L = 0.59)	1.4%	1.4%
Inlet (z/L = 0.04)	0.5%	0.4%

Table 3. Percent acceleration in velocity (equation 12) between chilled water limits (35 ^{o}C (T1) and 5 ^{o}C (T2))

Axial position	**Low heating (860 w/m^2)**	**High heating (2290 w/m^2)**
Outlet (z/L = 0.96)	30%	45%
Mid-channel (z/L = 0.59)	25%	21%
Inlet (z/L = 0.04)	10%	7%

(a) **(b)**

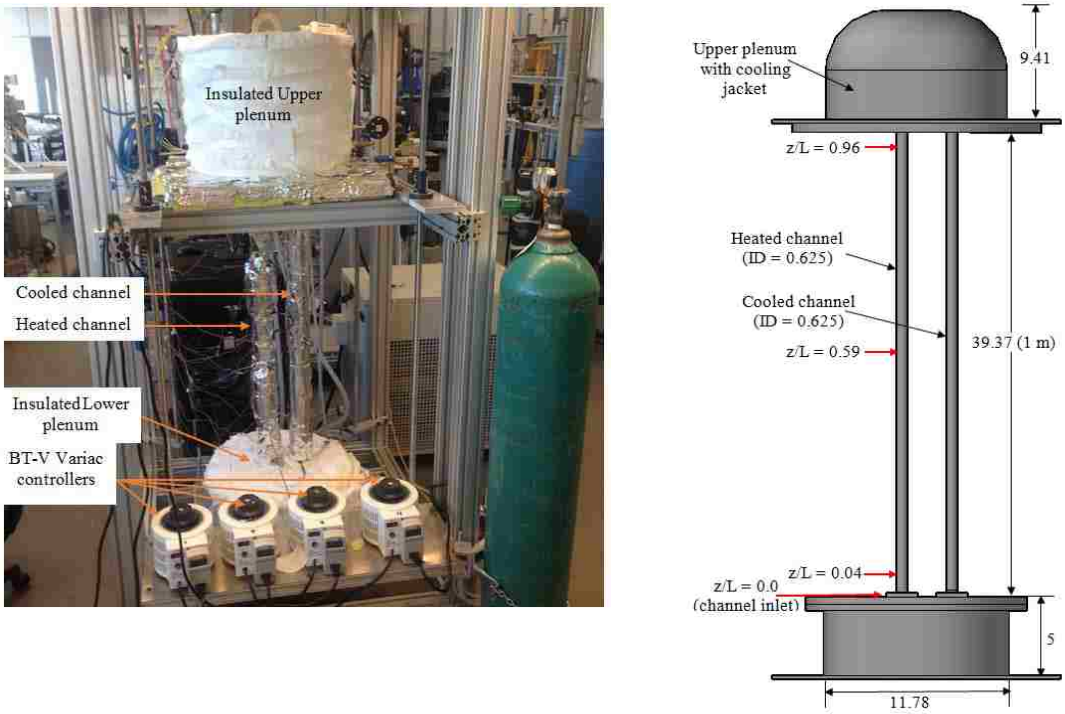

Figure 1. Missouri S&T dual channel test facility (a) Pictorial representation and (b) Schematic diagram with all dimensions in inches

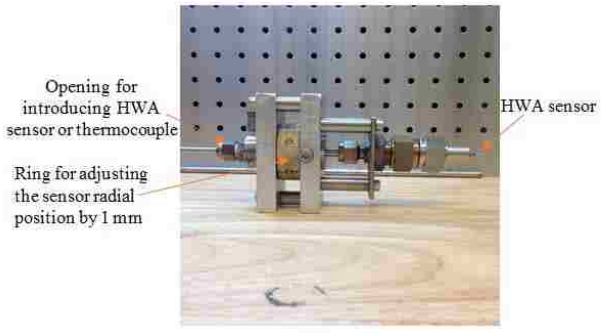

Figure 2. Mechanical part designed to allow the radial movement of the thermocouple and the HWA sensor by 1 mm interval

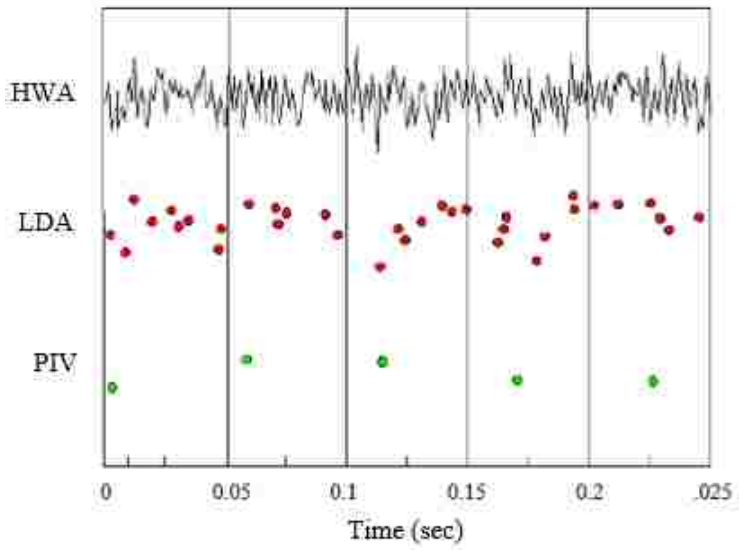

Figure 3. Representation of HWA, LDA, and PIV output signals

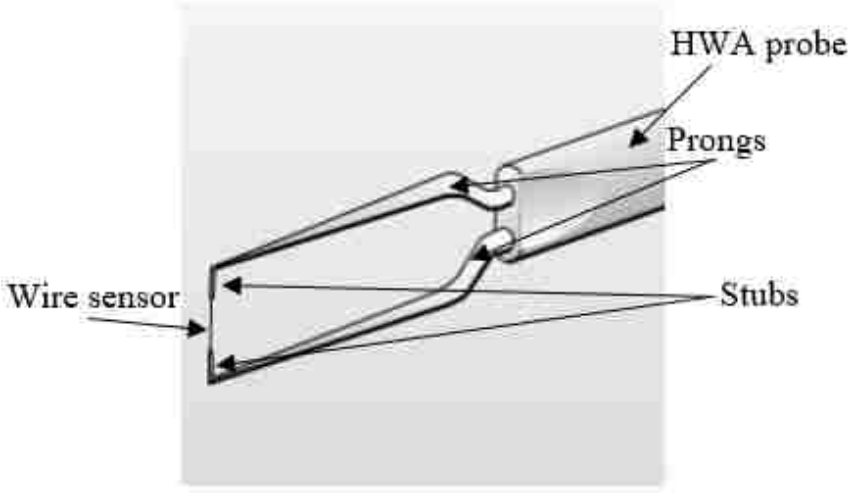

Figure 4. HWA sensor components

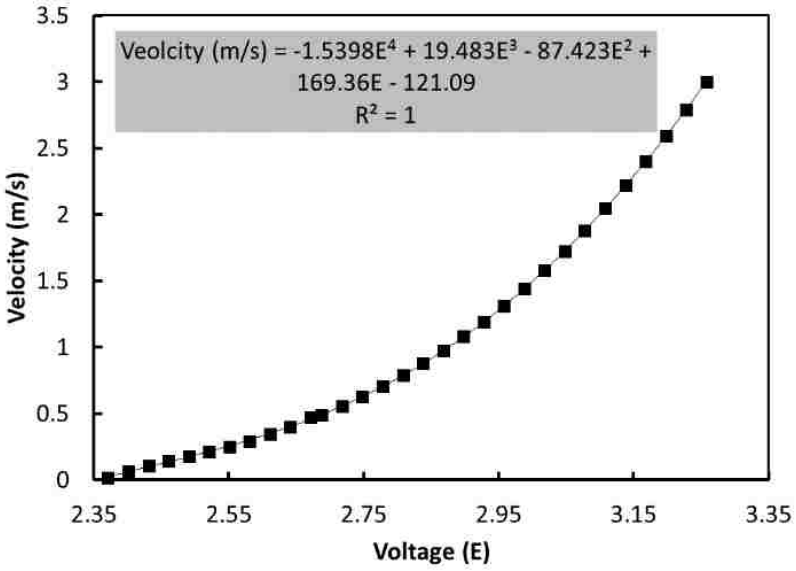

Figure 5. Sample result of HWA velocity-voltage calibration relationship

(a) **(b)**

Figure 6. Components of HWA data acquisition system (a) MiniCTA, (b) Automatic calibrator

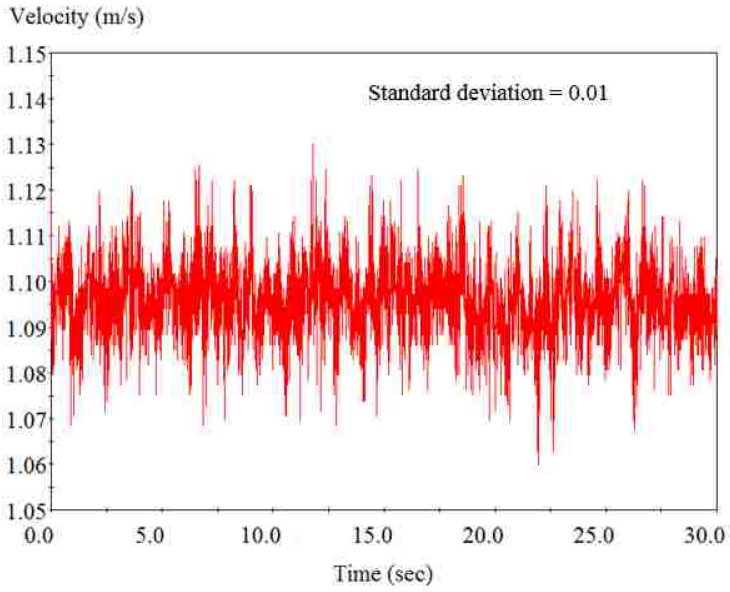

Figure 7. Sample results of velocity time series data

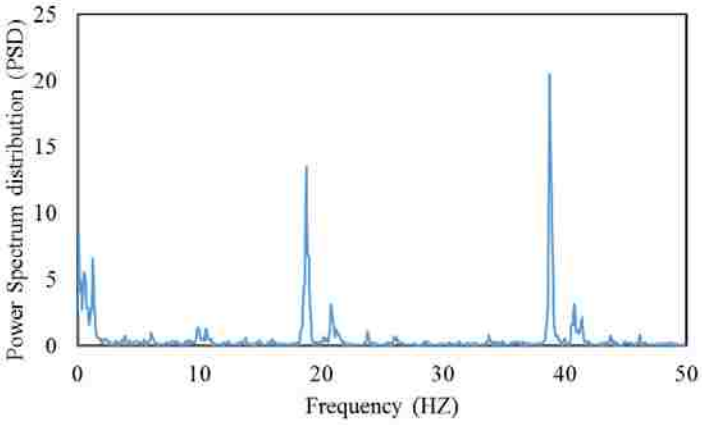

Figure 8. Sample results of instantaneous frequency analysis

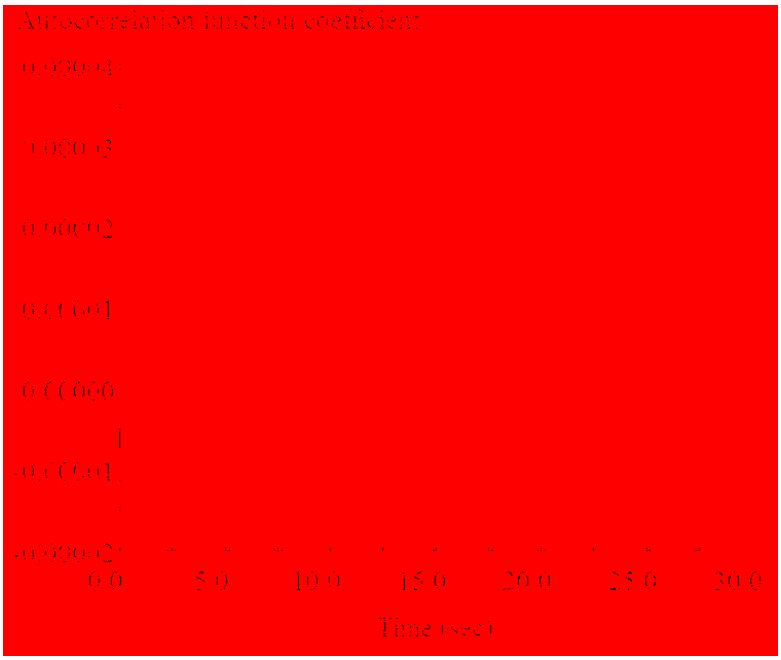

Figure 9. Sample results of obtained time series autocorrelation function coefficient

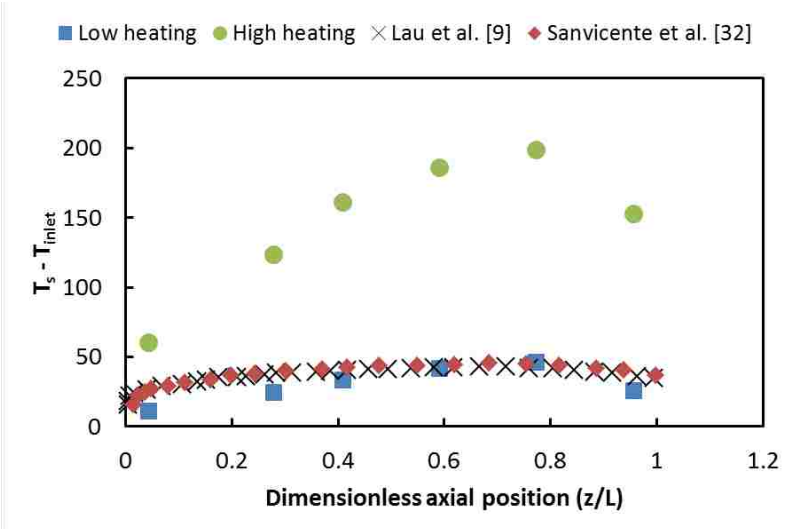

Figure 10. Axial distribution of inner wall surface temperature minus air inlet temperature to the heated channel

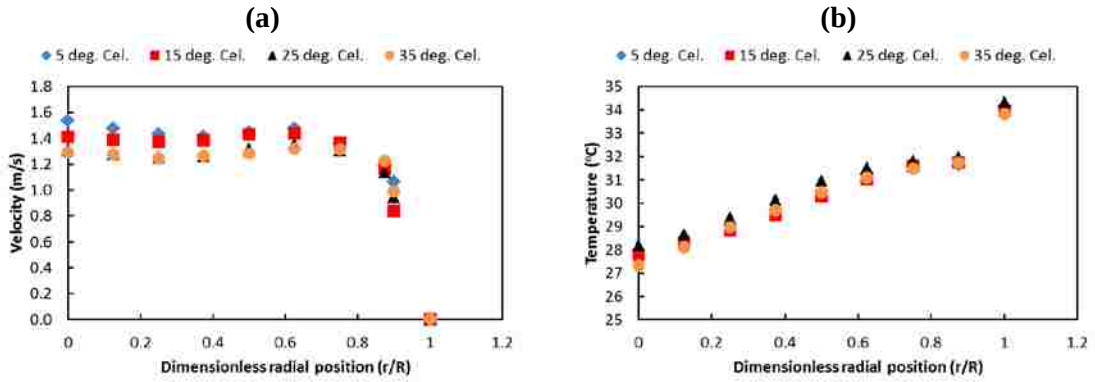

Figure 11. Radial distribution of air (a) velocity and (b) temperature at the channel inlet (z/L = 0.04) for four different chilled water temperatures and lower heat supplied (860 W/m^2)

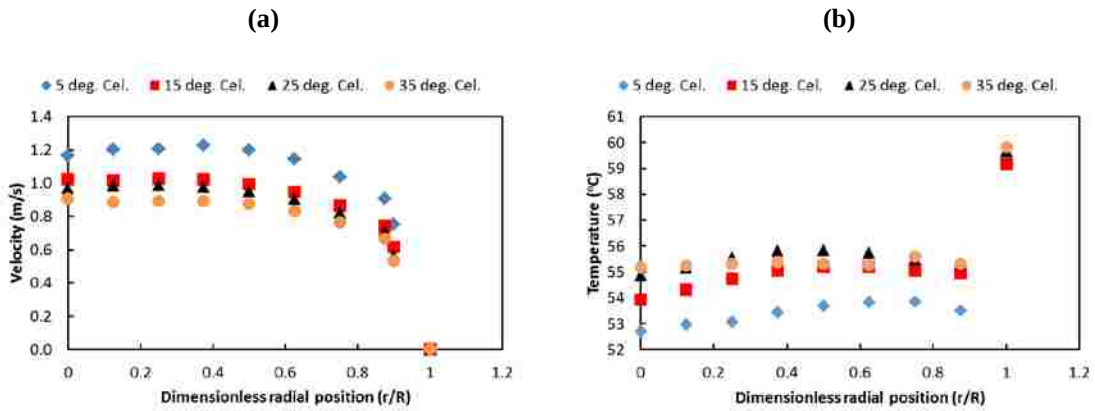

Figure 12. Radial distribution of air (a) velocity and (b) temperature at the mid-channel position (z/L = 0.95) for four different chilled water temperatures and lower heat supplied (860 W/m^2)

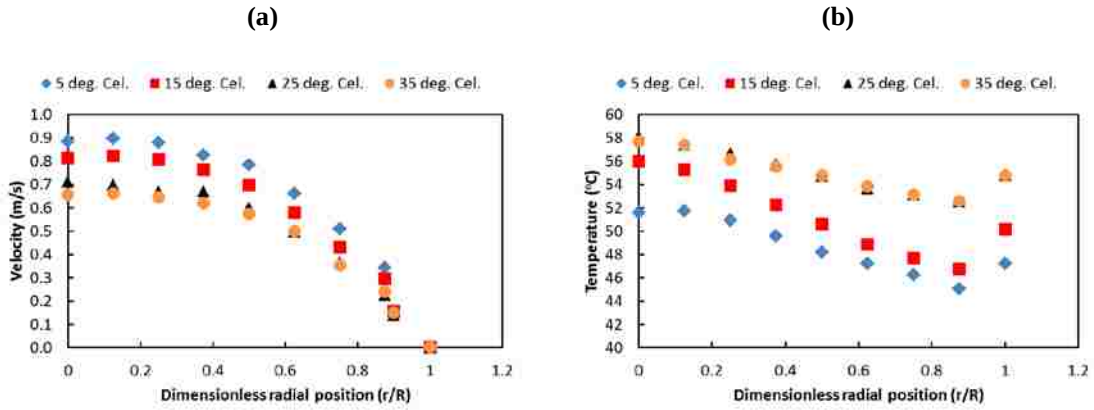

Figure 13. Radial distribution of air (a) velocity and (b) temperature at the channel outlet (z/L = 0.96) for four different chilled water temperatures and lower heat supplied (860 W/m^2)

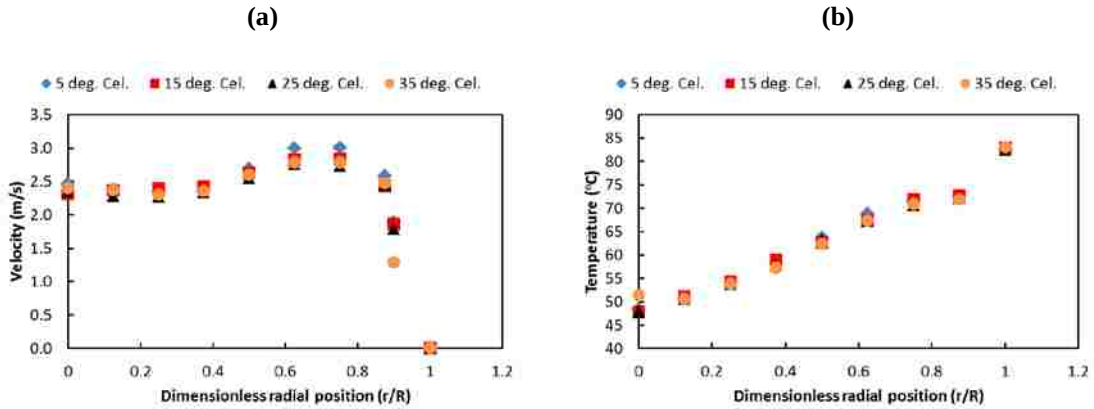

Figure 14. Radial distribution of air (a) velocity and (b) temperature at the channel inlet (z/L = 0.04) for four different chilled water temperatures and higher heat supplied (2290 W/m^2)

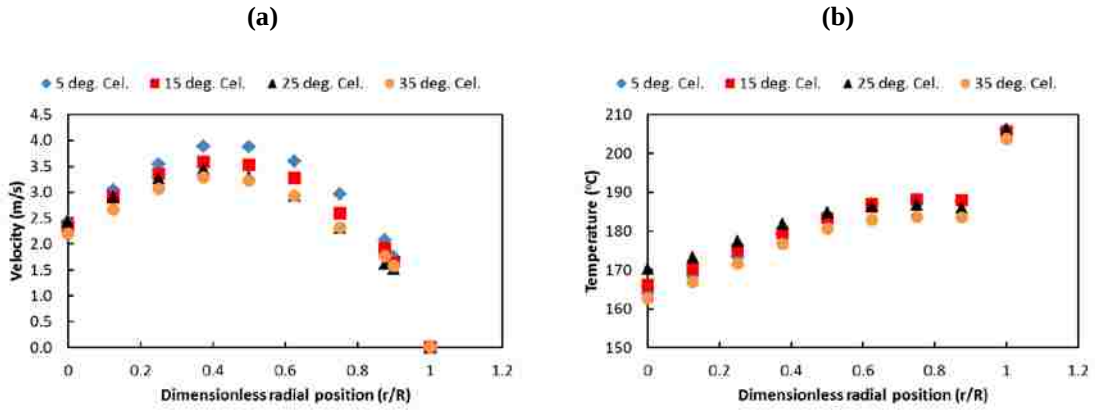

Figure 15. Radial distribution of air (a) velocity and (b) temperature at the mid-channel position (z/L = 0.95) for four different chilled water temperatures and higher heat supplied (2290 W/m^2)

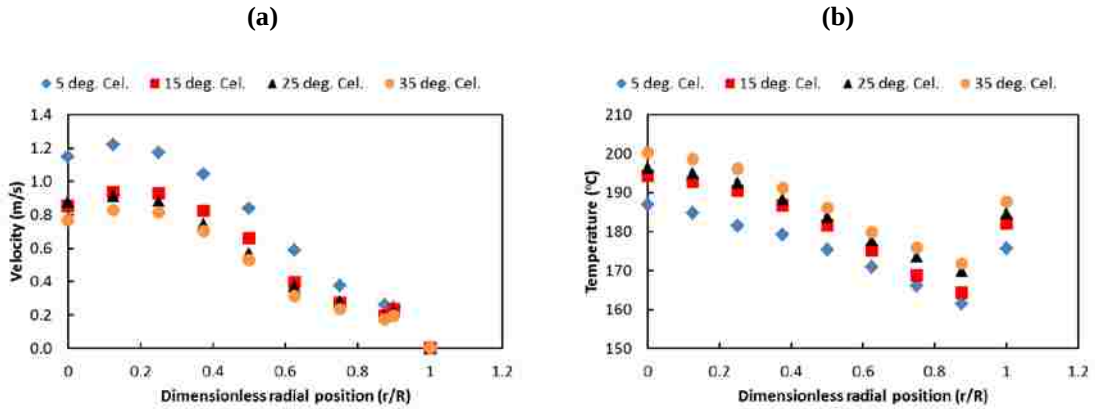

Figure 16. Radial distribution of air (a) velocity and (b) temperature at the channel outlet (z/L = 0.96) for four different chilled water temperatures and higher heat supplied (2290 W/m^2)

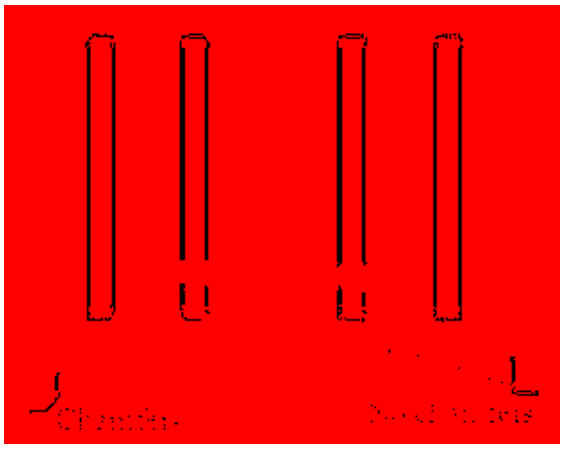

Figure 17. Schematic diagram showing the difference between channels with and without inlet chamfers

NOMENCLATURE

Symbols

A	Heat transfer area
C	Heat capacity
E	HWA output voltage
h	Heat transfer coefficient
H	Heat transferred to surrounding
I	Current supplied to the heated wire
n	Total number of radial positions
N	Total number of samples
Q	Thermal energy stored in wire
R	Resistance coefficient of the wire sensor

t	Time
T	Temperature
W	Power generated by Joule heating

Greek letters

ρ	Density
ν	Velocity

Subscript

c	Corrected value
f	Flowing air
i	Axial position
j	Radial position
k	Time series samples
o	Calibration condition
s	Inner wall surface
T	Chilled water temperature
w	Sensor wire
inlet	Air inlet to the channel
Exp	Experimental condition

Dimensionless group

z/L	Axial dimensionless position

r/R Radial dimensionless position

Abbreviations

CFD Computational fluid dynamics

CTA Constant temperature anemometry

PMRs Prismatic modular reactors

mReal Multiphase reactors engineering and applications laboratory

HWA Hot wire anemometry

LOFA Loss of flow accidents

P2P Plenum-to-plenum

DCC Depressurized conduction cooldown

OSU Oregon State University

HTTF High temperature test facility

REFERENCES

Aung, W., L. S. Fletcher and V. Sernas (1972). "Developing laminar free convection between vertical flat plates with asymmetric heating." International Journal of Heat and Mass Transfer 15(11): 2293-2308.

Ball, S. J., S. J. Ashforth-Frost, K. and C. F. Whitney (1999). "Appraisal of a hot-wire temperature compensation technique for velocity measurements in non-isothermal flows." International Journal of Heat and Mass Transfer 42(16): 3097-3102.

Bearman, P. W. (1971). "Corrections for the effect of ambient temperature drift on hot-wire measurements in incompressible flow." DISA Information 1971: 25-30.

Benjamin, S. F. and C. A. Roberts (2002). "Measuring flow velocity at elevated temperature with a hot wire anemometer calibrated in cold flow." International Journal of Heat and Mass Transfer 45(4): 703-706.

Bruun, H. H. (1995). Hot wire anemometry principles and signal analysis, Oxford University Press.

Celataa, G. P., F. Dannibale, A. Chiaradia and M. Cumo (1998). "Upflow turbulent mixed convection heat transfer in vertical pipes." International Journal of Heat and Mass Transfer 41(24): 4037-4054.

Fu, W.-S., W.-S. Chao, T.-E. Peng and C.-G. Li (2016). "Flow downward penetration of vertical parallel plates natural convection with an asymmetrically heated wall." International Communications in Heat and Mass Transfer 74: 55-62.

Habib, M. A., S. A. M. Said, S. A. Ahmed and A. Asghar (2002). "Velocity characteristics of turbulent natural convection in symmetrically and asymmetrically heated vertical channels." Experimental Thermal and Fluid Science 26(1): 77-87.

Hernández, J. and B. Zamora (2005). "Effects of variable properties and non-uniform heating on natural convection flows in vertical channels." International Journal of Heat and Mass Transfer 48(3-4): 793-807.

Hess, C. F. and C. W. Miller (1979). "Natural convection in a vertical cylinder subject to constant heat flux." International Journal of Heat and Mass Transfer 22(3): 421-430.

Jackson, R. B., E. Smith and B. G. Woods (2009). FLUENT modeling for heat transfer in upper plenum of VHTR. Transactions of the American Nuclear Society.

Jensen, K. D. (2004). "Flow measurements." Journal of the Brazilian Society of Mechanical Sciences and Engineering 26: 400-419.

Kao, M. T., P. Jain, S. Usman, I. A. Said, M. M. Taha, M. H. Al-Dahhan and Rizwan-Uddin (2015). Investigation of plenum-to-plenum heat transfer and gas dynamics under natural circulation in a scaled-down dual channel module mimicking prismatic VHTR core using CFD. International Topical Meeting on Nuclear Reactor Thermal Hydraulics 2015, NURETH 2015, American Nuclear Society.

Kihm, K. D., J. H. Kim and L. S. Fletcher (1995). "Onset of flow reversal and penetration lengths of natural convective flow between isothermal vertical walls." Journal of Heat Transfer 117(3): 776-779.

Kim, M.-H. and H.-S. Lim (2011). "Evaluation of the influence of bypass flow gap distribution on the core hot spot in a prismatic VHTR core." Nuclear Engineering and Design 241(8): 3076-3085.

King, L. V. (1914). On the convection of heat from small cylinders in a stream of fluid: determination of the convection constants of small Platinum wires, with applications to hot-wire anemometry. Philosophical Transactions of the Royal Society of London. Series A, Containing Papers of a Mathematical or Physical Character.

Lau, G. E., V. Timchenko, C. Menezo, S. Giroux-Julien, M. Fossa, E. Sanvicente, J. A. Reizes and G. H. Yeoh (2012). "Numerical and Experimental Investigation of Unsteady Natural Convection in a Vertical Open-Ended Channel." Computational Thermal Sciences 4(5): 443-456.

Lee, J. H., S. J. Yoon, E. S. Kim and G. C. Park (2014). "CFD analysis and assessment for cross-flow phenomena in VHTR prismatic core." Heat Transfer Engineering 35(11-12): 1152-1160.

Lomas, C. G. (1986). Fundamentals of hot wire anemometry, Cambridge University Press.

McVay, K. L., J.-H. Park, S. Lee, Y. A. Hassan and N. K. Anand (2015). "Preliminary tests of particle image velocimetry for the upper plenum of a scaled model of a very high temperature gas cooled reactor." Progress in Nuclear Energy 83: 305-317.

Mohammed, H. A. and Y. K. Salman (2007). "Heat transfer by natural convection from a uniformly heated vertical circular pipe with different entry restriction configurations." Energy Conversion and Management 48(7): 2244-2253.

Özahi, E. and M. Ö. Çarpınlıoğlu, Gündoğdu, M. Y. (2010). "Simple methods for low speed calibration of hot-wire anemometers." Flow Measurement and Instrumentation 21(2): 166-170.

Papanicolaou, E. and V. Belessiotis (2002). "Transient natural convection in a cylindrical enclosure at high Rayleigh numbers." International Journal of Heat and Mass Transfer 45(7): 1425-1444.

Sabharwall, P., T. Marshall, K. Weaver and H. Gougar (2007). CFD Analysis for Flow Behavior Characteristics in the Upper Plenum during low flow/low pressure transients for the Gas Cooled Fast Reactor (GCFR), Idaho National Laboratory (INL).

Said, I. A., M. M. Taha, U. Shoaib, B. G. Woods and M. H. Al-Dahhan (2017). "Investigation of Natural Convection Heat Transfer in a Unique Scaled-Down Dual-Channel Facility." AICHE Journal 63(1): 387-396.

Sanvicente, E., S. Giroux-Julien, C. Ménézo and H. Bouia (2013). "Transitional natural convection flow and heat transfer in an open channel." International Journal of Thermal Sciences 63: 87-104.

Schena, E., C. Massaroni, P. Saccomandi and S. Cecchini (2015). "Flow measurement in mechanical ventilation: A review." Medical Engineering and Physics 37(3): 257-264.

Shibahara, M., T. Takata and A. Yamaguchi (2013). "Numerical study on thermal stratification phenomena in upper plenum of LMFBR “MONJU”." Nuclear Engineering and Design 258: 226-234.

Sklar, B. (2001). Digital communications fundamentals and applications, Prentice Hall.

Sparrow, E. M., G. M. Chrysler and L. F. Azevedo (1984). "Observed flow reversals and measured-predicted Nusselt numbers for natural convection in one-sided heated vertical channel." Journal of Heat Transfer 106(2): 325-332.

Tak, N.-i., M.-H. Kim and W. J. Lee (2008). "Numerical investigation of a heat transfer within the prismatic fuel assembly of a very high temperature reactor." Annals of Nuclear Energy 35(10): 1892-1899.

Tanda, G. (1988). "Natural convection in partially heated vertical channels." Wärme- und Stoffübertragung 23(5): 307-312.

Tkachenko, O. A., V. Timchenko, S. Giroux-Julien, C. Menezo, G. H. Yeoh, J. A. Reizes, E. Sanvicente and M. Fossa (2016). "Numerical and experimental investigation of unsteady natural convection in a non-uniformly heated vertical open-ended channel." International Journal of Thermal Sciences 99: 9-25.

Van Dijk, A. and F. T. M. Nieuwstadt (2004). "The calibration of (multi-) hot-wire probes. 2. Velocity-calibration." Experiments in Fluids 36: 550-564.

Woods, B. G., R. B. Jackson, B. L. Nelson, S. R. Cadell and J. N. Reyes (2015). Scaling Analysis for the Very High Temperature Reactor Test Facility at Oregon State University. OSU-HTTF-000000-TECH-001-R0, Oregon State University.

III. BUOYANCY-DRIVEN GAS FLOW WITHIN PLENUM-TO-PLENUM FACILITY DOWN-COMER CHANNEL

ABSTRACT

Reliable measurements of thermal and velocity fields were experimentally investigated under different natural circulation intensities in a dual channel facility designed and developed with a representative geometry of prismatic modular reactor (PMR) core. Experiments were conducted under steady state conditions to obtain statistically stationary signals of temperature and velocity time series. Insignificant radial temperature variation was observed along the down-comer channel implying that the majority of supplied heat is removed through the upper plenum. Velocity results obtained emphasize the delicate nature of natural circulation phenomena in terms of flow destabilization, and recirculation penetration length. Observed air velocity distribution reveals that downward velocity is proportional to the extent of cooling applied to the setup. The calculated values of the dimensionless group Froude number (Fr) in the range of 2 to 10 indicate that air is dominated by momentum and is exiting the channel as a jet. Quantification of turbulent intensities implies that flow destabilization is noticeable along the down-comer channel particularly for the case of high cooling intensity. For 5^{o}C cooling water temperature, turbulent density ($\frac{v_{rms}}{v}$) peaks at the mid-channel (z/L = 0.5) reaching a value of 0.5. This value of turbulent intensity is much higher than the inlet (z/L = 0.96) and outlet (z/L = 0.04) turbulent intensities of 0.2 and 0.06 respectively. This destabilization is because of the flow reversal and heat conduction effects through stainless steel flanges connecting both channels. Current results provide detailed velocity and

temperature variation which can be useful for validating computational fluid dynamics (CFD) codes.

1. INTRODUCTION

In general, a heat source, a heat sink, and the pipes connecting them form a natural circulation loop (NCL) which transports heat from a source to a sink without the need for any machineries. Such systems are also called thermosiphon where fluid circulation is the result of the buoyancy forces, which in turn is the result of the density differences thermally induced by heat transport between the source and the sink under the influence of a body force field such as gravity. The absence of moving machineries makes it less susceptible to failures and thus maintenance and operating costs are reduced (Bejan 2013). Such loops are applicable to several heat exchange engineering applications such as electronic packaging and cooling systems, solar cells, and design of advanced nuclear reactors particularly for decay heat removal systems based on natural convection (Bar-Cohen et al. 1984, Kihm et al. 1995, Muresan et al. 2006, Yilmaz et al. 2007, Yilmaz et al. 2007, Pini et al. 2016, Tkachenko et al. 2016).

As a result of the nonlinear nature of natural circulation process and its low driving forces, such system is inherently unstable and subjected to oscillatory flow behavior (Vijayan 2002, Usman et al. 2017). Therefore, several experimental, numerical, and theoretical investigations have been performed and reported in the open literature concerning the stability analysis of NCLs (Mertol et al. 1981, Chen 1985, Vijayan 2002, Mousavian et al. 2004, Misale et al. 2007, Vijayan et al. 2007, Garibaldi et al. 2008, Misale et al. 2011, Cammi et al. 2016, Misale 2016). Comprehensive reviews of NCLs studies conducted and their applications have been also reported in the literature (Zvirin 1981,

Greif 1988, Vijayan et al. 1992, Misale 2016). These studies dealt with different NCLs geometries such as circular, rectangular, and toroidal loops under different flow regimes (i.e., laminar and turbulent) and different orientations of heating and cooling sources. Investigating buoyancy-driven flow inside the heat source regions of NCL (particularly vertical heated channels) started as early as 1942 by the innovative work of convective heat transfer phenomena in heated vertical channels conducted by Elenbaas (1942). Since this initiating work, there have been a number of investigations using various analytical, numerical, and experimental techniques for different heating conditions and geometries. Laminar natural convection flow in heated channels has been a subject of extensive investigations for both symmetrically and asymmetrically heating (Aung 1972, Aung et al. 1972, Dyer 1975, Martynenko et al. 1984, Sparrow et al. 1985, Cheng et al. 1988, Fujii et al. 1988). Later on, attention was directed to turbulent natural convection in vertical heated channels (Miyamoto et al. 1986) and as consequence several related works were published (Fedorov et al. 1997, Habib et al. 2002, Badr et al. 2006, Yilmaz et al. 2007, Yilmaz et al. 2007). Other natural convection associated phenomena studied include; flow destabilization and transient development (Jaluria et al. 1974, Bejan et al. 1990, Lau et al. 2012, Sanvicente et al. 2013), flow reversals (Sparrow et al. 1984, Kihm et al. 1995, Fu et al. 2016). However, to the best of authors' knowledge, no studies on natural convection along the cooled section of NCLs (i.e., down-comer channels) are reported in the open literature. Since coolant flow channels in nuclear reactors core are subjected to radial temperature gradients after the loss of flow accidents (LOFA) therefore some channels exhibit buoyancy-driven downward flow (Sabharwall et al. 2007, Said et al. 2017), thus a need for conducting studies along these channels within NCLs designed with a

representative geometry of prismatic modular reactors (PMR) core to deepen the knowledge and understanding of natural convection role in nuclear reactor's passive decay heat removal system. Designing and constructing such NCL with configuration representing the PMR core is a challenging task because of the significant effect of setup design and geometry on flow stability (Chen 1985). However, this was executed in a state-of-the-art manner by multiphase Reactors Engineering and Applications Laboratory (mReal) at Missouri S&T University (Taha et al. Under review 2017). This plenum-to-plenum facility (P2PF) was designed with two plena connected by two vertical channels to account for the PMR plena effect on flow along core channels. This study provides experimental results on natural circulation thermal hydraulics behavior within the test facility. Particularly, the effect of cooling configuration and intensity on air velocity and thermal fields inside the down-comer channel. Flow fields were characterized by implementing and integrating advanced measurement techniques including hot wire anemometry (HWA), wall flush mounted micro-foil sensors and thermocouples all working together to provide a comprehensive understanding of the phenomenon.

2. EXPERIMENTAL SETUP

A new natural circulation loop is designed with the experience gained from designing and constructing the high temperature test facility (HTTF) at Oregon State University (OSU) (Woods et al. 2015). This loop consists of two plena connected by two channels representing the PMRs core coolant channels. This design successfully demonstrates the plena effect on natural circulation inside core channels along with novel implementation of advanced measurement techniques for temperature and velocity measurements which

are missing in the open literature. A pictorial view of the experimental setup is shown in Figure 1.

The channels length (1 m ≈ 39.37 inch) is one half of the length utilized in the HTTF (2 m ≈ 78.74 inch) while channel internal diameter is kept the same as the HTTF coolant channels dimensions (0.016 m ≈ 0.625 inch). Since the HTTF core consists of 10 prismatic blocks arranged vertically (each block is 7.87 inch ≈ 20 cm of height), the current channel length accommodates only five vertical prismatic blocks. Additionally, the two plena are one quarter of the HTTF plena (Said et al. 2017, Taha et al. Under review).

The heated (riser) channel is located near the centerline of the core (x = 1.183 in or 3 cm) while the cooled (down-comer) channel is located away from the centerline (x = 3.549 in or 9 cm and y = 1.025 in or 2.6 cm) as shown in Figure 2. Selecting these locations is consistent with the radial temperature gradients occur within the core after loss of flow accidents (LOFA) in which the inner most regions are more heated than the periphery ones (Tung et al. 2011). The riser (i.e., the channel representing the heated regions of the core) is electrically heated by four 1 inch by 24 inch heavily insulated Duo-Tape electrical heaters, each with maximum capacity of 312 watts at 120 V. Each heater is connected to BT-V Variac power controller to adjust and control the amount of heat supplied from each heater separately. This allows conducting experiments under different heating intensities and axial flux shape (i.e., isoflux and non-isoflux). The heat sink region of the natural circulation loop is mimicked by circulating chiller water between an external chiller (Applied Thermal Control Ltd, K4 chiller) and cooling jacket surrounding the upper plenum and copper tubes (helical coil cooling heat exchanger) wrapping the down-comer channel (i.e., representing the less heated regions of the core). The temperature of the

chilled water can be varied by temperature controller with ±0.1℃ temperature stability built-in the chiller. To minimizing environmental interference and heat losses, the entire setup components (i.e., core channels and the two plena) are heavily insulated by ceramic fiber insulation. Detailed explanation of the experimental setup can be found elsewhere (Taha et al. Under review 2017).

3. EXPERIMENTAL WORK

3.1. EXPERIMENTS AND EXPERIMENTAL PROCEDURES

Dehumidified air is used in the current study as the gas phase. Each experiment is conducted in a batch manner in which the dehumidified air gas is compressed into the setup. Afterwards, the electrical heaters and external chiller are switched on to induce temperature difference within the setup and hence establishing natural circulation. Although the setup was constructed to withstand high pressure values up to 100 psi (Said et al. 2017, Taha et al. Under review 2017), current results represent experiments conducted at atmospheric pressure to avoid uncertain HWA measurements associated with high pressures. As natural circulation systems are susceptible to several kinds on instability (Chen 1985, Jiang et al. 2003, Cammi et al. 2016), preliminary experiments were conducted to identify the proper cooling configuration that minimize flow instabilities. Two configurations were examined with cooling is subjected to (1) both the upper plenum and the down-comer channel “configuration – 1” and (2) the upper plenum only while the down-comer channel is kept adiabatic “configuration – 2”. The capability of controlling the heat supplied from electrical heaters and chilled water temperatures enables characterizing flow behavior inside the down-comer channel under variant temperature

gradients that could exist within the prismatic core during accident scenarios. Four isoflux heating intensities ranging from 1500 to 2050 w/m^2 were investigated. The external chiller high capacity causes negligible change in the circulating chilled water temperature. Therefore, the degree of cooling can be expressed in terms of chilled water temperature. Four chilled water temperatures are examined typically; 5 to 35 ℃ with 10 ℃ temperature increments. The time needed to reach steady state varies depending on the experimental conditions and NCL geometry (Papanicolaou et al. 2002, Lau et al. 2012, Tkachenko et al. 2016). Therefore, each experiment is allowed sufficient time to reach thermal steady state conditions before recording readings of temperature and velocity in the down-comer. This steady state time is defined as the time needed for temperature measurements to be almost fixed with no observable change. Measurements were recorded three times for the first experiment repetition and then heaters and chiller were turned off, air vented and then the experiment was repeated again to obtain another three records under the same conditions for repeatability analysis.

3.2. INSTRUMENTATION

Thermal and velocity fields were characterized by implementing advanced measurement techniques that are integrated in a novel way to be used either separately or simultaneously during the experiments (Taha et al. Under review 2017, Taha et al. Under review 2017). Inner wall surface temperature (T_s) and local time-averaged air temperature (T) were measured by using micro-foil sensors that are flush mounted on the inner wall of the down-comer channel and T-type thermocouples with ±2℃ accuracy, respectively. Time series temperatures were obtained at frequencies of 0.05 kHz. Local time-averaged

air velocity was measured by using a DANTEC single component hot wire anemometry (HWA). Time series velocity measurements were collected at frequency 0.1 kHz. Both temperatures and velocity frequencies were selected to guarantee proper time series data points and sampling interval (Taha et al. Under review 2017). Since the HWA data acquisition system is a single channel (this means single HWA sensor can be used during experiment), each experiment was conducted for three locations, to obtain measurements at different axial positions along the down-comer channel namely: channel inlet (z/L = 0.96 near the top of the channel), mid-channel position (z/L = 0.5), and channel outlet (z/L = 0.04 near the bottom of the channel). For each location, experiments were repeated twice to ensure data reproducibility. Additionally, radial measurements were obtained from the inner wall (r/R = 1) to the centerline (r/R = 0.0) of the channel for each axial position by using a radial adjuster developed to allow adjusting radial measurement by 1 mm increment (Taha et al. Under review 2017). Detailed discussion of the measurement techniques implementation and raw time series obtained signals processing and analysis can be found elsewhere (Taha et al. Under review 2017).

4. RESULTS AND DISCUSSIONS

This section presents profile measurements of air temperatures and mean velocities that were obtained radially from the inner wall (r/R = 1) to the centerline (r/R = 0.0) at different axial locations along the down-comer channel (heat sink region of the circulation loop).

4.1. EFFECT OF COOLING CONFIGURATION

Preliminary experiments were conducted to compare the two cooling configurations (configuration – 1 and configuration – 2) and select the better one to be used for the rest of the experiments. Usually, NCLs are designed with a heat sink located above the heat source to promote circulation (Vijayan et al. 1994). Hence, two cooling configurations were investigated which are; (1) cooling is subjected to both the upper plenum and the down-comer channel "configuration – 1" and (2) cooling is subjected to the upper plenum only while the down-comer channel is kept adiabatic "configuration – 2".

Figure 3 and 4) show radial distribution of air temperature and mean velocity at three different axial locations for the chilled water temperature limits (i.e., 5℃ and 35℃). It was found that both temperature and velocity distributions are similar for the two configurations. However, subjecting the down-comer channel to cooling causes more reduction in temperature of air flowing inside the channel and subsequently higher downward velocity values are reported for cooling configuration (1). Small axial air temperature differences observed insides the channel for both configurations emphasize that the majority of heat supplied to the riser is removed through the upper plenum. This can be confirmed by radially averaged air temperatures at the top locations of both channels (outlet of the riser channel '$T_{avg,h}$' and inlet to the down-comer channel '$T_{avg,c}$') listed in Table 1. It is worth mentioning that air temperature at the exit of the riser channel is obtained from previous relevant study (Taha et al. Under review).

It is known that natural circulation phenomenon has a delicate nature, and time needed to reach circulation steady state is not only function of experimental conditions but loop geometrical conditions as well (i.e., geometry, cooling configuration, etc.). By

mentoring air temperatures change with time, it is found that cooling the upper plenum and channel simultaneously (configuration – 1) requires approximately 3 hours to reach thermal steady state while keeping the down-comer adiabatic (configuration – 2) increases system instabilities and thus 6 hours are needed to reach steady state conditions. Thus from experimental feasibility point of view and to avoid protracted experiments duration, cooling configuration (1) is preferred to be used for the remaining experiments.

4.2. TEMPERATURE CHARACTERIZATION

Figure 5 shows air temperature radial distribution at different axial positions along the down-comer channel. The reported radial temperature change is not noticeable except at channel both ends at 5℃ chilled water temperature. For intense cooling (i.e., 5℃ chilled water temperature), air temperature is found to slightly decrease towards the centerline of the channel (r/R = 0.0) at both ends of the channel. This higher temperature near the channel wall is attributed to the heat transfer by conduction through the stainless-steel O-ring plate, connecting the plena and channels, between heated and cooled regions as shown in Figure 6.

The effect of the heat transfer by conduction through the stainless-steel plate between both channels is presented by measuring air temperature axially along the down-comer channel at different chilled water temperatures as shown in Figure 7. Ideally, it is expected that the air temperature will continuously decrease as air moves downwards inside the channel subjected to uniform cooling. This trend of temperature distribution is observed only at low degree of cooling (higher chilled water temperature = 35℃). However, increasing cooling intensity (decreasing chilled water temperature) causes a noticeable

reduction in air temperature at the mid-channel position until it becomes less than air temperatures at down-comer outlet at the bottom that is affected by heat transfer by conduction through lower plenum stainless-steel flange. On the other hand, the reported mean velocity of air at different axial positions does not show such variations with changing chilled water temperature. Detailed illustration of mean velocity axial distribution is discussed in the following section.

4.3. VELOCITY CHARACTERIZATION

Natural circulation downward flow fields along the down-comer channel is shown in Figure 8. For all axial locations, the downward mean velocity values are proportional to the degree of cooling (inverse with chilled water temperature). As chilled water temperature decrease, air becomes denser and is accelerated in the downward direction along the down-comer channel.

At both ends of the channel, the mean velocity radial distribution can be divided into two regions: one region near the wall (r/R=1) of the channel in which the velocity approaches zero at the wall as a result of the wall shear stress and then increases with distance towards the radial positon at r/R ≅ 0.6. The second region lasts from the radial position r/R ≅ 0.5 towards the centerline of the channel (r/R = 0.0) in which there is no significant variation in the radial distribution of the temporal mean velocity. This radial distribution is consistent with the air temperature radial distribution that shows insignificant radial variation as mentioned earlier in Figure 5. Further explanation of the observed mean velocity and data repeatability analysis for these positions is discussed below.

For the mid-channel position (z/L = 0.5), the observed mean velocity values near the wall (from r/R = 1 to 0.6) are small (i.e., approaches zero). This small net mean velocity value indicates bidirectional air flow (i.e., flow reversal) in the midsection of the channel near the wall. As shown earlier in Figure 7, air temperature is found to decrease from the channel inlet to the mid-channel position and then increases (or almost remains constant) beyond mid-channel to the outlet. Thus certainly, near the wall air flows downwards from the top to the mid-channel position however there are air plumes that move upward from the bottom to the mid-channel position near the wall. Since the HWA with one sensor is only recording net velocity, hence the mean velocity close to the wall in the midsection channel approaches zero. Therefore, bidirectional flow exits and causes recirculation of air plumes inside the channel and it is concluded that the penetration length of recirculation can approach the mid-channel position of the channel. This bidirectional flow would lead to apparent flow stagnation and high turbulence as discussed later in the paper.

Sample results of air mean velocity radial distribution along the down-comer channel axis is presented for 35℃ chilled water temperature in Figure 9. It is worth mentioning that the mean velocity radial and axial distribution are not strongly influenced by degree of cooling (same trends are observed for other chilled water temperatures). However, the plena effect seems to highly affecting flow at both ends of the channel. Ideally, the mean velocity is expected to continuously increase as air flows downward inside the channel as a result of subjecting the channel to continuous cooling. In the current study, it is found that observed mean velocity at both ends exhibits higher values than the reported values at the mid-channel position. This increase in reported mean velocity is attributed to the interaction between air flow inside the channel and mixed air plumes in both plena and

heat conduction through stainless steel O-rings from the riser to the down-comer channel that cause jet like flow behavior at these positions. The reduced mean velocity values reported at the mid-channel position is caused by the recirculation and bidirectional air flow that occurs inside the midsection of the channel which necessitates further investigations.

4.4. REPEATABILITY, TURBULENT INTENSITIES AND FLOW DESTABILIZATION INSIDE THE CHANNEL

Each experiment was replicated twice and for each repetition three measurements of temperature and velocity were recorded to study signals stability, as shown in figure 10. Although these measurements seem to be almost superposed, there are slight discrepancies are found between the results of the twice experimental replications (Figure 11) since there is no control of external conditions and indeed natural circulation is highly sensitive to minor variation in environmental conditions. The observed oscillations in these instantaneous time series results of air mean velocity are considered statistically stationary flow signals for which simple time-averaged can be defined according to this formula (Bradshaw 2013).

$$v = \frac{1}{N} \sum_{i=0.0}^{i=N} v_i \qquad (1)$$

where v and v_i are the time-averaged and instantaneous mean velocities, respectively. The index i refers to sampling points that have maximum N numbers.

Turbulent intensities (I) indicates the level of turbulence or chaotic behavior associated with flow. They quantify for the velocity fluctuations (root mean square; rms) divided by the time-averaged flow velocity recorded at each radial position (r/R) for each

axial section (z/L). In the current study, the turbulent intensities are based on the HWA measured air mean velocities as follows.

$$v_{rms} = \left(\frac{1}{N\text{-}1} \sum_{i=0.0}^{i=N} (v_i - v)^2 \right)^{0.5} \quad (2)$$

$$I = \frac{v_{rms}}{v} \quad (3)$$

where v_{rms} indicates to the root mean square (or standard deviation) of the mean velocity results and I represents turbulent intensity.

Figure 12 shows turbulent intensities radial distribution from the inner wall (r/R = 1) to the centerline of the channel (r/R = 0.0) at channel inlet (top at z/L = 0.96). It is found that intense flow destabilization occurs in the inner wall vicinity regions. This destabilization is attributed to boundary layer separation occurs near the wall for the flow entering the down-comer channel from the upper plenum. This flow separation is caused by the non-chamfer effect at the down-comer channel entry (Lau et al. 2012, Sanvicente et al. 2013) and the interaction between upper plenum mixed plumes with downward flow through the cooled channel (McVay et al. 2015). Boundary layer separation was reported previously in the open literature for vertical heated channels with 30° and 45° entry chamfers and it denotes that sharp entry edges (no chamfer or 90° edge entry that is the same case in this study as shown in Figure 13) exhibits larger eddies and flow separation at channel inlet. It is observed that turbulent intensity increases with increasing cooling intensity (decreasing cooling water temperature) as a result of increasing the buoyancy force driving the flow downwards through the channel. As mentioned earlier, the majority of supplied heat is removed in the upper plenum and the mixed cooled air plumes there is affecting air flow inside the channel. Decreasing chilled water temperature increases air

plumes mixing intensity in the upper plenum and thus increasing the channel inlet interaction between air flow entering the down-comer channel and mixed cooled air plumes in the upper plenum that induces turbulences and flow destabilization near channel inlet at the top (z/L = 0.96) as seen by observed high turbulent intensity near wall (see figure 12).

Figure 14 shows radial distribution of turbulent intensity (I) at three axial locations along the down-comer channel at 5 and 35℃ of chilled water temperatures. It is clearly seen that turbulent intensity is maximized at the mid-height of the channel (z/L = 0.5). This observation is consistent with the previous explanation of low mean air velocity measured at this locations due to the bidirectional flow occurring with penetration length reaching the midsection of the channel. At the channel outlet (z/L = 0.04), reported turbulent intensity (I) is found to be less than that reported at upstream positions. Although flow reversal starts at this position especially in the vicinity regions to the channel inner wall flow, destabilization is found to be less noticeable than upstream position. Previously reported air mean velocity shows that maximum air flow occurs in the centerline of the channel and flow exiting the channel as almost like a jet. More characterization of flow at this position is conducted by calculating the dimensionless group Densitometric Froude number (Fr) that describes flow behavior inside open channel flow in the context of Boussinesq approximation. The Fr is calculated as follows:

$$Fr = \frac{v}{\sqrt{g \frac{\Delta T}{T_{upper}} \ell}} \tag{4}$$

where v is the radially-averaged mean velocity, g acceleration gravity, and ℓ is the characteristic length that is defined in this study as channel inner diameter, $\Delta T = T - T_{upper}$ is

the temperature difference between the radially-averaged temperature at this position (z/L = 0.04) and the bulk fluid temperature in the upper plenum T_{upper}.

High Fr values are obtained, ranging from 2 to 10, implying that flow at channel outlet is classified as fast and rapid flow, as a result the simultaneously acting of inertial and gravity forces in pushing the flow in the downward direction and this confirms the jet flow behavior at channel outlet.

5. REMARKS

In the current study, thermal and velocity fields along the down-comer channel was experimentally investigated under different natural circulation intensities using the dual-channel separate-effects test facility with a representative geometry of prismatic modular reactor core for investigating natural circulation phenomena that has been designed, developed, and tested in the Multiphase Reactors Engineering and Applications Laboratory (mReal) at Missouri S&T. Findings of the current study are summarized as follows:

- Natural circulation has a delicate nature and achieving steady state stability is dependent on setup geometrical specifications and experimental conditions.
- The majority of heat supplied through the riser channel is found to be removed by heat transfer in the upper plenum.
- Increasing cooling intensity (decreasing chilled water temperature) increases air mean velocity in the downward direction inside the channel as a result of increased air density.
- Small temperature variations have been observed radially along the down-comer channel.

- Air thermal and velocity fields at down-comer channel boundaries is affected by heat conduction through stainless steel flanges connecting both channels and interaction between mixed air plumes especially between the upper plenum and channel inlet at the top.
- High values obtained for the dimensionless group Froude number (Fr) implies that fast and rapid flow is observed at channel outlet and thus flow exiting the channel is momentum driven and acts like a jet where the maximum velocity is observed at the centerline of the channel.
- Large turbulent intensities (I) values observed at the channel mid-height (z/L = 0.5) confirm the flow reversal flow inside the channel and reveal that the penetration length could reach the mid-height of the channel.

This paper presents precise measurements of velocity and thermal fields aimed to establish universal understanding/knowledge of the natural circulation for decay heat removal system in prismatic modular reactors (PMR). The benchmark results obtained are useful for computational fluid dynamics (CFD) validation that can be reliably and widely used for better understanding of natural circulation phenomena in complex systems like Very High Temperature Reactor (VHTR).

Table 1. Radially average air temperature at riser exit ($T_{avg,h}$) (Taha et al. Under review) and down-comer inlet ($T_{avg,c}$) at 1500 w/m^2

$\mathbf{T_{chilled\ water}}$ (°C)	**5**	**15**	**25**	**35**
$\mathbf{T_{avg,h}}$ (°C)	175.76	181.78	184.69	187.49
$\mathbf{T_{avg,c}}$ (°C)	15.43	22.89	30.34	35.55

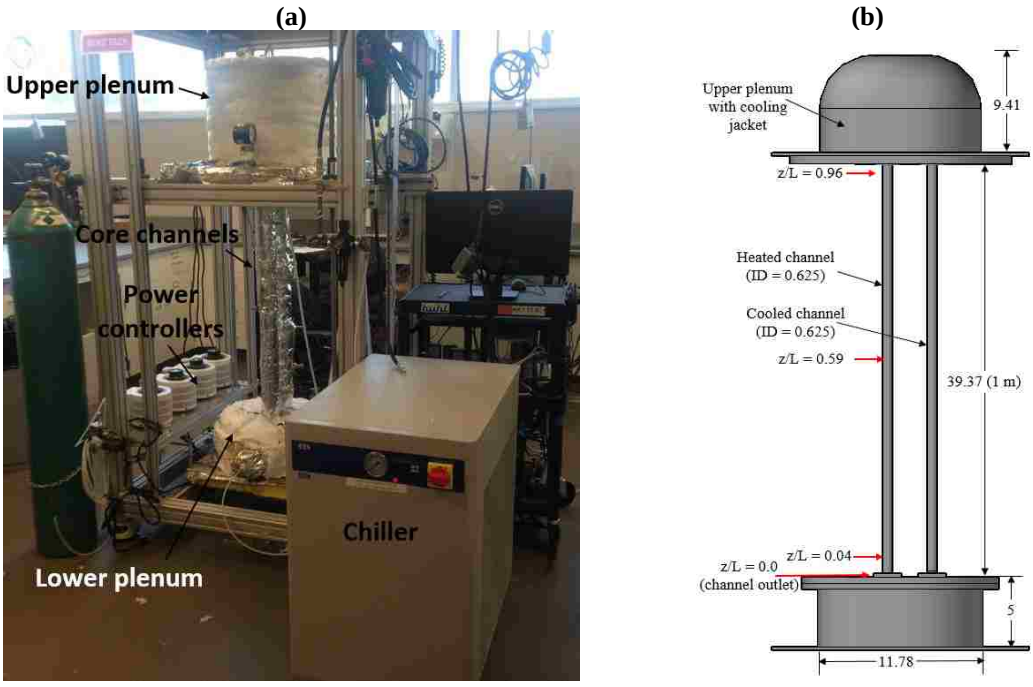

Figure 1. Plenum-to-plenum facility with two channels mimicking prismatic modular reactor (PMR) core (a) pictorial view and (b) schematic diagram

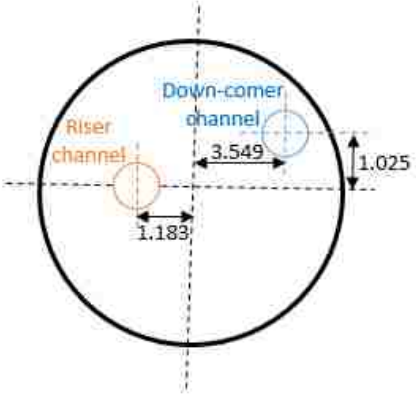

Figure 2. Schematic showing the two channels locations with respect to the center of the plena (dimensions in inches)

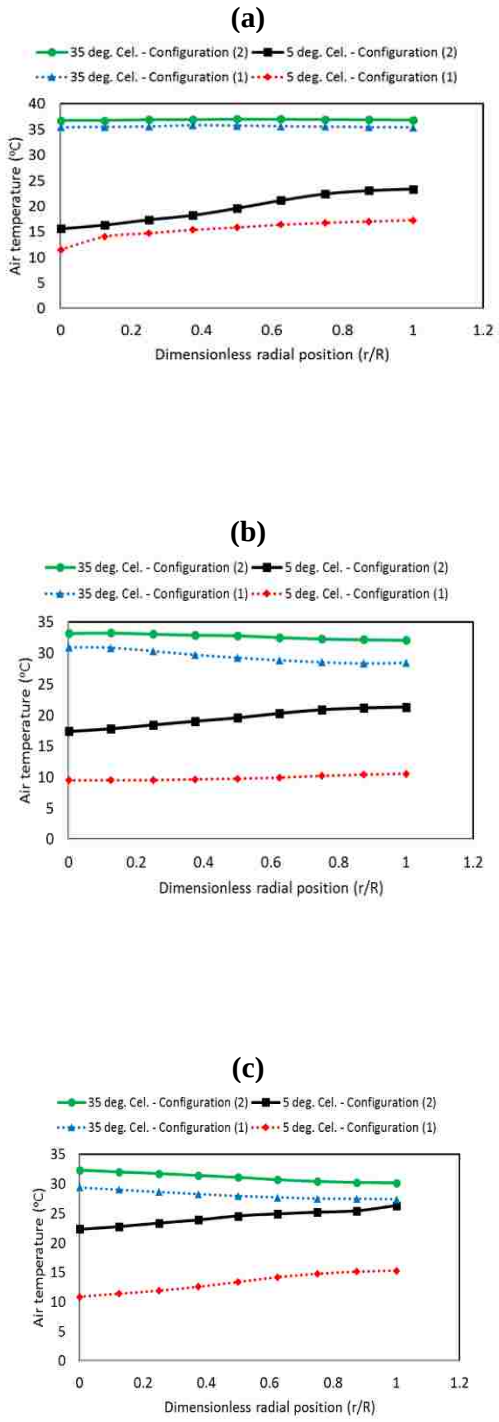

Figure 3. Radial air temperature distribution for both cooling configurations at different axial locations along the down-comer channel (a) Channel inlet (z/L = 0.96 at top), (b) Mid-channel height (z/L = 0.5), and (c) Channel outlet (z/L = 0.04 at bottom)

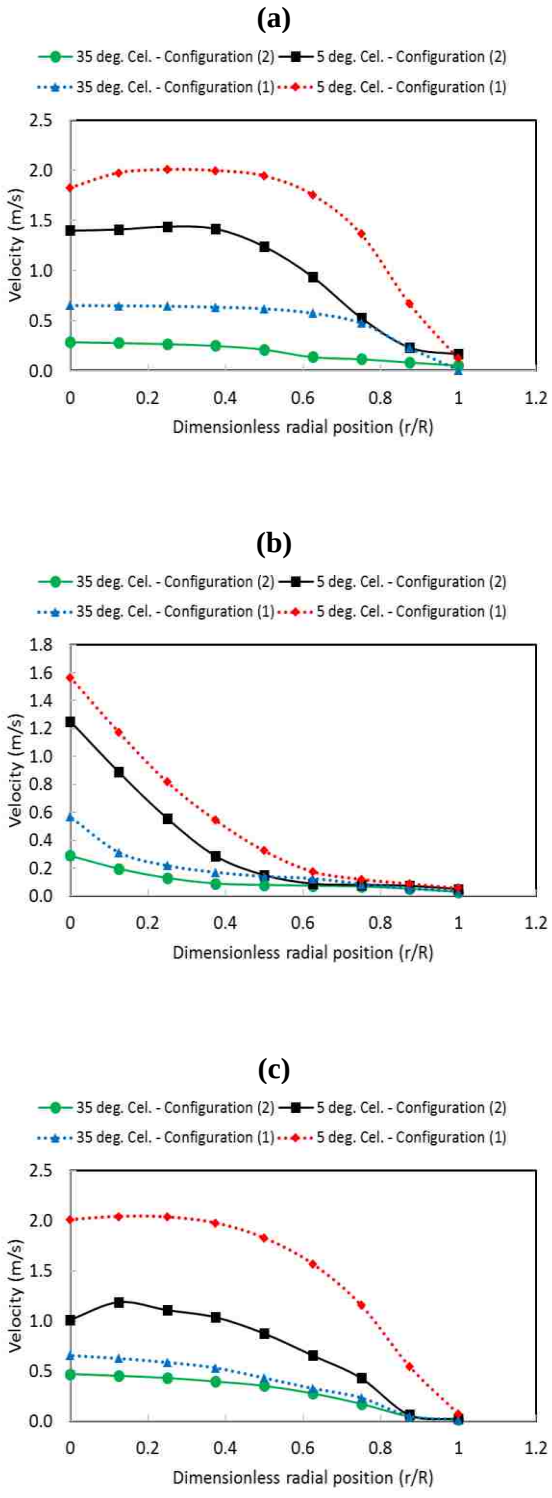

Figure 4. Radial distribution of air mean velocity for both cooling configurations at different axial locations along the down-comer channel (a) Channel inlet (z/L = 0.96 at top), (b) Mid-channel height (z/L = 0.5), and (c) Channel outlet (z/L = 0.04 at bottom)

(a)

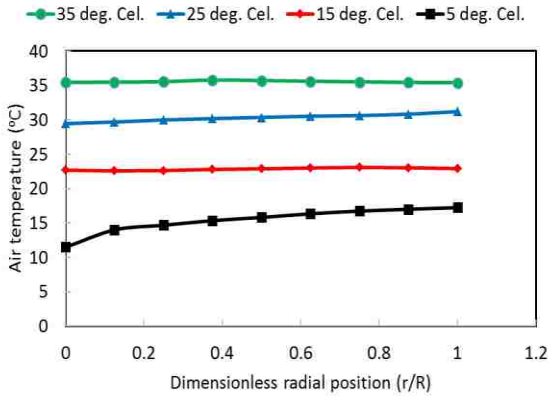

(b)

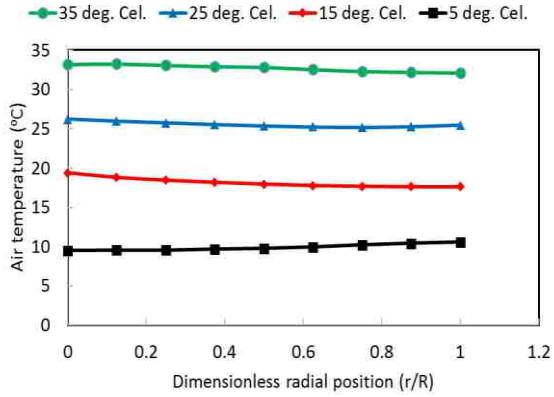

(c)

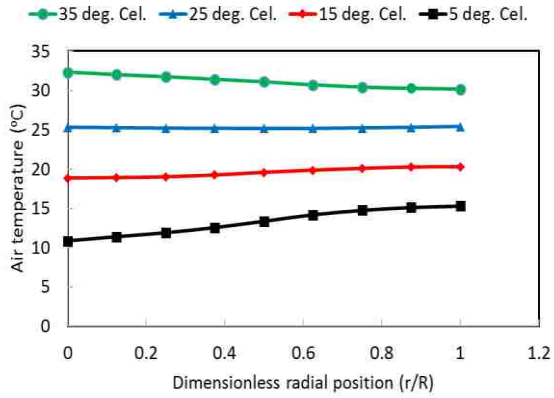

Figure 5. Radial distribution of air temperature for cooling configurations (1) at different axial locations along the down-comer channel (a) Channel inlet (z/L = 0.96 at top), (b) Mid-channel height (z/L = 0.5), and (c) Channel outlet (z/L = 0.04 at bottom)

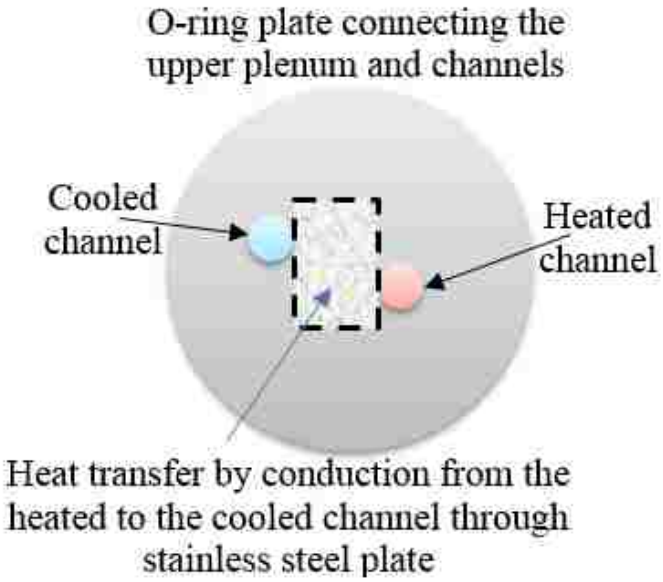

Figure 6. Top view of the channel and the stainless steel plate connecting channels ends with plena

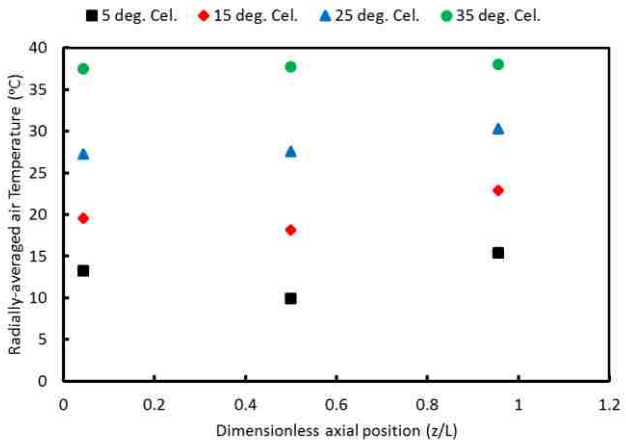

Figure 7. Axial distribution of radially averaged air temperature for cooling configurations (1) at different chilled water temperatures

(a)

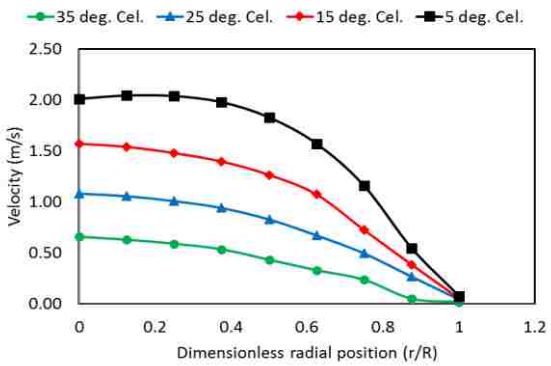

(b)

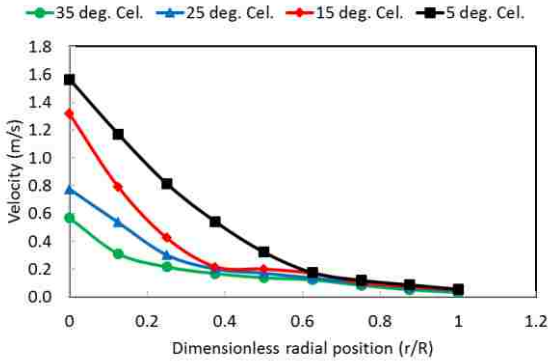

(c)

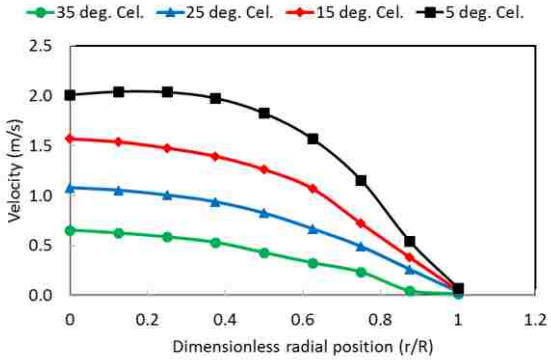

Figure 8. Radial distribution of air mean velocity for cooling configurations (1) at different axial locations along the down-comer channel (a) Channel inlet (z/L = 0.96 at top), (b) Mid-channel height (z/L = 0.5), and (c) Channel outlet (z/L = 0.04 at bottom)

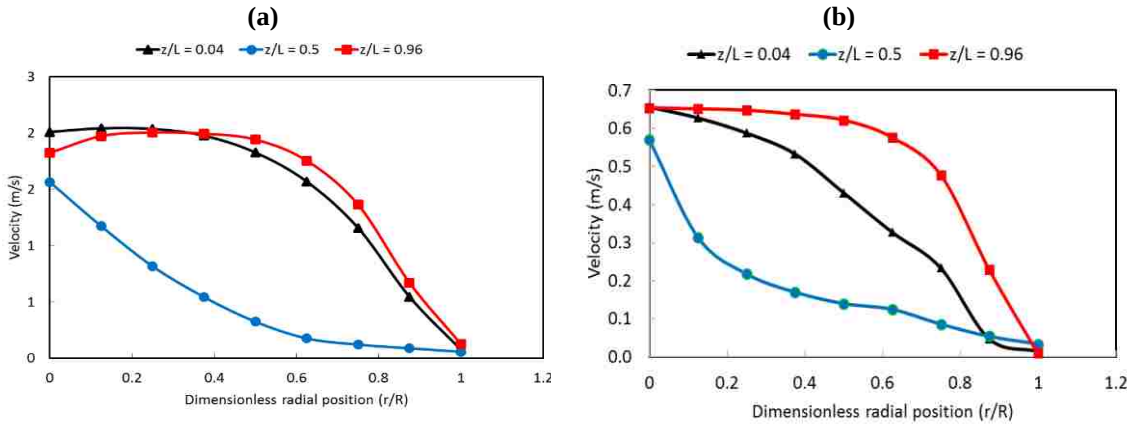

Figure 9. Radial distribution of air mean velocity along the channel axis for cooling configurations (1) at (a) 5^{o}C and (b) 35^{o}C chilled water temperatures

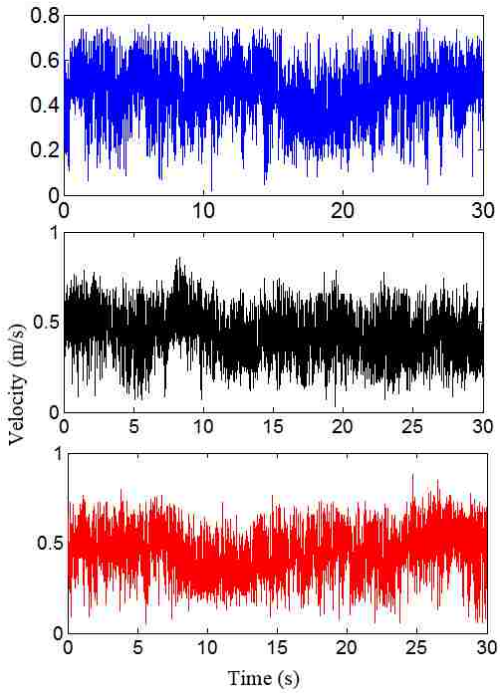

Figure 10. Sample results of time series air velocity for three measurements for single replication

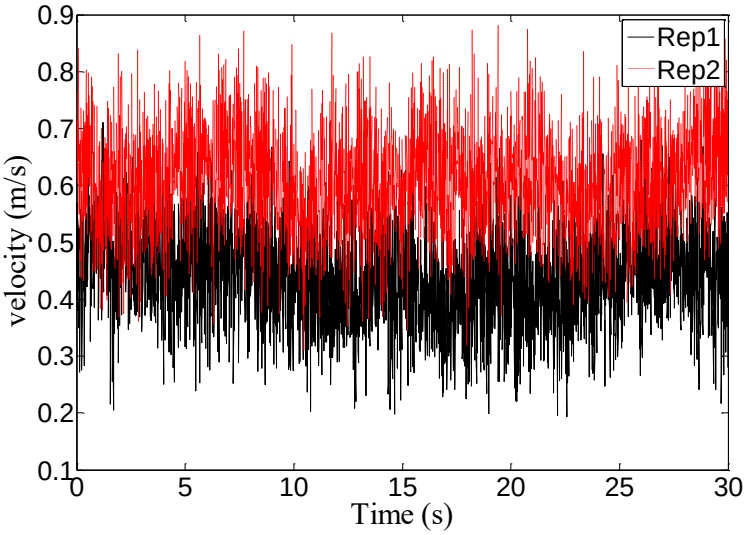

Figure 11. Comparison of average air velocity time series raw data for two different replications under same conditions

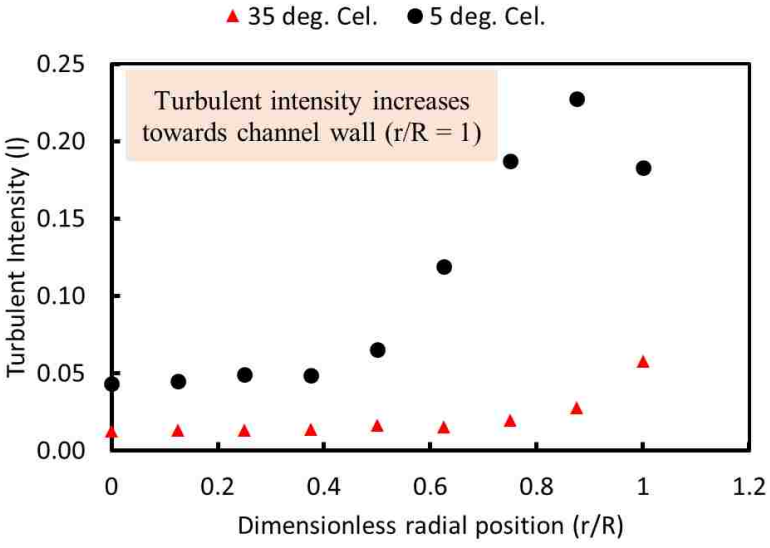

Figure 12. Turbulent intensity (I) radial distribution at channel inlet (z/L = 0.96)

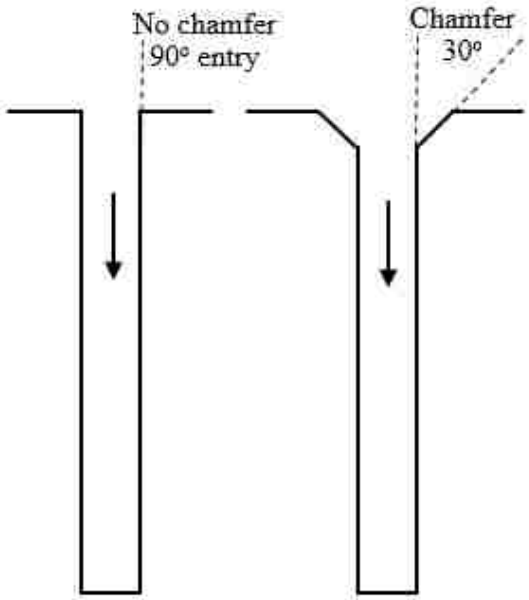

Figure 13. Schematic diagram showing down-comer channel entry with and without chamfer

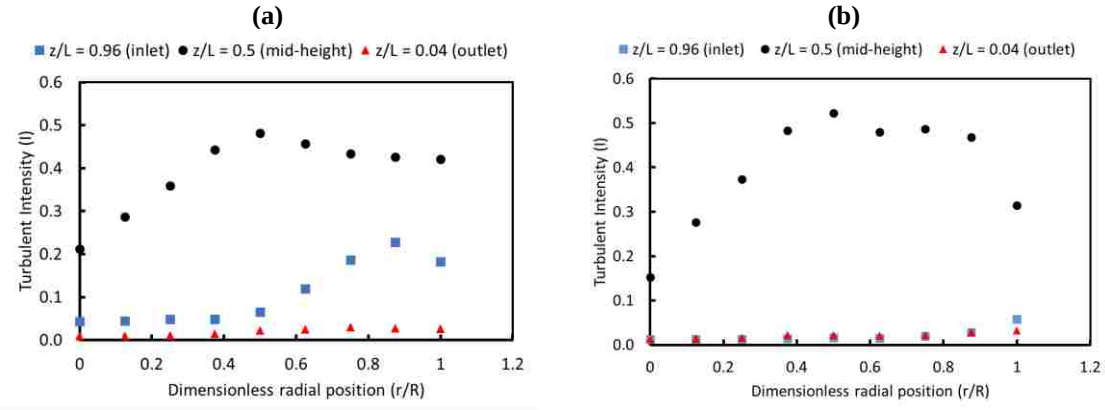

Figure 14. Turbulent intensity (I) radial distribution at different axial locations along the down-comer channel at (a) at 5 ^{o}C and (b) 35 ^{o}C chilled water temperature

NOMENCLATURE

Symbols

I	Turbulent intensity
T	Temperature
v	time-averaged mean velocity
v_i	Instantaneous mean velocity
ℓ	Characteristic length
g	Acceleration gravity

Subscript

c	Cooled channel
h	Heated channel
i	sampling point index
s	Inner wall surface
avg	average
chilled temp	Chilled water temperature
rms	root men square
upper	Upper plenum

Dimensionless group

z/L	Axial dimensionless position
r/R	Radial dimensionless position
Fr	Froude number

Abbreviations

NCLs Natural circulation loops

LOFA Loss of flow accidents

PMRs Prismatic modular reactors

HWA Hot wire anemometry

HTTF High temperature test facility

OSU Oregon state university

CFD Computational fluid dynamics

REFERENCES

Aung, W. (1972). "Fully developed laminar free convection between vertical plates heated asymmetrically." International Journal of Heat and Mass Transfer 15(8): 1577-1580.

Aung, W., L. S. Fletcher and V. Sernas (1972). "Developing laminar free convection between vertical flat plates with asymmetric heating." International Journal of Heat and Mass Transfer 15(11): 2293-2308.

Badr, H. M., M. A. Habib, S. Anwar, R. Ben-Mansour and S. A. M. Said (2006). "Turbulent natural convection in vertical parallel-plate channels." Heat and Mass Transfer/Waerme- und Stoffuebertragung 43(1): 73-84.

Bar-Cohen, A. and W. M. Rohsenow (1984). "Thermally optimum spacing of vertical, natural convection, cooled, parallel plates." Journal of Heat Transfer 106(1): 116-123.

Bejan, A. (2013). Convection Heat Transfer: Fourth Edition, John Wiley and Sons.

Bejan, A. and J. L. Lage (1990). "Prandtl number effect on the transition in natural convection along a vertical surface." Journal of Heat Transfer 112(3): 787-790.

Bradshaw, P. (2013). An introduction to turbulence and its measurement: thermodynamics and fluid mechanics series, Elsevier.

Cammi, A., L. Luzzi and A. Pini (2016). "The influence of the wall thermal inertia over a single-phase natural convection loop with internally heated fluids." Chemical Engineering Science 153: 411-433.

Chen, K. (1985). "On the oscillatory instability of closed-loop thermosyphons." Journal of Heat Transfer 107: 826-832.

Cheng, C.-H., W.-H. Huang and H.-S. Kou (1988). "Laminar free convection of the mixing flows in vertical channels." Numerical Heat Transfer 14(4): 447-463.

Dyer, J. R. (1975). "The development of laminar natural-convective flow in a vertical uniform heat flux duct." International Journal of Heat and Mass Transfer 18(12): 1455-1465.

Elenbaas, W. (1942). "Heat dissipation of parallel plates by free convection." Physica 9(1): 1-28.

Fedorov, A. G. and R. Viskanta (1997). "Turbulent natural convection heat transfer in an asymmetrically heated, vertical parallel-plate channel." International Journal of Heat and Mass Transfer 40(16): 3849-3860.

Fu, W.-S., W.-S. Chao, T.-E. Peng and C.-G. Li (2016). "Flow downward penetration of vertical parallel plates natural convection with an asymmetrically heated wall." International Communications in Heat and Mass Transfer 74: 55-62.

Fujii, T., S. Koyama and N. S. Buenconsejo (1988). "Laminar free convection flow rate in a vertical tube." International Journal of Heat and Mass Transfer 31(4): 831-841.

Garibaldi, P. and M. Misale (2008). "Experiments in Single-Phase Natural Circulation Miniloops With Different Working Fluids and Geometries." Journal of Heat Transfer 130(10): 1-5.

Greif, R. (1988). "Natural circulation loops." Journal of Heat Transfer 110: 1243-1258.

Habib, M. A., S. A. M. Said, S. A. Ahmed and A. Asghar (2002). "Velocity characteristics of turbulent natural convection in symmetrically and asymmetrically heated vertical channels." Experimental Thermal and Fluid Science 26(1): 77-87.

Jaluria, Y. and B. Gebhart (1974). "On transition mechanisms in vertical natural convection flow." Journal of Fluid Mechanics 66: 309-337.

Jiang, Y. Y. and M. Shoji (2003). "Flow stability in a natural circulation loop : influences of wall thermal conductivity." Nuclear Engineering and Design 222: 16-28.

Kihm, K. D., J. H. Kim and L. S. Fletcher (1995). "Onset of flow reversal and penetration lengths of natural convective flow between isothermal vertical walls." Journal of Heat Transfer 117(3): 776-779.

Lau, G. E., V. Timchenko, C. Menezo, S. Giroux-Julien, M. Fossa, E. Sanvicente, J. A. Reizes and G. H. Yeoh (2012). "Numerical and Experimental Investigation of Unsteady Natural Convection in a Vertical Open-Ended Channel." Computational Thermal Sciences 4(5): 443-456.

Martynenko, O. G., A. A. Berezovsky and Y. A. Sokovishin (1984). "Laminar free convection from a vertical plate." International Journal of Heat and Mass Transfer 27(6): 869-881.

McVay, K. L., J.-H. Park, S. Lee, Y. A. Hassan and N. K. Anand (2015). "Preliminary tests of particle image velocimetry for the upper plenum of a scaled model of a very high temperature gas cooled reactor." Progress in Nuclear Energy 83: 305-317.

Mertol, A., R. Greif and Y. Zvirin (1981). "The transient, steady state and stability behavior of a thermosyphon with throughflow." International Journal of Heat and Mass Transfer 24(4): 621-633.

Misale, M. (2016). "Experimental study on the influence of power steps on the thermohydraulic behavior of a natural circulation loop." International Journal of Heat and Mass Transfer 99: 782-791.

Misale, M., P. Garibaldi, J. C. Passos and G. G. de Bitencourt (2007). "Experiments in a single-phase natural circulation mini-loop." Experimental Thermal and Fluid Science 31(8): 1111-1120.

Misale, M., P. Garibaldi, L. Tarozzi and G. S. Barozzi (2011). "Influence of thermal boundary conditions on the dynamic behaviour of a rectangular single-phase natural circulation loop." International Journal of Heat and Fluid Flow 32(2): 413-423.

Miyamoto, M., Y. Katoh, J. Kurima and H. Sasaki (1986). Turbulent free convection heat transfer from vertical parallel plates in air (heat transfer characteristics). Proceedings of the 8th Internation Heat Transfer Conference.

Mousavian, S. K., M. Misale, F. D'Auria and M. A. Salehi (2004). "Transient and stability analysis in single-phase natural circulation." Annals of Nuclear Energy 31(10): 1177-1198.

Muresan, C., C. Ménézo, R. Bennacer and R. Vaillon (2006). "Numerical simulation of a vertical solar collector integrated in a building frame: Radiation and turbulent natural convection coupling." Heat Transfer Engineering 27(2): 29-42.

Papanicolaou, E. and V. Belessiotis (2002). "Transient natural convection in a cylindrical enclosure at high Rayleigh numbers." International Journal of Heat and Mass Transfer 45(7): 1425-1444.

Pini, A., A. Cammi, M. Cauzzi, F. Fanale and L. Luzzi (2016). An Experimental Facility to Investigate the Natural Circulation Dynamics in Presence of Distributed Heat Sources. Energy Procedia, The Author(s).

Sabharwall, P., T. Marshall, K. Weaver and H. Gougar (2007). CFD Analysis for Flow Behavior Characteristics in the Upper Plenum during low flow/low pressure transients for the Gas Cooled Fast Reactor (GCFR), Idaho National Laboratory (INL).

Said, I. A., M. M. Taha, U. Shoaib, B. G. Woods and M. H. Al-Dahhan (2017). "Investigation of Natural Convection Heat Transfer in a Unique Scaled-Down Dual-Channel Facility." AICHE Journal 63(1): 387-396.

Sanvicente, E., S. Giroux-Julien, C. Ménézo and H. Bouia (2013). "Transitional natural convection flow and heat transfer in an open channel." International Journal of Thermal Sciences 63: 87-104.

Sparrow, E. M. and L. F. A. Azevedo (1985). "Vertical-channel natural convection spanning between the fully-developed limit and the single-plate boundary-layer limit." International Journal of Heat and Mass Transfer 28(10): 1847-1857.

Sparrow, E. M., G. M. Chrysler and L. F. Azevedo (1984). "Observed flow reversals and measured-predicted Nusselt numbers for natural convection in one-sided heated vertical channel." Journal of Heat Transfer 106(2): 325-332.

Taha, M. M., I. A. Said, U. Shoaib and M. H. Al-Dahhan (Under review). "Investigation of natural circulation in a separate effects facility of two channels representing prismatic modular reactors (PMRs) core." International Journal of Thermal Sciences.

Taha, M. M., I. A. Said, U. Shoaib and M. H. Al-Dahhan (Under review 2017). "Investigation of natural circulation in a separate effects facility of two channels representing prismatic modular reactors (PMRs) core." International Journal of Thermal Sciences.

Taha, M. M., I. A. Said, U. Shoaib, B. G. Woods and M. H. Al-Dahhan (Under review). "Design and development of an experimental test facility with a representative geometry of prismatic block modular reactor core." Nuclear Engineering and Design.

Taha, M. M., I. A. Said, U. Shoaib, B. G. Woods and M. H. Al-Dahhan (Under review 2017). "Design and development of an experimental test facility with a representative geometry of prismatic block modular reactor core." Nuclear Engineering and Design.

Tkachenko, O. A., V. Timchenko, S. Giroux-Julien, C. Menezo, G. H. Yeoh, J. A. Reizes, E. Sanvicente and M. Fossa (2016). "Numerical and experimental investigation of unsteady natural convection in a non-uniformly heated vertical open-ended channel." International Journal of Thermal Sciences 99: 9-25.

Tung, Y. H. and R. W. Johnson (2011). CFD calculations of natural circulation in a high temperature gas reactor following pressurized circulator shutdown. ASME 2011 International Mechanical Engineering Congress and Exposition, IMECE 2011.

Usman, S. and S. Anwar (2017). Narual convection - A case of simple harmonics. ICONE 2017 - International Conference of Nuclear Engineering. China.

Vijayan, P. K. (2002). "Experimental observations on the general trends of the steady state and stability behaviour of single-phase natural circulation loops." Nuclear Engineering and Design 215(1): 139-152.

Vijayan, P. K. and H. Austregesilo (1994). "Scaling laws for single-phase natural circulation loops." Nuclear Engineering and Design 152(1-3): 331-347.

Vijayan, P. K. and A. W. Date (1992). "The limits of conditional stability for single-phase natural circulation with throughflow in a figure-of-eight loop." Nuclear Engineering and Design 136: 361-380.

Vijayan, P. K., M. Sharma and D. Saha (2007). "Steady state and stability characteristics of single-phase natural circulation in a rectangular loop with different heater and cooler orientations." Experimental Thermal and Fluid Science 31(8): 925-945.

Woods, B. G., R. B. Jackson, B. L. Nelson, S. R. Cadell and J. N. Reyes (2015). Scaling Analysis for the Very High Temperature Reactor Test Facility at Oregon State University. OSU-HTTF-000000-TECH-001-R0, Oregon State University.

Yilmaz, T. and S. M. Fraser (2007). "Turbulent natural convection in a vertical parallel-plate channel with asymmetric heating." International Journal of Heat and Mass Transfer 50: 2612-2623.

Yilmaz, T. and A. Gilchrist (2007). "Temperature and velocity field characteristics of turbulent natural convection in a vertical parallel-plate channel with asymmetric heating." Heat and Mass Transfer/Waerme- und Stoffuebertragung 43(7): 707-719.

Zvirin, Y. (1981). "A review of natural circulation loops in pressurized water reactors and other systems." Nuclear Engineering and Design 67: 203-225.

IV. NATURAL CONVECTION INSIDE HEATED CHANNEL OF A FACILITY REPRESENTING MODULAR REACTOR CORE

ABSTRACT

Thermal and velocity fields inside a separate effects dual channel facility have been investigated under different natural circulation intensities. Flow characterization inside the heated channel is illustrated by dividing the channel into three sections (i) inlet, (ii) midsection, and (iii) outlet. It is found that temperature and velocity radial profiles differ axially from one section to another. These profiles are also function of the amount of heat supplied. Atypical thermal and velocity radial profiles observed at the outlet section of the channel. This discrepancy it attributed to the temperature reduction observed at axial position (z/L = 0.8) close to the channel exit. Temperature inflection is adopted as a criterion for initiation of naturally driven flow destabilization. In the current study, amplifications of turbulent intensities (I) and local modified Rayleigh number (Ra_{mx}) were observed to coincide with the location of temperature inflection confirming the dependence of destabilization on temperature. Quantification of the overall Rayleigh number (Ra) versus overall Reynold number (Re) are found to be related by $Re\ \alpha\ Ra^{0.58}$. Upper plenum mixing was characterized by determining the modified Reynold number (Re_m) and Froude number $(1/Fr^2)$ dimensionless groups. Interaction of cooled plenum air with hot rising plumes along with turbulence amplifications strengthen the macroscopic mixing between fluid layers and subsequently causes the observed temperature drop. Therefore flow reversal of the cooled air along the channel wall occurs and consequently heat transfer reversal (i.e., fluid-to-wall) at the top section of the hot channel. Additionally, dimensional analysis and comparison of distortion factors reveal a good similarity between

the Plenum-to-Plenum Facility (P2PF) and the Modular High Temperature Gas-cooled Reactor (MHTGR). Current results provide detailed high resolution velocity and temperature measurements which can be useful for validating computational fluid dynamics (CFD) codes.

1. INTRODUCTION

The terminology single-phase natural circulation loops (NCLs), also called thermosyphon or natural convection systems, refers to any closed systems in which fluid is transported between diversely heated regions, naturally without need for pumping machinery. The circulating fluid absorbs heat from heated regions and rejects it to cooled (less heated) ones. Fluid motion between these regions is resulting from the buoyancy forces caused by the thermally induced density differences in a gravitational force field. Buoyancy forces overcome the fluid inertia and the frictional resistance in the loop and hence passive circulation exists and continue as long as temperature gradient is maintained. Steady state natural convection can be achieved since heating and cooling conditions are kept constant. However, under certain circumstances, it is found that steady state has a nonlinear nature and is inherently unstable and subjected to oscillatory flow behavior (Vijayan et al. 1992, Vijayan 2002). Such loops are applicable to several heat exchange engineering applications such as electronic cooling systems, solar cells, gas turbine blade cooling, and advanced nuclear reactors (Greif 1988, Basu et al. 2014).

For advanced nuclear reactors, natural convection is utilized as a safety feature to passively remove the decay heat released after loss of flow accidents (LOFA). Prismatic Modular Reactors (PMRs), one of the Generation IV proposed systems is capable of

providing electric power and/or high temperature process heat at about 1000 °C. During normal operation, this high temperature is removed by gas-cooled forced circulation system. In case of LOFA, forced cooling system is lost but radial temperature gradients exist within the reactor core (Tung et al. 2011) which can provide passive cooling. Hence under LOFA conditions, flow direction is reversed after initiation of intra-core natural circulation that the heated gas coolant moves upward along the core heated regions and flowing downward through the core less heated regions (Ghose et al. 1989, Wu et al. 2002, Southworth et al. 2003, LaBar et al. 2004, Zhang et al. 2006, Basu et al. 2014). This intra-core natural convection dissipates the released decay heat and avoid reaching the reactor core failure temperatures. Significant attention was directed to PMRs passive safety systems especially after the Fukushima Daiichi nuclear power plant accident in 2011 (Zohuri 2016). Thus understanding thermal-hydraulics of natural circulation phenomena was advanced by several computational studies available in the open literature (Tak et al. 2008, Sato et al. 2010, Yoon et al. 2011, Travis et al. 2013). However, experimental validation of simulations and computational fluid dynamics (CFD) codes is crucial. Validation is conducted by providing high quality data obtained from separate-and-integral test facilities designed with reference to the corresponding reference PMRs. It is worth mentioning that the General Atomics 350 MW-Th Modular High Temperature Gas-cooled Reactor (MHTGR) is selected as the reference facility for designing PMRs (McDonald 1992, Sato et al. 2010). For this reason, many studies ((Reyes et al. 2010, King 2012, Castañeda 2014, Woods et al. 2015)) including current are based on the scaling down of MHTGR.

Naturally driven flow behavior inside heated channels has been intensively reported in the open literature since the innovative work conducted by Elenbaas (1942). These studies investigated different natural convection flow regimes (i.e., laminar and turbulent) (Aung 1972, Aung et al. 1972, Dyer 1975, Sparrow et al. 1985, Miyamoto et al. 1986, Cheng et al. 1988, Fujii et al. 1988, Fedorov et al. 1997, Habib et al. 2002, Badr et al. 2006, Yilmaz et al. 2007, Yilmaz et al. 2007), transition criteria (Jaluria et al. 1974, Sanvicente et al. 2013), and flow reversal (Sparrow et al. 1984, Kihm et al. 1995, Fu et al. 2016). It is found that the majority of these studies focus on heat transfer and global correlation between dimensionless groups. Few studies, listed in Table 1, concern with flow kinematics and thermal behavior. It is obvious that these studies were conducted for simplified geometries with different dimensions than that employed in real nuclear systems hence it cannot be directly extended to PMRs applications (Celataa et al. 1998).

On the other hand, there are few experimental studies investigating natural circulation for closed loops with the specific goal of addressing MHTGR's passive safety. One such effort is the integral tests conducted in the High Temperature Test Facility (HTTF) developed at Oregon State University (OSU) (King 2012, Woods et al. 2015). Since integral testing facilities are generally large and long-term investment. Thus there is a need for designing test facilities to provide consistent separate effects tests complement these ongoing integral tests. As well, these facilities must be designed in a flexible manner to investigate different thermal boundary intensities. Designing and constructing such NCL facility with configuration representing the PMRs core is a challenging task because of the significant effect of setup design and geometry on flow stability (Chen 1985). However, this was executed in a state-of-the-art manner by multiphase Reactors Engineering and

Applications Laboratory (mReal) at Missouri S&T University (Taha et al. Under review 2017). This developed experimental setup called the Plenum-*to*-Plenum Facility (P2PF) and was designed with a representative geometry of PMRs core. The aim of designing the P2PF is to investigate intra-core natural circulation thermal-hydraulic phenomena. Flow fields characterization is conducted by novel implementation of advance sophisticated measurement techniques including hot wire anemometry (HWA), wall flush mounted micro-foil sensors, and thermocouples. Novel integration of these measurement techniques will aid overcoming the insufficiency of experimental benchmark data available for thermal-hydraulics natural convection inside the core channels.

2. EXPERIMENTAL SETUP

Missouri S&T has designed and developed a separate-effects test facility to advance knowledge and understanding of plenum-to-plenum (P2P) natural circulation thermal-hydraulics phenomena in the PMRs. This P2PF is fabricated with a representative geometry of the PMR main components (i.e., plena and core). A schematic diagram of the facility is shown in Figure 1. Current phase of the facility design consists of two plena (i.e., upper and lower) connected by two core channels via flanges, all made of stainless steel. Facility design is flexible enough to upgrade the current phase to involve multichannel core for future investigations. The dual channels locations were selected to represent the core regions that are diversely heated as a result of the radial temperature gradient which exist within the core after LOFA (Tung et al. 2011). The heated (riser) channel is located near the centerline of the core (x = 1.183 inch or 3 cm) while the cooled (down-comer) channel is located away from the centerline (x = 3.549 inch or 9 cm and y = 1.025 inch or 2.6 cm)

as shown in Figure 2. Both channels have the same dimensions of 1 m (39.37 inch) height accommodating five vertical prismatic blocks, and 0.016 m (0.625 inch) ID as same utilized in the reference MHTGR core channels. The upper and lower plena heights are 0.24 m (9.41 inch) and 0.13 m (5 inch), respectively, see Figure 1.

Natural circulation is mimicked by electrically heating the inner-most channel by four 1 inch by 24 inch heavily insulated Duo-Tape electrical heaters, each with maximum capacity of 312 watts at 120 V. Each heater is connected to BT-V Variac power controller to adjust and control the amount of heat supplied from each heater separately. This allows conducting experiments under different heating intensities and profiles (i.e., isoflux and non-isoflux). The outer channel as well the upper plenum are cooled by using an external chiller (Applied Thermal Control Ltd, K4 chiller). The channel is wrapped by copper tube in which chilled water is introduced. Simultaneously, chilled water is pumped into the jacket surrounding the upper plenum. The temperature of the chilled water can be varied by temperature controller within ±0.1℃ temperature stability built-in the chiller. Since natural circulation has a delicate nature and highly sensitive to surrounding changes, the entire facility (i.e., channels and plena) are heavily insulated by ceramic fiber insulation. Detailed explanation of the design stages of the facility can be found elsewhere (Taha et al. Under review 2017).

3. EXPERIMENTAL WORK

3.1. EXPERIMENTAL PROCEDURES AND THERMAL BOUNDARY CONDITIONS

In the current study, the effect of four isoflux heating intensities ranging from 100 to 700 with an increment of 200 W/m^2 on thermal and velocity fields inside the heated channel

has been investigated. Each experiment was considered as a batch process in which dehumidified air is compressed in the facility before turning on the electrical heaters and the chiller. Although the facility is capable of withstanding pressures up to 100 psi (Said et al. 2017, Said et al. In press, Taha et al. Under review 2017), the results discussed in this study are for experiments conducted at atmospheric pressure to avoid HWA measurements uncertainties associating high pressures. Flow field measurements were obtained after reaching thermal steady state that is distinguished by observing insignificant temperature change with time. Since steady state time is a function of the amount of heat supplied and the measurements position (Hess et al. 1979), time needed to reach steady state has been observed for each experimental condition examined in the current study. Thus it is guaranteed that each experiment is allowed sufficient time to reach thermal steady state conditions before obtaining flow fields results. Measurements were obtained at six axial positions (z/L) along the channel namely; 0.04, 0.28, 0.41, 0.59, 0.77, 0.96. For each axial position, radial measurements were obtained from the inner wall (r/R = 1) to the centerline (r/R = 0.0) of the channel. The chilled water temperature is fixed at 5℃ for all experiments. Each experiment was repeated twice to ensure data reproducibly and for each repetition three measurement replications have been recorded. The variables examined in this study are listed in Table 2.

3.2. INSTRUMENTATION

Naturally driven air thermal and velocity fields have been characterized by implementing advanced measurement techniques in a novel way to be utilized either separately or simultaneously during experiments (Taha et al. Under review 2017, Taha et

al. Under review 2017). Instantaneous inner wall surface temperature $(T_{s,i})$ and instantaneous air temperatures (T_i) were measured by using micro-foil sensors that are flush mounted in a noninvasive way to the inner wall of the heated channel and T-type thermocouples with ±2℃ accuracy, respectively. Time series temperatures were obtained at frequencies of 0.05 kHz. Local instantaneous air velocities (U_i) were measured by using a DANTEC single component hot wire anemometry (HWA). Time series velocity measurements were collected at frequency 0.1 kHz. Both temperatures and velocity frequencies were selected to guarantee proper time series data points and sampling interval based on time-and-frequency domain analysis discussed elsewhere (Taha et al. Under review 2017). Since the HWA data acquisition system is a single channel (this means single HWA sensor can be used during experiment), same experiment was repeated by introducing the sensors through small blocks, shown in Figure 3, manufactured in-house and installed at six axial positions along the channel. These blocks were designed in a novel way so that the thermocouple readings are not disturbed by the HWA sensor. For each axial position, radial velocity and temperature measurements obtained from the inner wall (r/R = 1) to the centerline (r/R = 0.0) of the channel by using a radial adjuster, shown in Figure 4. This adjuster enables varying sensors radial positions by 1 mm step while the experiment is running. Measurements were obtained for each position after waiting few seconds to avoid perturbations due to the probes displacements. Detailed discussion of the measurement techniques implementation and raw time series obtained signals processing and analysis can be found elsewhere (Taha et al. Under review 2017).

4. RESULTS AND DISCUSSION

The effect of heat flux on temperature and velocity distributions at six axial position (z/L) along the uniformly heated channel (riser) is being presented in this section. Results are presented in terms of (i) local time-averaged wall and air temperatures, (ii) local time-averaged air velocity, and (iii) dimensionless analysis and quantification.

4.1. TIME-AVERAGED TEMPERATURE MEASUREMENTS

Large number of temperature measurements were recorded after reaching thermal steady state conditions to ensure statistical convergence of the results. These instantaneous readings have been averaged with respect to time (Bradshaw 2013):

$$T = \frac{1}{N}\sum_{i=0.0}^{i=N} T_i \tag{1}$$

$$T_s = \frac{1}{N}\sum_{i=0.0}^{i=N} T_{s,i} \tag{2}$$

where $(T\ and\ T_s)$ are the time-averaged air and channel inner surface temperatures; and $(T_i\ and\ T_{s,i})$ are the instantaneous air and channel inner surface temperature measurements, respectively. The index (i) refers to the number of sample readings that have a maximum number of (N).

Figure 5 shows temperatures axial and radial distribution along the heated channel for the lowest (i.e., 100 W/m^2) and highest (i.e., 700 W/m^2) uniform heat supplied. Channel inner wall surface temperature (r/R = 1) is clearly illustrated by plotting axial temperature difference $\left(\Delta T_{s,j}\right)$ versus channel height (z/L) as shown in Figure 6. The $\left(\Delta T_{s,j}\right)$ is calculated as follows:

$$\Delta T_{s,j} = T_{s,j+1} - T_{s,j} \quad (3)$$

where the index (j) refers to the axial position along the channel.

It is obvious that the channel can be divided into three section; (i) inlet, (ii) midsection, and (iii) outlet. In the inlet section (0.0 < z/L < 0.3), surface temperature is found to increase rapidly, as shown in Figure 6. The midsection is defined where temperature increases linearly with a reduced gradient. Thus concisely, surface temperature increases from the leading edge to an axial position of (z/L = 0.8) where maximum temperature is noticed. Beyond this position, surface temperature is observed to decrease towards the channel outlet (z/L = 1).

Surface temperature inflection position was observed in previous studies at certain axial positions close to where detected in the current study, approximately at z/L = 0.8 (Miyamoto et al. 1986, Fedorov et al. 1997, Lau et al. 2012, Sanvicente et al. 2013). In these studies, temperature drop is attributed to environmental losses which is equivalent to heat transfer by conduction through the heated channel and the flange connecting both channels to the facility cooled upper plenum. The significant effect of this heat conduction was examined by computational simulations carried out for the same facility (Kao et al. 2015, Kao et al. 2015). Surface temperature inflection was reported as a significant criterion of flow destabilization (i.e., flow regime transition or flow reversal) which emphasize the delicate nature of buoyancy-driven flow (Jaluria et al. 1974, Muresan et al. 2006, Lau et al. 2012, Sanvicente et al. 2013). This destabilization is verified by flow dynamics analysis discussed in the following section.

Axial air temperature distribution is found to have similar trend of surface temperature of being increased from the channel inlet (z/L = 0.0) to the inflection axial

position at z/L = 0.8. This temperature rise is followed by subsequent reduction along the outlet section (0.8 < z/L < 1). Air radial temperature profile is found to be a function of the axial position. In the region from the entrance to the inflection point, sample plotting shown in Figure 7, temperature is observed to decrease from the inner wall (r/R = 1) towards the centerline (r/R = 0.0) of the channel. This temperature distribution implies that wall-to-fluid heat transfer is maintained along this height. Beyond the axial position (z/L = 0.8), radial temperature distribution is observed to be reversed with an increase in temperature towards the centerline of the channel (r/R = 0.0) as shown in Figure 8. This temperature radial profile indicates that a reversal in the heat transfer direction occurs near the channel outlet. This heat transfer reversal was investigated and quantified in a previous related study (Said et al. 2017) in which negative heat flux values, denoting heat transfer reversal, were observed and measured at the channel top section near the outlet. Indeed, this heat transfer directional reversal affects the temperature inflection position and influences flow stability inside the channel as discussed in the subsequent sections.

4.2. TIME-AVERAGED VELOCITY MEASUREMENTS AND TURBULENT INTENSITY

Air velocity contours, shown in Figure 9, represents kinematical flow characterization for all heating intensities examined in this study. Air velocities are expressed in terms of normalized velocity ($U_{normalized}$) that is calculated as follows.

$$U_{normalized} = \frac{U}{U_{max}} \tag{4}$$

where (U_{max}) is the maximum value of velocity obtained among all heating intensities investigated. This value is obtained approximately at the mid-height of the channel at

central radial position between the inner wall and the centerline of the channel (at r/R = 0.5) in case of 700 W/m^2 heating. As well, (U) is the time-averaged air velocity and is calculated similar to time-averaged temperatures mentioned earlier.

$$U = \frac{1}{N}\sum_{i=0.0}^{i=N} U_i \tag{5}$$

where (U_i) is the instantaneous air velocity and the index (i) refers to the number of sampling readings that have a maximum number of (N).

By assuming non-slip flow conditions at channel inner wall (r/R = 1), it is found that velocity increase in the vicinity regions of the heated channel. Velocity profiles are significantly depend on the axial position and the amount of heat supplied. Thus, as previously discussed, channel length is divided into three sections: (i) inlet (0.0 < z/L 0.3), (ii) midsection (0.3 < z/L < 0.8), and (iii) outlet (0.8< z/L < 1).

Along the inlet section, velocity is found to increase in the vicinity of the heated channel and then remains constant towards the centerline (r/R = 0.0) of the channel (Figure 5 a). This flow behavior was obtained in previous studies (Ayinde et al. 2006, Daverat et al. 2013) and attributed to suction at the entry resulting from the buoyant effects. These suction effects are defined as chimney effect (Daverat et al. 2013, Daverat et al. 2014). It is worth mentioning that this chimney effect was not reported in numerous natural convection studies as mostly vertical parallel plates used to mimic the channel geometry. On contrast to parallel plates, channel geometry impacts flow behavior and could lead to occurrence of such chimney effects (Daverat et al. 2014). In the current study, chimney effect is observed at inlet section of the channel only in case of low amount of heat supplied (i.e., 100 W/m^2, figure 5 a). By increasing the amount of heat supplied, a typical naturally

driven flow profiles are obtained, as shown in Figure 5 (c, d) and sample results plotted in Figure 10. Under these conditions, velocity peak is observed in the vicinity regions of the heated channel followed by a decrease in velocity towards the centerline of the channel (r/R = 0.0). Similarly to previous studies (Habib et al. 2002), this velocity peak increases with increasing the amount of heat supplied along the axial position (increase of z/L) and shifted towards the centerline (r/R = 0.0) of the channel. Thus it is noted that, for higher heat supply the maximum velocity is observed in the mid-section of the channel and close to the radial position of r/R~0.5.

For the outlet section of the channel, velocity profiles are atypical as a consequence of temperature inflection and atypical profiles. Similarly, minimum velocities are observed at the channel wall. While the velocity peak is shifted from the regions near the channel heated wall towards the centerline of the channel. This shift in velocity radial profiles is accompanied with a reduction in the velocity measurements obtained in this top section than that obtained at upstream positions as observed in Figure 9.

For better illustration of flow dynamics inside the channel and quantification of the level of turbulence or system chaotic behavior, turbulent intensities associated with flow measurements are vital. Turbulent intensities (I) quantifies for the velocity fluctuations (root mean square; rms) divided by the time-averaged flow velocity recorded at each radial (r/R) and axial (z/L) positions. Turbulent intensities have been effectively used previously to define onset of natural convection turbulence on inclined plates by using HWA measurements (Rodríguez-Sevillano et al. 2011).

In the current study, the turbulent intensities are also based on the HWA measured air velocities as follows.

$$U_{rms}=\left(\frac{1}{N\text{-}1}\sum_{i=0.0}^{i=N}(U_i\text{-}U)^2\right)^{0.5} \quad (6)$$

$$I=\frac{U_{rms}}{U} \quad (7)$$

where (U_{rms}) indicates to the root mean square (or standard deviation) of the mean velocity results, $(U_i \; and \; U)$ are the instantaneous and time averaged air velocities, respectively, and I represents turbulent intensity. The index (i) refers to the number of sampling readings that have a maximum number of (N).

Since flow field characterization has been conducted in the current study by investigating flow in three distinct regions: (i) inlet, (ii) midsection, and (iii) outlet of the channel. Thus, turbulent intensities have been measured at three axial positions along the channel (i.e, z/L = 0.28, 0.6, and 0.96). It is found that values obtained at the inlet and midsection approximately are similar. Hence, only midsection results are plotted in Figure 11 in which it is shown that high turbulence intensities are obtained near the outlet of the channel (z/L = 0.96). This increase in turbulence intensities emphasize that flow destabilization occurs near channel exit. It is vital to examine whether this destabilization occurs only at the outlet or below this axial position. In other words, it is necessary to determine the exact axial position where flow destabilization starts to take place. This is distinguished by the position where turbulent intensity starts to grow (Rodríguez-Sevillano et al. 2011). Therefore, turbulent intensities were calculated at an axial position of z/L =0.77 and results were compared with midsection ones. As shown in Figure 12, no variation in turbulent intensities values exists around the centerline of the channel (r/R = 0.0). While turbulence values starts to grow close to the heated walls of the channel. Thus it is concluded that flow destabilization starts at an axial position (z/L = 0.77)

approximately where wall surface temperature starts to decrease. This finding emphasize the conclusion that existence of temperature inflection point is a key criterion that can be adopted to indicate flow destabilization in naturally driven flow inside vertical channels.

All in all, temperature inflection (initiation of flow destabilization) within the P2PF is attributed to; (1) heat losses by conduction, (2) heat transfer reversal, and (3) upper plenum mixing. Heat losses by conduction occurs through stainless steel material of the channels and the flange connecting the upper plenum with dual channels. These heat conduction losses were observed in CFD simulations conducted for the current facility (Kao et al. 2015, Kao et al. 2015). Temperature distributions reveal that fluid-to-wall heat transfer occurs near the channel outlet which was quantified in more details by authors of the current study (Said et al. 2017).

Furthermore, gas plumes mixing phenomenon occurring in the upper plenum has been computationally and experimentally studied (Sabharwall et al. 2007, King 2012, McVay et al. 2015). For the current facility, naturally driven air exiting the heated channel enters the upper plenum which is subjected to cooling. Air is cooled and subsequently its density increases and tends to flow downwards. Thus air plumes are mixed in the upper plenum and interacted with upcoming heated air from the channel. The previously reported dependency of flow on chilled water temperatures (i.e., upper plenum wall temperatures) ensure the interaction between cooled air plumes near channel exit (Taha et al. Under review 2017). This flow interaction along with heat losses by conduction give rise to heat transfer reversal and subsequently flow reversal and recirculation of cooled plumes inside the heated channel. It is expected that cooled air plumes are recirculated near the channel wall and hence inflection temperature arises and consequently velocity peak is shifted

towards the centerline (r/R = 0.0) of the channel near the outlet. This flow reversal phenomenon was observed in previous studies with remarking that recirculated flow penetration length could reach the mid-height of the channel (Sparrow et al. 1984, Kihm et al. 1995, Li et al. 2013, Fu et al. 2016).

4.3. DIMENSIONLESS APPROACH ANALYSIS

Dimensionless groups can be used to further the discussion of current findings and to provide a means for comparison with other experimental results. Overall and local quantification of these dimensionless parameters were adopted as the phenomenon of natural convection and flow reversal is local in nature.

4.3.1. Flow Inside Heated Channel.

- Quantification of overall dimensionless groups

Dimensionless groups, governing natural convection, used in this section of analysis are listed in Table 3.

The volumetric expansion coefficient of air (β) is defined as

$$\beta = \frac{1}{T_{mf}} \tag{8}$$

where mean film temperature (T_{mf}) is the reference temperature chosen to characterize the average thermal-energy state of the fluid and at which all air physical properties (Brereton et al. 2006). In this study, the reference temperature is defined to be

$$T_{mf} = \frac{T_{ms} + T_f}{2} \tag{9}$$

where (T_{ms}) is the mean value of channel inner wall time-averaged surface temperatures (eq. 2) that are measured a different axial positions along the channel. This mean film temperature is calculated as follows

$$T_{ms} = \frac{1}{L} \int_{o}^{L} T_s \; dL \tag{10}$$

where (L) is height of the channel.

Also $\left(T_f\right)$ is the characteristic temperature of the fluid. In the literature, there are several definitions of this temperature. For instance, it was selected to be the channel wall temperature (eq. 10) in the pioneering work conducted by Elenbaas (1942) and it was chosen to be the gas temperature at the inlet of the channel (Sanvicente et al. 2013). In the current analysis, it is determined by averaging the radially-averaged temperatures obtained at different axial positions along the channel as follows

$$T_f = \frac{1}{L} \int_{o}^{L} \bar{T} \; dL \tag{11}$$

where $(\bar{T})$ is the radially averaged air temperature obtained at each axial position and is calculated as

$$\bar{T} = \frac{1}{R} \int_{0}^{R} T \; dr \tag{12}$$

where (R) is the channel radius.

The characteristic velocity $\left(U_f\right)$ is calculated as the same manner for calculating the characteristic temperature. It is calculated by averaging the radially-averaged velocities $(\bar{U})$ obtained at different axial positions along the channel as:

$$U_f = \frac{1}{L} \int_{0}^{L} \bar{U} \; dL \tag{13}$$

where $(\overline{U})$ is calculated as:

$$\overline{U} = \frac{1}{R} \int_0^R U \ dr \tag{14}$$

where (U) is the time averaged velocity that is obtained as shown in (eq. 5).

Figure 13 shows the overall Reynolds number versus overall Rayleigh number for all heating intensities investigated in the current study. It is concluded that (Ra) is proportional to the (Re) according to the following relationship:

$$Re \ \alpha \ Ra^{0.58} \tag{15}$$

This relationship was found to be qualitatively consistent but quantitatively deviating from Daverat et al. (2013) relationship correlating same dimensionless groups.

$$Re \ \alpha \ Ra^{0.33} \tag{16}$$

The reported deviation could be resulted from the difference in the characteristic temperature and velocity definitions. In this previous study, these characteristic parameters were determined based on mean values obtained at inlet and outlet of the channel.

- Local quantification of dimensionless groups

In addition to estimating the overall Rayleigh number, variation of same parameter has been quantified locally at different axial positions (z/L) along the channel. Same general formula for Ra has been implemented in this section

$$Ra = \frac{g \ \beta \ \ell^4 \ q}{\alpha \ \upsilon \ k} \tag{17}$$

where (g) is acceleration by gravity, (β) is the volumetric expansion coefficient, (q) is the amount of supplied heat flux, (ℓ) is the characteristic length, (k) is the thermal conductivity, (υ) is kinematic viscosity.

The characteristic temperature at which all air physical properties have been calculated is selected to be the radially averaged air temperature ($\bar{T}$) obtained for each axial position (see eq. 12). In order to account for the variation of the axial position, local distance from the leading edge of the channel (z) has been utilized to be the characteristic length (Ambrosini et al. 2006). Since the total channel height is 1 m, the distance (z) is found to be equivalent to the dimensionless axial position (z/L). The expression of the Rayleigh number can be rewritten to quantify for local Ra as follows:

$$Ra_x = \frac{g\,\beta\,z^4\,q}{\alpha\,\upsilon\,k} \tag{18}$$

Where (Ra_x) is local Rayleigh number. Another term representing channel aspect ratio (d/L) is added to this expression in order to estimate local modified Rayleigh number (Ra_{mx}) that is calculated as:

$$Ra_{mx} = \frac{g\,\beta\,z^4\,q}{\alpha\,\upsilon\,k}\,\frac{d}{L} \tag{19}$$

Where ($d\ and\ L$) are channel diameter and height, respectively.

Axial distribution of (Ra_{mx}) at different heating intensities is shown in Figure 14. It is observed that the local measurements of (Ra_{mx}) increases with a smaller gradient from the leading edge (z/L = 0.0) to a certain axial position (approximately z/L = 0.8) where amplification of (Ra_{mx}) is observed and continues towards the outlet of the channel. It is adopted that high values of Rayleigh number implies natural convection flow destabilization takes place (i.e., flow regime transition) (Habib et al. 2002, Ayinde et al. 2006). Thus the obtained results of (Ra_{mx}) emphasize that flow destabilization starts to occur approximately where temperature inflection exists (z/L = 0.8). This instability in flow is due to intensification of turbulent intensities along with flow reversal at the top

section of the channel. Muresan et al. (2006) stated that this instability is due to appearance of eddies and vortices that strengthen the macroscopic mixing between the fluid layers. As degree of mixing increases, the boundary region is broken and hence resistance to heat transfer is reduced. It was also provided that such heat transfer enhancement is also a significant factor affecting temperature inflection observed. Detailed analysis of heat transfer enhancement at the top section of the channel can be found elsewhere (Said et al. 2017).

4.3.2. Upper Plenum Mixing. Once exiting the heated channel (riser), heated air enters the upper plenum which is subjected to cooling. Although one of the dual channels is also cooled, the majority of heat supplied is found to be removed through the upper plenum surrounding jacket (Taha et al. Under review 2017). It is necessary to quantify the amount of mixing in the upper plenum for better understanding of thermal-hydraulic phenomena in PMRs and also for providing needed benchmark data for validating CFD codes. Thus several studies have been conducted and reported in the literature for better visualization and quantification of this phenomenon (Sabharwall et al. 2007, Jackson et al. 2009, King 2012, Shibahara et al. 2013, McVay et al. 2015).

There is an ongoing study related to plenum-to-plenum (P2P) natural circulation thermal-hydraulics behavior is being conducted at Oregon State University (OSU). Hence, detailed scaling analysis have been conducted to design and construct the HTTF with reference to the MHTGR (Reyes et al. 2010, King 2012, Castañeda 2014, Woods et al. 2015). This scaling analysis is based on the Hierarchical Two-Tired Scaling (H2TS) methodology that was described by Zuber et al. (1998). The analytical solution of this methodology yields design specification of the integral effects HTTF at OSU and the

scaling dimensionless parameters that accounts for the degree of mixing in the upper plenum. These dimensionless parameters obtained are Reynolds (Re) number, densimetric Froude (Fr) number, and the ratio of inlet plenum length to flow channel diameter (Woods et al. 2015).

Generally, the Reynolds number (Re) is calculated as follows;

$$Re = \frac{\rho_{exit}\, \bar{U}_{exit}\, \ell}{\mu_{exit}} \tag{20}$$

where $(\bar{U})$ is radially averaged velocity (eq. 13), $(\rho\ and\ \mu)$ are fluid density and viscosity, respectively, and (ℓ) is the characteristic length. The subscript $(exit)$ indicates that parameters are calculated for conditions at channel exit.

The densimetric Froude number (Fr) is a dimensionless value describes different flow regimes of open channel flow. It is a ratio of inertial to buoyant forces. By considering the Boussinesq approximation, it is calculated by;

$$Fr = \frac{\bar{U}_{exit}}{\sqrt{g\, \frac{\Delta T}{\bar{T}_{exit}}\, \ell}} \tag{21}$$

where $(\bar{T}_{exit})$ is radially averaged air temperature at channel exit (z/L = 0.96) and (ΔT) is the temperature difference between the $(\bar{T}_{exit})$ and the upper plenum wall temperature (T_{up}), as in eq. 22. The plenum temperature (T_{up}) is found to approximately equals the chilled water temperature used in this study which is 5℃.

$$\Delta T = \bar{T}_{exit} - T_{up} \tag{22}$$

It is worth mentioning that the Reynolds numbers here is calculated using the channel diameter as the characteristic length, while the densimetric Froude number is calculated using the height of the upper plenum (L_{up}). This length is shown in Figure 1 to be 0.24 m

(9.41 inch). Thus these dimensionless groups can be formulated as follows (Woods et al. 2015)

$$Re = \frac{\rho_{exit}\,\bar{U}_{exit}\,d}{\mu_{exit}} \tag{23}$$

$$Fr = \frac{\bar{U}_{exit}}{\sqrt{g\,\frac{\Delta T}{\bar{T}_{exit}}\,L_{up}}} \tag{24}$$

The other dimensionless number, ratio of inlet plenum length to flow channel diameter is represented as:

$$\Pi = \frac{L_{up}}{d} \tag{25}$$

Available results obtained for the HTTF and the MHTGR presented these dimensionless groups in terms of modified Reynold number (Re_m) and ($1/Fr^2$) (King 2012). Therefore, same formulas have been adopted to quantify the similarity between current facility and the MHTGR. The modified Reynold number is obtained by combining the Reynolds number and the ratio of inlet plenum length and flow channel diameter as follows:

$$Re_m = \frac{1}{Re}\,\frac{L_{up}}{d} = \frac{L_{up}\,\mu_{exit}}{\rho_{exit}\,\bar{U}_{exit}\,d^2} \tag{26}$$

Values of these dimensionless groups for the experimental conditions of this study and that obtained for the HTTF and the MHTGR are listed in Table 4.

It is clear that dimensionless groups numbers do not p match and hence exact similarity cannot be achieved between test facilities and prototypes because of the differences in geometric scales and fluid properties (Kline 1965). Thus quantification of the fractional difference in the dimensionless group numbers between current facility

(P2PF) and the reference MHTGR is calculated by the following equation (Woods et al. 2015):

$$\text{Distortion Factor} = \frac{[\Pi]_{\text{MHTGR}} - [\Pi]_{\text{P2PF}}}{[\Pi]_{\text{MHTGR}}} \tag{27}$$

where (Π_{MHTGR}) is any of the dimensionless groups calculated for the MHTGR and (Π_{P2PF}) is the corresponding value of same dimensionless group for the P2PF. The distortions calculated for the results obtained for the P2PF for the current study experimental conditions and that for HTTF facility relative to the reported values for MHTGR are listed in Table 5.

The importance of this analysis is to determine the discrepancy between the two facilities cause by scaling distortions. As one can observe, (Re_m) distortion for the HTTF is significantly higher than that for the P2PF. For Helium test the (Re_m) distortion is 253% and for Nitrogen 354%. The P2PF's (Re_m) distortion seems to be decreasing with higher heat flux. For smallest heat flux test of 100 W/m^2, the observed distortion is 86%. On the other hand, $(1/Fr^2)$ for the HTTF is better in the range of 2-3%, while P2PF distortion is as high as 53%. This distortion is observed to be reducing with heat flux of the experiment to 16.6% for the highest heat flux of 700 W/m^2. Operation at even higher heat flux was not feasible because of the concern of the possible damage to the micro-foil sensors. These sensors are needed for surface temperature and heat flux measurements. This limitation can be addressed if an advanced sensor capable of withstanding higher temperature becomes available. Since these distortions have been estimated, experimental and computational results from this facility can be rescaled to predict data needed to model the reference reactor. Moreover, these distortions will need further work for testing different experimental conditions to minimize these deviations as possible.

5. REMARKS

Effect of uniform heating on natural convection flow fields within the plenum-to-plenum facility (P2PF) has been investigated. The key findings of the current study are summarized as follows:

- Temperature and velocity axial and radial profiles depend on the amount of heat supplied and the axial position along the channel.
- The axial temperature increase along the heated channel is followed by a sudden reduction at an approximate axial position of z/L = 0.8.
- Typical radial temperature and velocity profiles were observed from the leading edge (z/L = 0.0) till this temperature inflection position (z/L = 0.8).
- Atypical radial distributions are observed at the top section of the heated channel in which temperature and velocity peak is shifted towards the centerline (r/R = 0.0) of the channel.
- Amplifications of turbulent intensities (I) and local modified Rayleigh number (Ra_{mx}) are noticed at the same axial location of temperature inflection.
- Local flow dynamics quantification confirms that temperature inflection can be adopted as a significant criteria for naturally driven flow destabilization inside heated channels.
- Flow interaction between air plumes cooled in the upper plenum and heated air exiting the channel as well reported turbulence amplifications strengthen the macroscopic mixing between fluid layers and subsequently causes temperature inflection. This inflection is accompanied by heat transfer reversal (i.e., fluid-to-

wall) as well flow recirculation of the cooled air plumes penetrating the heated channel along the wall to various lengths.

- Dimensionless groups characterizing the amount of mixing in the upper plenum (i.e., $Re_m \; and \; 1/Fr^2$) have been calculated. Quantification of distortions of these parameters shows a good similarity between the P2PF and the reference MHTGR.
- It is expected that these distortions could be minimized and improving similarity between facilities by examining different experimental conditions such as increasing heat intensity.

The P2PF is shown to be an innovative separate effects test facility designed with a representative geometry of PMRs core for investigating thermal-hydraulics intra-core natural circulation and complement the ongoing work within integral HTTF. In the current study, detailed velocity and temperature measurements were provided for validating CFD codes that are crucial from safety analysis and PMRs design perspectives.

Table 1. Previous studies of natural convection kinematical and thermal behavior inside vertical heated channels

Author	**Channel configuration**	**Channel dimensions**	**Heating intensity (W/m^2)**	**Measurement techniques**
(Hess et al. 1979)	Channel	L = 38 cm D = 24 cm	50, 250, 600	LDA
(Lau et al. 2012)	Parallel plates	L = 150 cm D = 10 cm	One plate heated with 220 W/m^2	Thermocouples PIV
(Sanvicente et al. 2013)	Parallel plates	L = 150 cm D = 5-30 cm	One plate heated with 225 W/m^2	Thermocouples PIV
(Daverat et al. 2013)	Parallel plates	L = 65 cm D = 4.5 cm	190, 382, 764, 1147, 2305 W/m^2	Thermocouples LDA
(Daverat et al. 2014)	Parallel plates	L = 65 cm D = 4.5 cm	1150	Thermocouples LDA
(Tkachenko et al. 2016)	Parallel plates	L = 150 cm D = 10 cm	Non-uniform heating of 220 W/m^2	Numerical and experimental using Thermocouples PIV

Table 2. Experimental variables examined in the current study

Variables	**Ranges**
1. Isoflux heating intensity	4 heating intensities namely: 100, 300, 500, 700 (W/m^2)
2. Axial position (z/L)	6 values namely: 0.04, 0.28, 0.41, 0.59, 0.77, 0.96
3. Radial location (r/R)	9 readings from the inner wall (r/R = 1) to the centerline (r/R = 0.0) of the channel

Table 3. List of dimensionless groups

Symbol	Dimensionless group	Defined as
Gr	Grashof number	$Gr = \frac{g\,\beta\,\ell^4\,q}{k\,\upsilon^2}$
Pr	Prandtl number	$\Pr = \frac{\mu\,C_p}{k}$
Ra	Rayleigh number	$Ra = Gr\,\Pr = \frac{g\,\beta\,\ell^4\,q}{\alpha\,\upsilon\,k}$
Re	Reynold's number	$Re = \frac{U_f\,\ell}{\upsilon}$

Table 4. Calculated values for the dimensionless groups obtained for the MHTGR, HTTF (King 2012), and P2PF

		Dimensionless groups		
	Heating intensity	$\boldsymbol{Re_m}$	$\boldsymbol{1/Fr^2}$	**Π**
P2PF (air)	100 W/m^2	0.023	2.73	15
	300 W/m^2	0.025	3.17	15
	500 W/m^2	0.03	3.9	15
	700 W/m^2	0.038	4.85	15
HTTF (Helium)	91 kW	0.603	6.03	53
HTTF (Nitrogen)	149 kW	0.777	5.926	53
MHTGR	350 MW	0.17	5.814	224

Table 5. Natural circulation distortions between the P2PF and the HTTF relative to the reference MHTGR

Facility		**Distortion Factor**		
HTTF (King 2012)		Re_m	$1/Fr^2$	**Π "Geometrical group"**
Helium		2.53	0.0372	0.763
Nitrogen		3.54	0.0193	0.763
P2PF		Re_m	$1/Fr^2$	**Π "Geometrical group"**
Air	100 W/m^2	0.864	0.531	0.933
	300 W/m^2	0.851	0.454	0.933
	500 W/m^2	0.821	0.329	0.933
	700 W/m^2	0.776	0.166	0.933

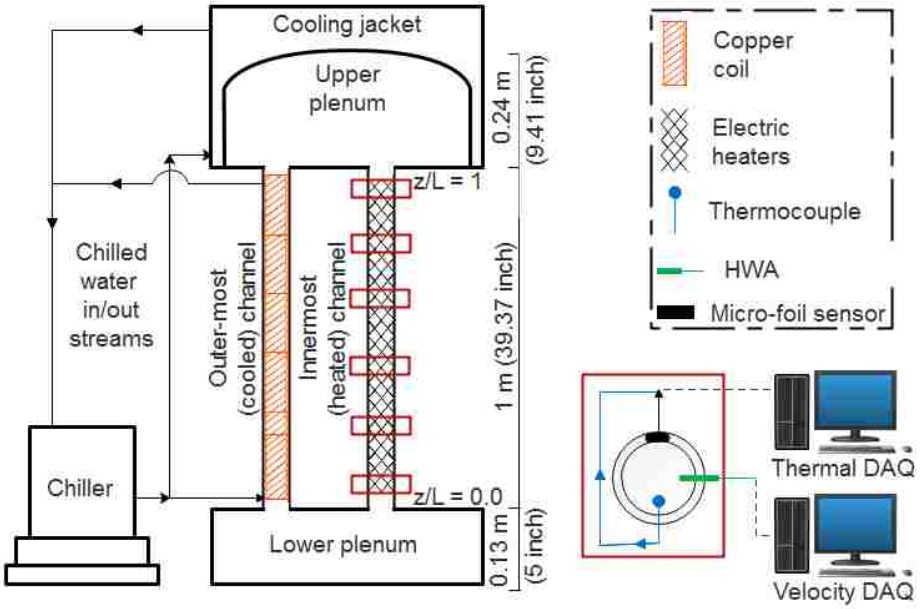

Figure 1. Schematic diagram of the P2PF

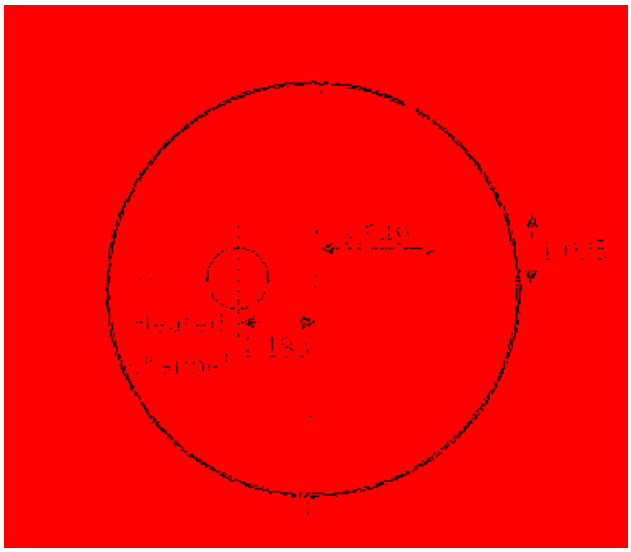

Figure 2. Schematic diagram of the dual channels locations (dimensions in inches)

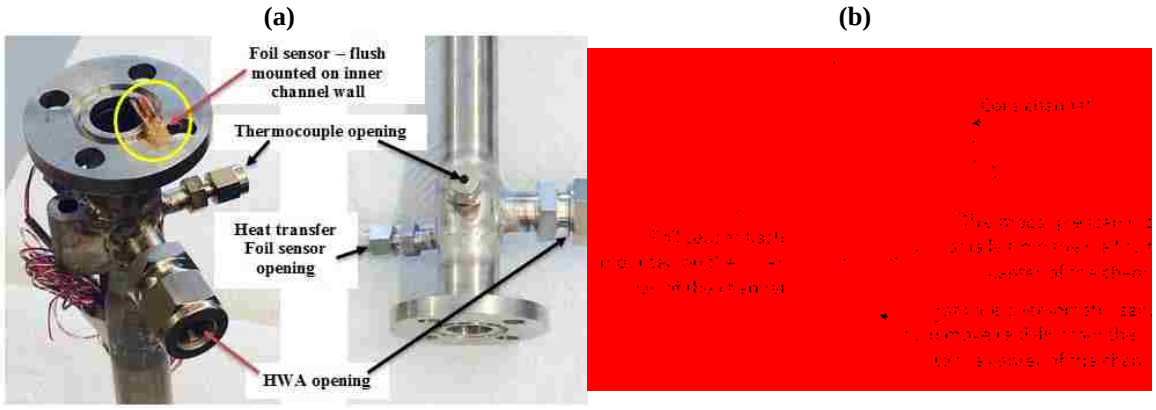

Figure 3. (a) Physical picture and (b) Schematic diagram of the blocks integrating the thermocouples and HWA sensors simultaneously

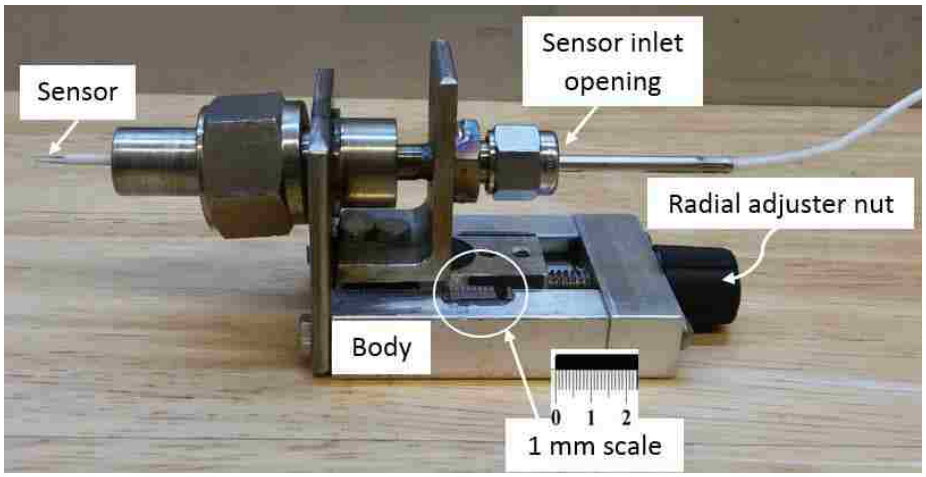

Figure 4. Mechanical radial adjusted for the HWA and thermocouples

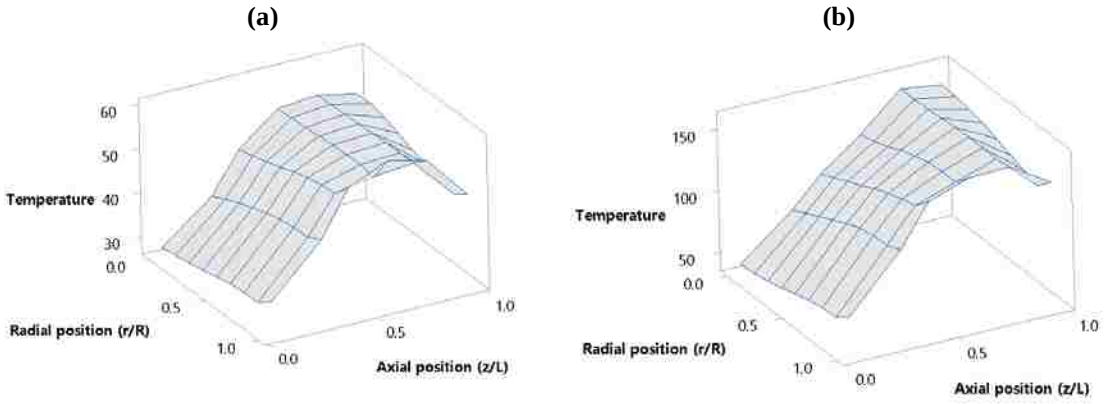

Figure 5. Local time-averaged temperature distribution along the heated channel (a) 100 W/m^2 (lowest heating) and (b) 700 W/m^2 (highest heating)

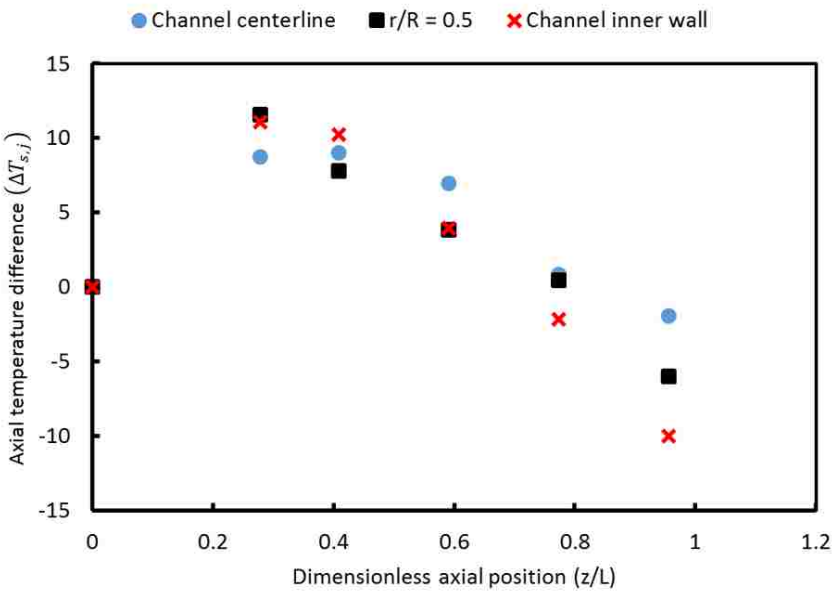

Figure 6. Air temperature axial difference at different radial location inside the channel at 100 W/m^2

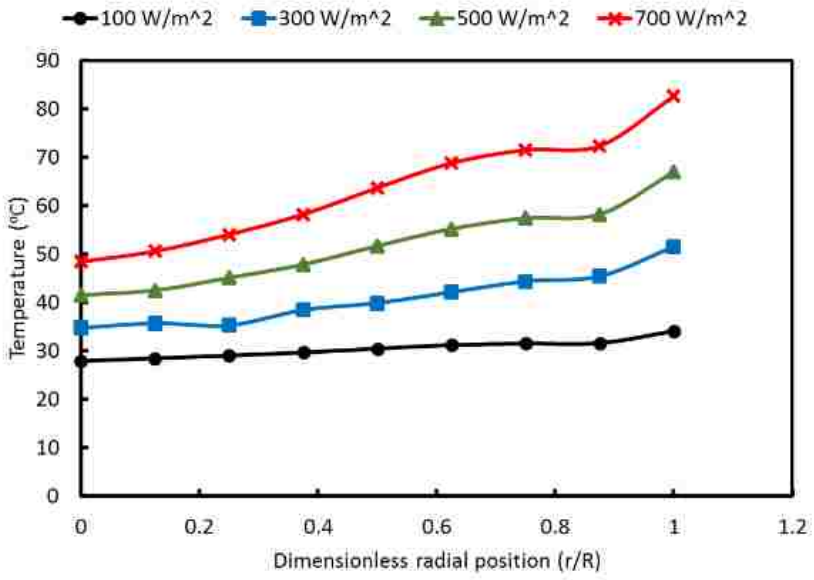

Figure 7. Air temperature radial distribution for different heating intensities at axial position z/L = 0.044

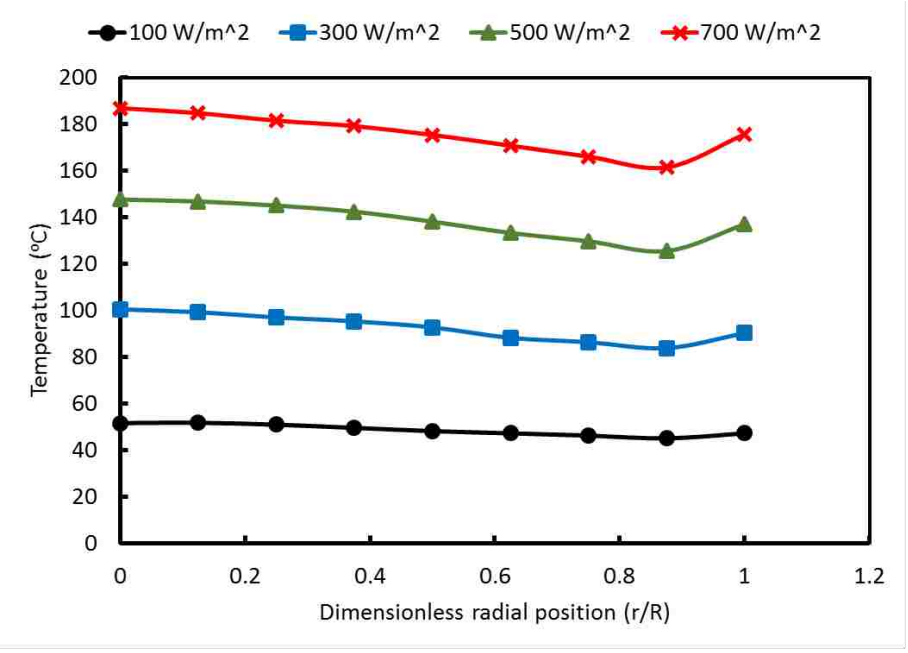

Figure 8. Air temperature radial distribution at different heating intensities at axial position z/L = 0.96

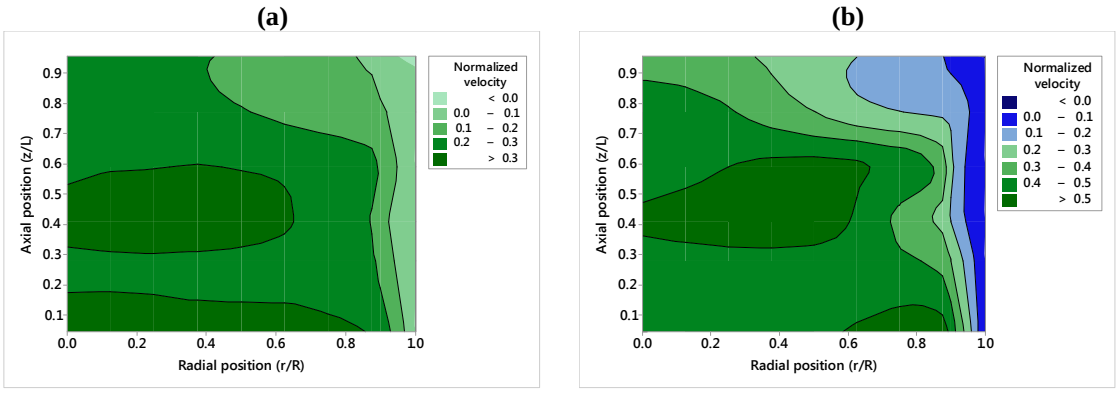

Figure 9. Air time-averaged velocity contours at different heating intensities (a) 100 W/m^2, (b) 300 W/m^2, (c) 500 W/m^2, and (d) 700 W/m^2

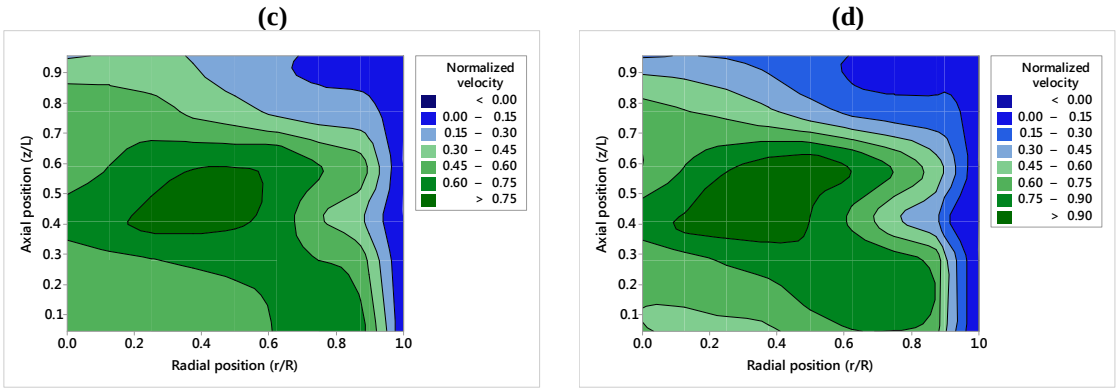

Figure 9 (cont.). Air time-averaged velocity contours at different heating intensities (a) 100 W/m^2, (b) 300 W/m^2, (c) 500 W/m^2, and (d) 700 W/m^2

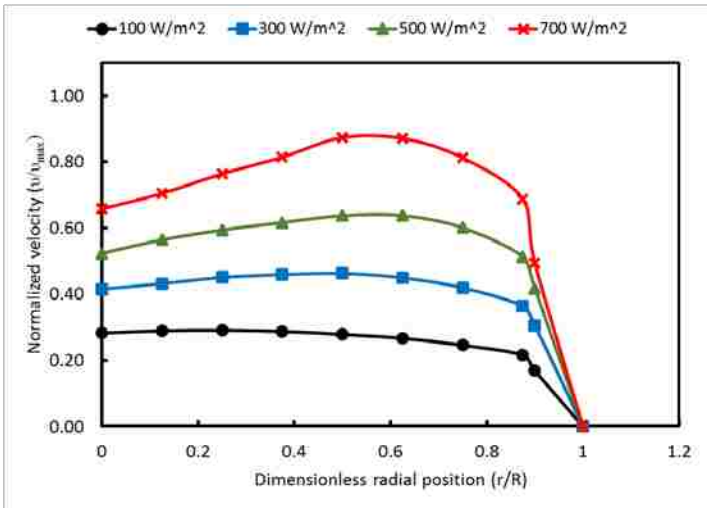

Figure 10. Sample result of typical velocity profiles for different heating intensities at z/L = 0.28

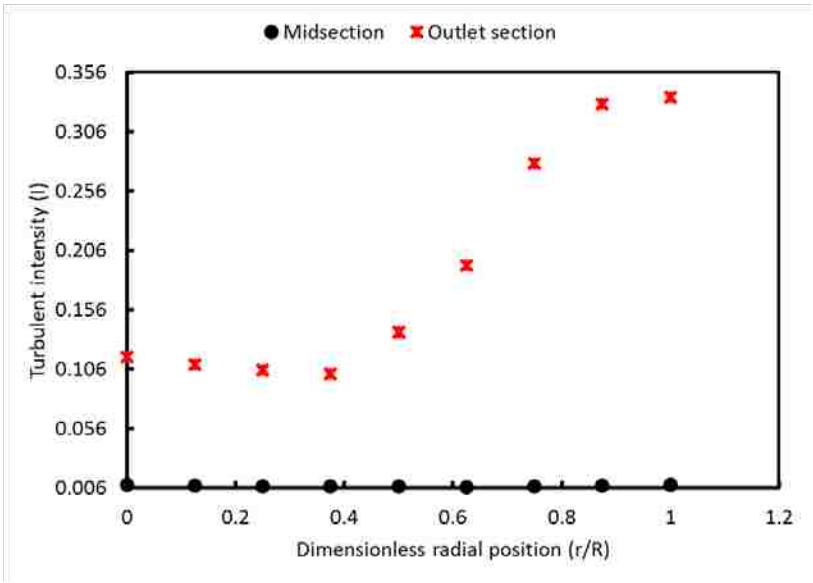

Figure 11. Radial distribution of turbulent intensity (I) at different axial sections along the channel

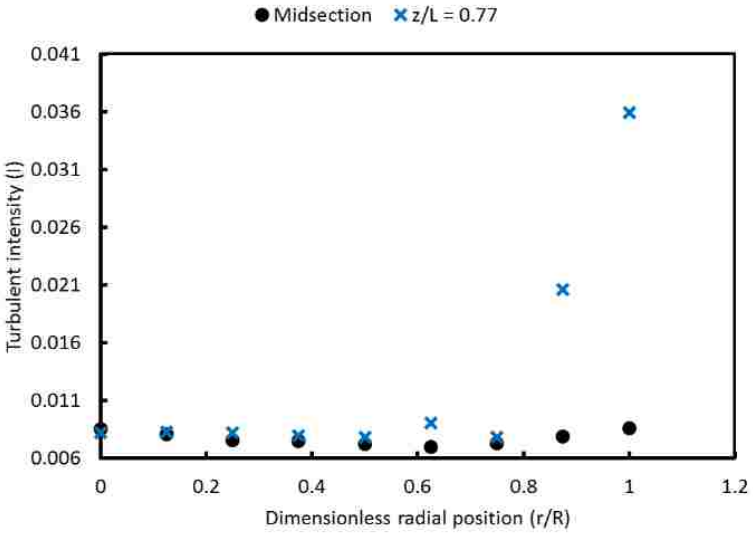

Figure 12. Radial distribution of turbulent intensity (I) at midsection (z/L = 0.6) and z/L = 0.77

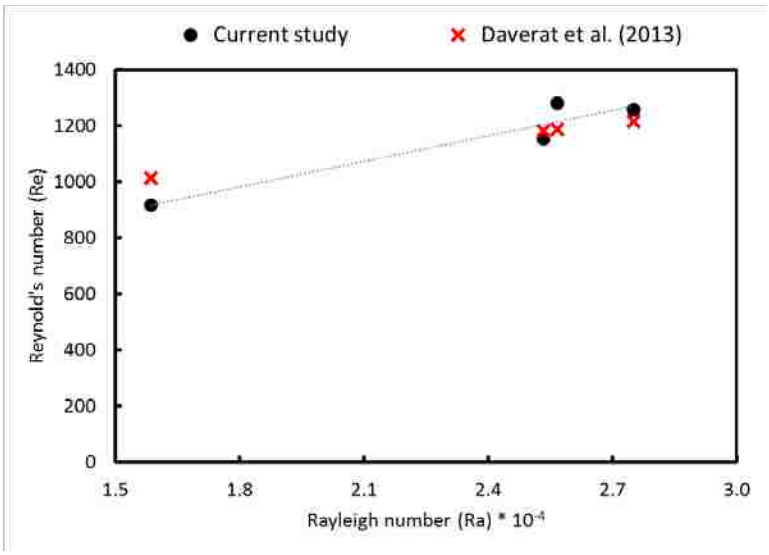

Figure 13. Reynolds number versus Rayleigh number for the heating intensities investigated

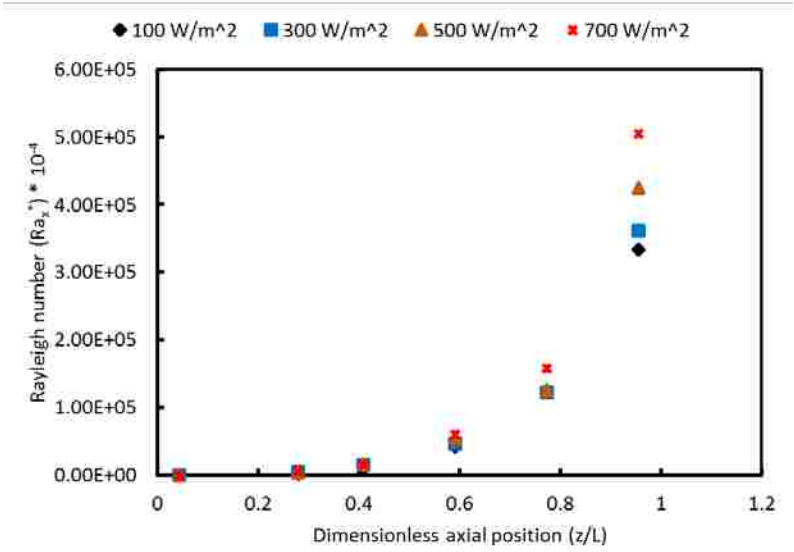

Figure 14. Axial distribution of local modified Rayliegh number (Ra^*_x)

NOMENCLATURE

Symbols

C_p	Heat capacity
g	Acceleration by gravity
I	Turbulent intensity
k	Thermal conductivity
L	Height
N	Number of data points
q	Heat flux
R	Channel radius
T	Temperature
ΔT	Temperature difference
U	Velocity
x	Channel axial distance

Greek letters

β	Volumetric expansion coefficient
υ	Kinematic viscosity
μ	Dynamic viscosity
α	Thermal conductivity
ℓ	Characteristic length

Superscript

i	Number of samples readings
s	Surface temperature
j	Channel axial position
normalized	Normalized
max	Maximum
rms	Root mean square
f	Flow characteristic parameter
mf	Mean film
ms	Mean value of surface temperature
exit	Channel exit
up	Upper plenum
m	Modified
z	Local value

Subscripts

$\bar{}$	Average

Dimensionless groups

z/L	Dimensionless axial group
r/R	Dimensionless radial group
Fr	Froude number
Gr	Grashof number

Pr	Prandtl number
Ra	Rayleigh number
Re	Reynold number
Π	Dimensionless group

Abbreviations

CFD	Computational fluid dynamics
HTTF	High temperature test facility
HWA	Hot wire anemometry
LDA	Laser Doppler anemometry
MHTGR	Modular high temperature gas-cooled reactor
mReal	Multiphase reactors and applications laboratory
OSU	Oregon State University
P2PF	Plenum-to-plenum facility
PIV	Particle image velocimetry
PMRs	Prismatic modular reactors
NCLs	Natural circulation loops

REFERENCES

Ambrosini, D. and G. Tanda (2006). "Comparative measurements of natural convection heat transfer in channels by holographic interferometry and schlieren." European journal of physics 27(1): 159.

Aung, W. (1972). "Fully developed laminar free convection between vertical plates heated asymmetrically." International Journal of Heat and Mass Transfer 15(8): 1577-1580.

Aung, W., L. S. Fletcher and V. Sernas (1972). "Developing laminar free convection between vertical flat plates with asymmetric heating." International Journal of Heat and Mass Transfer 15(11): 2293-2308.

Ayinde, T. F., S. A. M. Said and M. A. Habib (2006). "Experimental investigation of turbulent natural convection flow in a channel." Heat and Mass Transfer/Waerme- und Stoffuebertragung 42(3): 169-177.

Badr, H. M., M. A. Habib, S. Anwar, R. Ben-Mansour and S. A. M. Said (2006). "Turbulent natural convection in vertical parallel-plate channels." Heat and Mass Transfer/Waerme- und Stoffuebertragung 43(1): 73-84.

Basu, D. N., S. Bhattacharyya and P. K. Das (2014). "A review of modern advances in analyses and applications of single-phase natural circulation loop in nuclear thermal hydraulics." Nuclear Engineering and Design 280: 326-348.

Bradshaw, P. (2013). An introduction to turbulence and its measurement: thermodynamics and fluid mechanics series, Elsevier.

Brereton, G. J. and Y. Jiang (2006). "Convective heat transfer in unsteady laminar parallel flows." Physics of Fluids 18(10): 1-15.

Castañeda, J. A. (2014). Scaling Analysis of the OSU High Temperature Test Facility during a Pressurized Conduction Cooldown Event using RELAP5-3D. M.Sc, Oregon State University.

Celataa, G. P., F. Dannibale, A. Chiaradia and M. Cumo (1998). "Upflow turbulent mixed convection heat transfer in vertical pipes." International Journal of Heat and Mass Transfer 41(24): 4037-4054.

Chen, K. (1985). "On the oscillatory instability of closed-loop thermosyphons." Journal of Heat Transfer 107: 826-832.

Cheng, C.-H., W.-H. Huang and H.-S. Kou (1988). "Laminar free convection of the mixing flows in vertical channels." Numerical Heat Transfer 14(4): 447-463.

Daverat, C., Y. Li, H. Pabiou, S. Xin, D. Lyon and D. Lyon (2014). Natural Convection in an Open Vertical Channel With Heated Walls At High Rayleigh Number. Proceedings of the 15th International Heat Transfer Conference, IHTC-15.

Daverat, C., H. Pabiou, C. Ménézo, H. Bouia and S. Xin (2013). "Experimental investigation of turbulent natural convection in a vertical water channel with symmetric heating: Flow and heat transfer." Experimental Thermal and Fluid Science 44: 182-193.

Dyer, J. R. (1975). "The development of laminar natural-convective flow in a vertical uniform heat flux duct." International Journal of Heat and Mass Transfer 18(12): 1455-1465.

Elenbaas, W. (1942). "Heat dissipation of parallel plates by free convection." Physica 9(1): 1-28.

Fedorov, A. G. and R. Viskanta (1997). "Turbulent natural convection heat transfer in an asymmetrically heated, vertical parallel-plate channel." International Journal of Heat and Mass Transfer 40(16): 3849-3860.

Fu, W.-S., W.-S. Chao, T.-E. Peng and C.-G. Li (2016). "Flow downward penetration of vertical parallel plates natural convection with an asymmetrically heated wall." International Communications in Heat and Mass Transfer 74: 55-62.

Fu, W. S., W. S. Chao, T. E. Peng and C. G. Li (2016). "Flow downward penetration of vertical parallel plates natural convection with an asymmetrically heated wall." International Communications in Heat and Mass Transfer 74: 55-62.

Fujii, T., S. Koyama and N. S. Buenconsejo (1988). "Laminar free convection flow rate in a vertical tube." International Journal of Heat and Mass Transfer 31(4): 831-841.

Ghose, S. K. and A. S. Shenoy (1989). Natural circulation air cooling system for MHTGR. Proceedings of the Intersociety Energy Conversion Engineering Conference.

Greif, R. (1988). "Natural circulation loops." Journal of Heat Transfer 110: 1243-1258.

Habib, M. A., S. A. M. Said, S. A. Ahmed and A. Asghar (2002). "Velocity characteristics of turbulent natural convection in symmetrically and asymmetrically heated vertical channels." Experimental Thermal and Fluid Science 26(1): 77-87.

Hess, C. F. and C. W. Miller (1979). "Natural convection in a vertical cylinder subject to constant heat flux." International Journal of Heat and Mass Transfer 22(3): 421-430.

Jackson, R. B., E. Smith and B. G. Woods (2009). FLUENT modeling for heat transfer in upper plenum of VHTR. Transactions of the American Nuclear Society.

Jaluria, Y. and B. Gebhart (1974). "On transition mechanisms in vertical natural convection flow." Journal of Fluid Mechanics 66: 309-337.

Kao, M. T., P. Jain, S. Usman, I. A. Said, M. M. Taha, M. H. Al-Dahhan and Rizwan-Uddin (2015). Investigation of plenum-to-plenum heat transfer and gas dynamics under natural circulation in a scaled-down dual channel module mimicking prismatic VHTR core using CFD. International Topical Meeting on Nuclear Reactor Thermal Hydraulics 2015, NURETH 2015, American Nuclear Society.

Kao, M. T., P. Jain, S. Usman, I. A. Said, M. M. Taha, M. H. Al-Dahhan and U. Rizwan (2015). Study of Plenum to Plenum (P2P) natural cireulation phenomena in a dual channel scaled module of very high temperature reactor design by using CFD. Nuclear Engineering Division 2015 - Core Programming Area at the 2015 AIChE Annual Meeting.

Kihm, K. D., J. H. Kim and L. S. Fletcher (1995). "Onset of flow reversal and penetration lengths of natural convective flow between isothermal vertical walls." Journal of Heat Transfer 117(3): 776-779.

King, B. M. (2012). Natural Circulation Scaling of a Pressurized Conduction Cooldown Event in the Upper Plenum of the Modular High Temperature Gas Reactor. Master, Oregon State University.

Kline, S. J. (1965). Similtude and approximation theory. New York, McGraw-Hill.

LaBar, M. P., A. S. Shenoy, W. A. Simon and E. M. Campbell (2004). "Introducing the GT-MHR." Nuclear Engineering International 49(596): 18-23.

Lau, G. E., V. Timchenko, C. Menezo, S. Giroux-Julien, M. Fossa, E. Sanvicente, J. A. Reizes and G. H. Yeoh (2012). "Numerical and Experimental Investigation of Unsteady Natural Convection in a Vertical Open-Ended Channel." Computational Thermal Sciences 4(5): 443-456.

Li, R., M. Bousetta, E. Chénier and G. Lauriat (2013). "Effect of surface radiation on natural convective flows and onset of flow reversal in asymmetrically heated vertical channels." International Journal of Thermal Sciences 65: 9-27.

McDonald, C. F. (1992). "Gas-cooled reactor opportunities in the 21st century." SAE Technical Papers.

McVay, K. L., J.-H. Park, S. Lee, Y. A. Hassan and N. K. Anand (2015). "Preliminary tests of particle image velocimetry for the upper plenum of a scaled model of a very high temperature gas cooled reactor." Progress in Nuclear Energy 83: 305-317.

Miyamoto, M., Y. Katoh, J. Kurima and H. Sasaki (1986). Turbulent free convection heat transfer from vertical parallel plates in air (heat transfer characteristics). Proceedings of the 8th Internation Heat Transfer Conference.

Muresan, C., C. Ménézo, R. Bennacer and R. Vaillon (2006). "Numerical simulation of a vertical solar collector integrated in a building frame: Radiation and turbulent natural convection coupling." Heat Transfer Engineering 27(2): 29-42.

Reyes, J. N., J. T. Groome, B. G. Woods, B. Jackson and T. D. Marshall (2010). "Scaling analysis for the high temperature Gas Reactor Test Section (GRTS)." Nuclear Engineering and Design 240(2): 397-404.

Rodríguez-Sevillano, A., I. Pérez-Grande and J. Meseguer (2011). "On the onset of turbulence in natural convection on inclined plates." Experimental Thermal and Fluid Science 35(1): 68-72.

Sabharwall, P., T. Marshall, K. Weaver and H. Gougar (2007). CFD Analysis for Flow Behavior Characteristics in the Upper Plenum during low flow/low pressure transients for the Gas Cooled Fast Reactor (GCFR), Idaho National Laboratory (INL).

Said, I. A., M. M. Taha, Rizwan-Uddin, U. Shoaib and M. H. Al-Dahhan (In press). "Effect of helium pressure on natural convection heat transfer in a dual-channel circulation loop." International Journal of Thermal Sciences.

Said, I. A., M. M. Taha, U. Shoaib, B. G. Woods and M. H. Al-Dahhan (2017). "Investigation of Natural Convection Heat Transfer in a Unique Scaled-Down Dual-Channel Facility." AICHE Journal 63(1): 387-396.

Sanvicente, E., S. Giroux-Julien, C. Ménézo and H. Bouia (2013). "Transitional natural convection flow and heat transfer in an open channel." International Journal of Thermal Sciences 63: 87-104.

Sato, H., R. Johnson and R. Schultz (2010). "Computational fluid dynamic analysis of core bypass flow phenomena in a prismatic VHTR." Annals of Nuclear Energy 37(9): 1172-1185.

Shibahara, M., T. Takata and A. Yamaguchi (2013). "Numerical study on thermal stratification phenomena in upper plenum of LMFBR “MONJU”." Nuclear Engineering and Design 258: 226-234.

Southworth, F. H., P. E. MacDonald, D. J. Harrell, C. V. Park, E. L. Shaber, M. R. Holbrook and D. A. Petti (2003). The Next Generation Nuclear Plant (NGNP) project. Global 2003: Atoms for Prosperity: Updating Eisenhowers Global Vision for Nuclear Energy.

Sparrow, E. M. and L. F. A. Azevedo (1985). "Vertical-channel natural convection spanning between the fully-developed limit and the single-plate boundary-layer limit." International Journal of Heat and Mass Transfer 28(10): 1847-1857.

Sparrow, E. M., G. M. Chrysler and L. F. Azevedo (1984). "Observed flow reversals and measured-predicted Nusselt numbers for natural convection in one-sided heated vertical channel." Journal of Heat Transfer 106(2): 325-332.

Taha, M. M., I. A. Said, U. Shoaib and M. H. Al-Dahhan (Under review 2017). "Buoyancy-driven air flow within plenum-to-plenum facility down-comer channel." Experimental Thermal and Fluid Science.

Taha, M. M., I. A. Said, U. Shoaib and M. H. Al-Dahhan (Under review 2017). "Investigation of natural circulation in a separate effects facility of two channels representing prismatic modular reactors (PMRs) core." International Journal of Thermal Sciences.

Taha, M. M., I. A. Said, U. Shoaib, B. G. Woods and M. H. Al-Dahhan (Under review 2017). "Design and development of an experimental test facility with a representative geometry of prismatic block modular reactor core." Nuclear Engineering and Design.

Tak, N.-i., M.-H. Kim and W. J. Lee (2008). "Numerical investigation of a heat transfer within the prismatic fuel assembly of a very high temperature reactor." Annals of Nuclear Energy 35(10): 1892-1899.

Tkachenko, O. A., V. Timchenko, S. Giroux-Julien, C. Menezo, G. H. Yeoh, J. A. Reizes, E. Sanvicente and M. Fossa (2016). "Numerical and experimental investigation of unsteady natural convection in a non-uniformly heated vertical open-ended channel." International Journal of Thermal Sciences 99: 9-25.

Travis, B. W. and M. S. El-Genk (2013). "Thermal–hydraulics analyses for 1/6 prismatic VHTR core and fuel element with and without bypass flow." Energy Conversion and Management 67: 325-341.

Tung, Y. H. and R. W. Johnson (2011). CFD calculations of natural circulation in a high temperature gas reactor following pressurized circulator shutdown. ASME 2011 International Mechanical Engineering Congress and Exposition, IMECE 2011.

Vijayan, P. K. (2002). "Experimental observations on the general trends of the steady state and stability behaviour of single-phase natural circulation loops." Nuclear Engineering and Design 215(1): 139-152.

Vijayan, P. K. and A. W. Date (1992). "The limits of conditional stability for single-phase natural circulation with throughflow in a figure-of-eight loop." Nuclear Engineering and Design 136: 361-380.

Woods, B. G., R. B. Jackson, B. L. Nelson, S. R. Cadell and J. N. Reyes (2015). Scaling Analysis for the Very High Temperature Reactor Test Facility at Oregon State University. OSU-HTTF-000000-TECH-001-R0, Oregon State University.

Wu, Z., D. Lin and D. Zhong (2002). "The design features of the HTR-10." Nuclear Engineering and Design 218: 25-32.

Yilmaz, T. and S. M. Fraser (2007). "Turbulent natural convection in a vertical parallel-plate channel with asymmetric heating." International Journal of Heat and Mass Transfer 50: 2612-2623.

Yilmaz, T. and A. Gilchrist (2007). "Temperature and velocity field characteristics of turbulent natural convection in a vertical parallel-plate channel with asymmetric heating." Heat and Mass Transfer/Waerme- und Stoffuebertragung 43(7): 707-719.

Yoon, S. U. J., C. Y. Jin, M. H. Kim and G. C. Park (2011). "Experimental and computational assessment of core bypass flow in block-type very high temperature reactor." Nuclear Technology 175(2): 419-434.

Zhang, Z., Z. Wu, Y. Sun and F. Li (2006). "Design aspects of the Chinese modular high-temperature gas-cooled reactor HTR-PM." Nuclear Engineering and Design 236: 485-490.

Zohuri, B. (2016). Nuclear Energy for Hydrogen Generation through Intermediate Heat Exchangers: A renewable source of energy, Springer.

Zuber, N., G. E. Wilson, M. Ishii, W. Wulff, B. E. Boyack, A. E. Dukler, P. Griffith, J. M. Healzer, R. E. Henry, J. R. Lehner, S. Levy, F. J. Moody, M. Pilch, B. R. Sehgal, B. W. Spencer, T. G. Theofanous and J. Valente (1998). "An integrated structure and scaling methodology for severe accident technical issue resolution: Development of methodology." Nuclear Engineering and Design 186(1-2): 1-21.

SECTION

2. CONCLUSIONS

Separate-and-mixed effects test facility (named Plenum-to-Plenum facility "P2PF") has been designed, developed, and tested by multiphase Reactors Engineering and Applications Laboratory (mReal) at Missouri S&T University. This facility was designed with a representative geometry of Prismatic Modular Reactors (PMRs) for experimental investigations of coolant gas thermal and velocity fields under different natural circulation intensities to advance knowledge and understanding of natural circulation phenomenon as a passive safety system in advanced nuclear systems. Flow fields have been characterized by novel implementation and integration of advanced sophisticated measurement techniques such as the hot wire anemometry (HWA), flush-mounted micro-foil sensors, and thermocouples that will provide local time-averaged measurements at different axial and radials positions along the channels. The major findings of this study can by summarized as follows:

1. Natural circulation has a delicate nature and achieving steady state stability is dependent on geometrical specifications and experimental conditions.
2. Since heat is supplied to the inner-most channel and both the outer channel and the upper plenum are subjected to cooling, heat is primarily removed through the cooling jacket surrounding the upper plenum not through the helical copper coils surrounding the cooled (down-comer) channel.
3. Thermal and velocity fields along the cooled (down-comer) channel can be summarized as follows:
    - Gas velocity is found to be proportional to the cooling intensity.

- Small radial temperature variations have been observed along the cooled channel.
- Large turbulent intensity values observed at the channel mid-height (z/L = 0.5) indicates that significant flow destabilization (i.e., bidirectional flow) exits along the cooled channel.

4. Thermal and velocity fields along the heated (riser) channel can be summarized as follows:
    - Flow fields inside the heated channel is significantly affected by the degree of heating subjected to the channel.
    - Channel inner wall surface temperature is found to increase from the leading edge of the channel to z/L = 0.8 where and inflection point is observed.
    - Flow fields radial distribution near the top section of the heated channel implies that reversal in heat transfer direction to be existing from the gas to the channel and subsequently flow reversal is predicted at the top section of the heated channel.
5. Thermal-hydraulic mixing phenomenon in both plena
    - High values obtained for the dimensionless group Froude number (Fr) at the exit of both channels to both plena (gas flow exiting the heated channel into the upper plenum and flow exiting cooled channel towards the lower plenum) implies that fast and rapid flow exiting both channels and acts like a jet. This jet flow ensures that gas plumes mixing phenomenon exits within both plena.

This proposed work has significant impact on advancing the knowledge and understanding of the plenum-to-plenum natural circulation thermal and provides high quality benchmark

data that are much needed for verification and validation (V&V) of computational fluid dynamics (CFD) models and codes which will enhance the reliability of their use in designing reliable passive safety systems for prismatic Very High Temperature Reactors (VHTRs) and in safety analysis and assessment.

APPENDIX

OPERATING PROCEDURES OF HOT WIRE ANEMOMETRY (HWA)

All the hot wire anemometry (HWA) data acquisition system components are discussed in manuscript (II) and in this section the procedures of using the software of the hot wire anemometry are illustrated. The operating steps start with selecting the HWA icon shown as:

- After opening the HWA steamwire software the following page is seen.

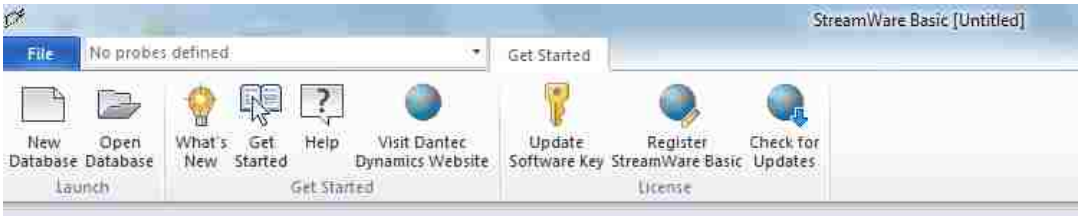

- If new set of experiments will start then “open database” is selected and then select this set by the name it was saved as. While, to start new experiments with new calibration, “open database” is selected and the next page appears.

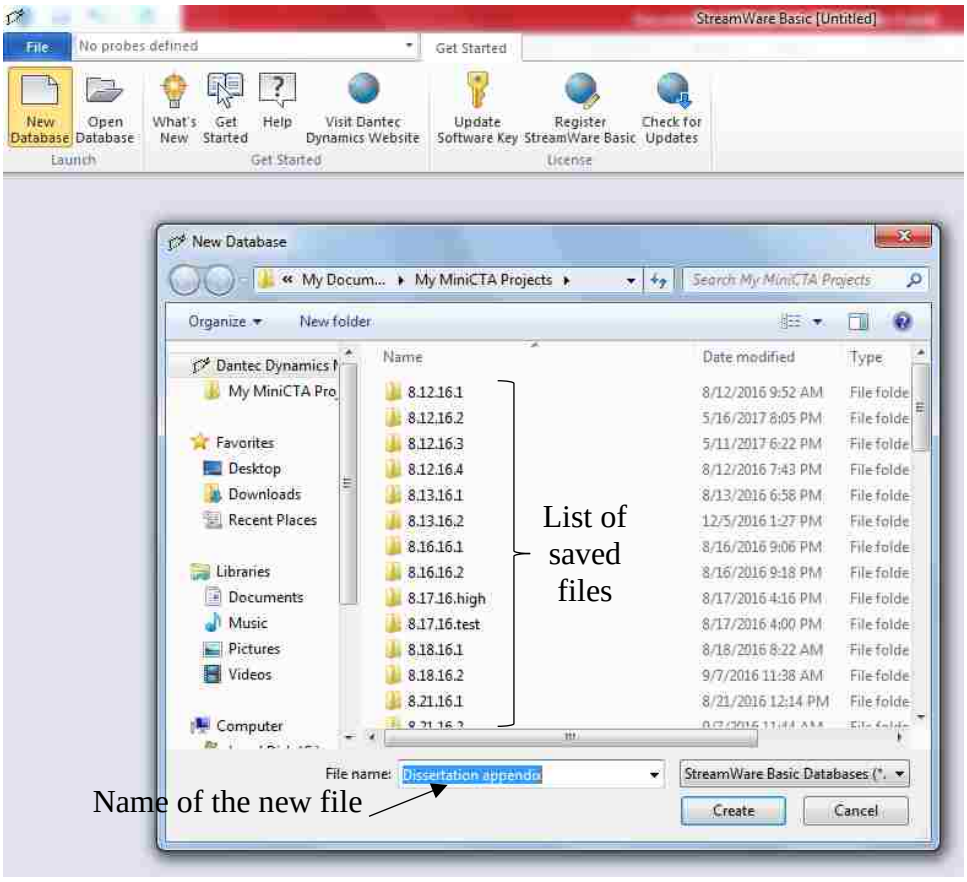

- After pressing create, the following window appear in which the ID name is defined and who creates it as follows:

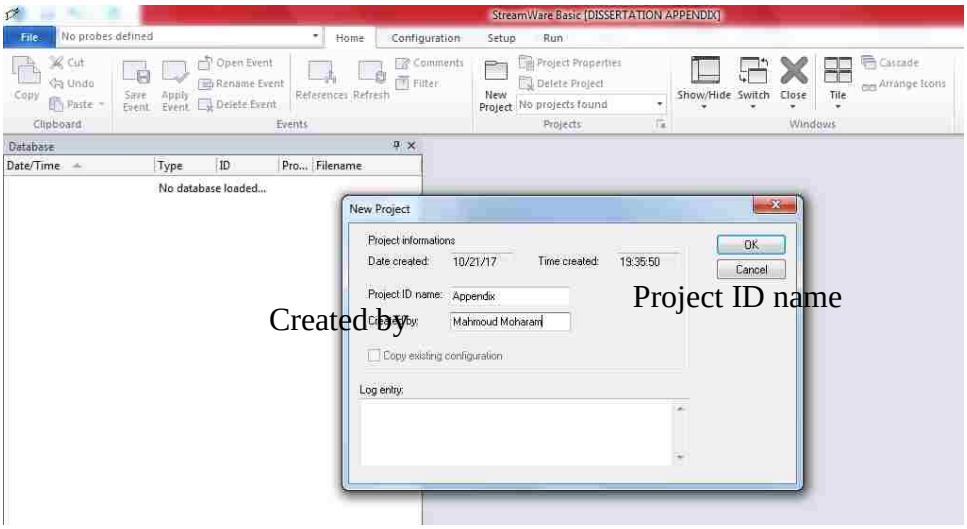

- After pressing “ok”, the following window appears asking to define the sensor configuration and the data acquisition system (DAQ).

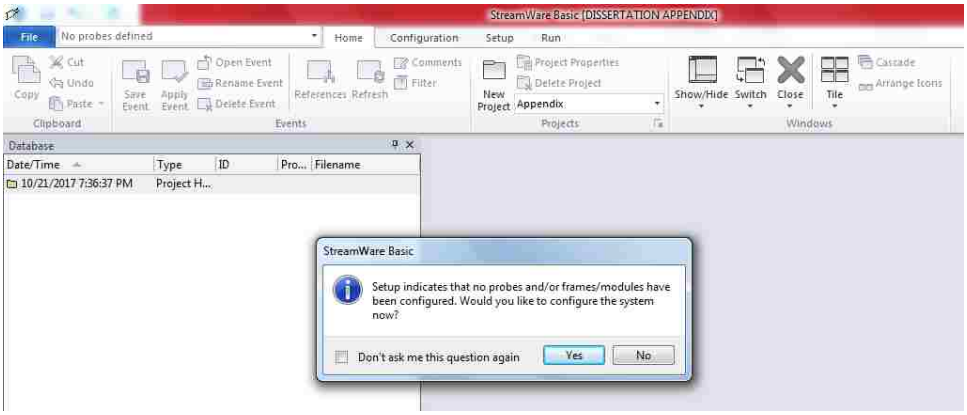

- Now press “yes” to start defining the sensor and the DAQ as follows.

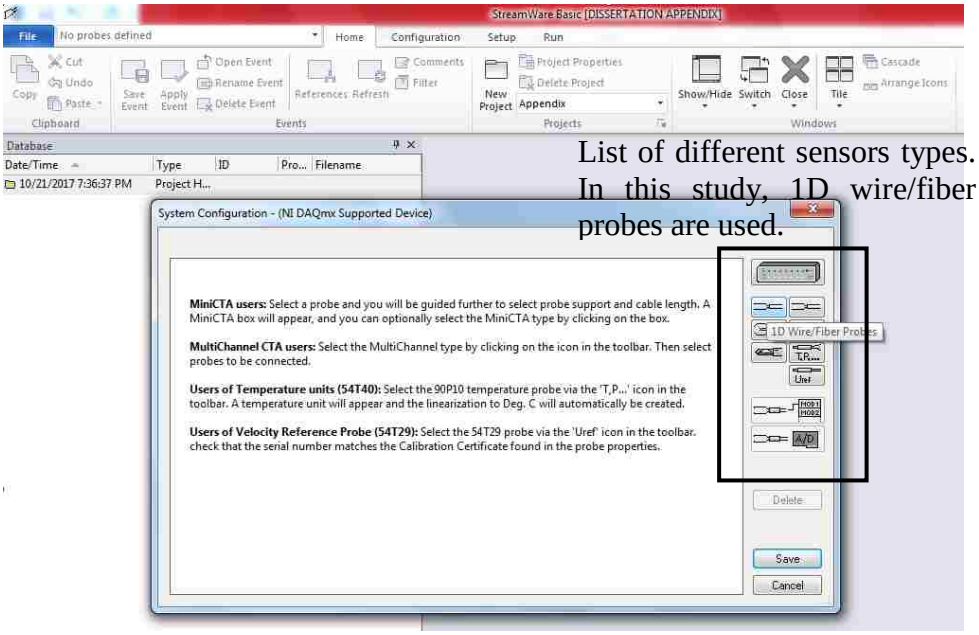

List of different sensors types. In this study, 1D wire/fiber probes are used.

- After choosing 1D wire/fiber probes icon, the following window opens.

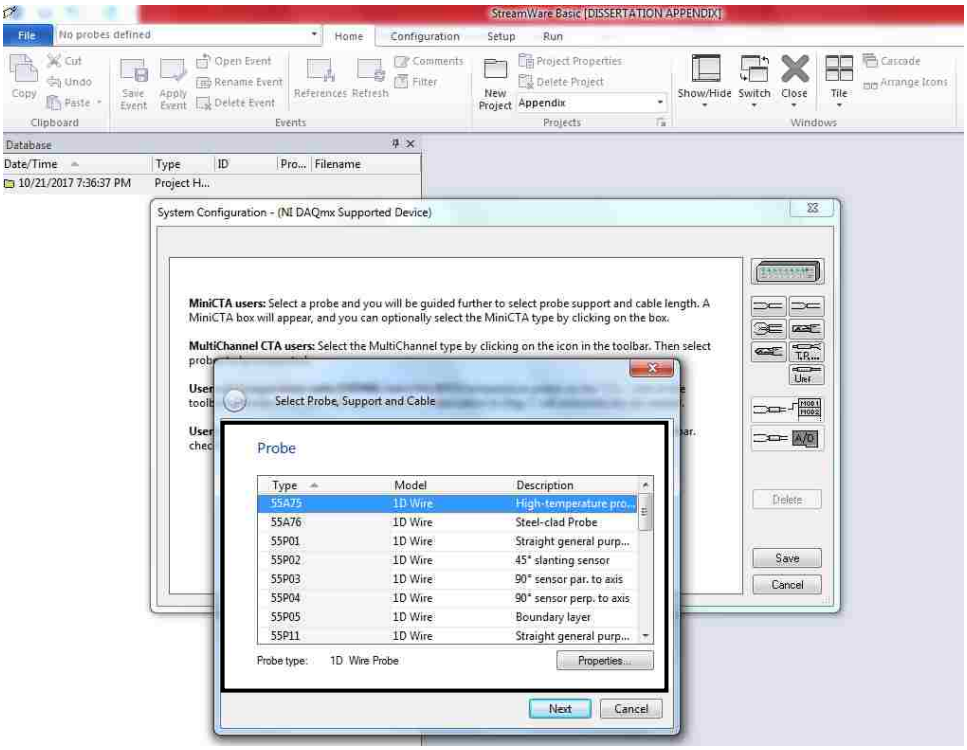

Select the probe type used. In this study (55A75) was used.

- Defining the support probe and the cables used is carried out as follows:

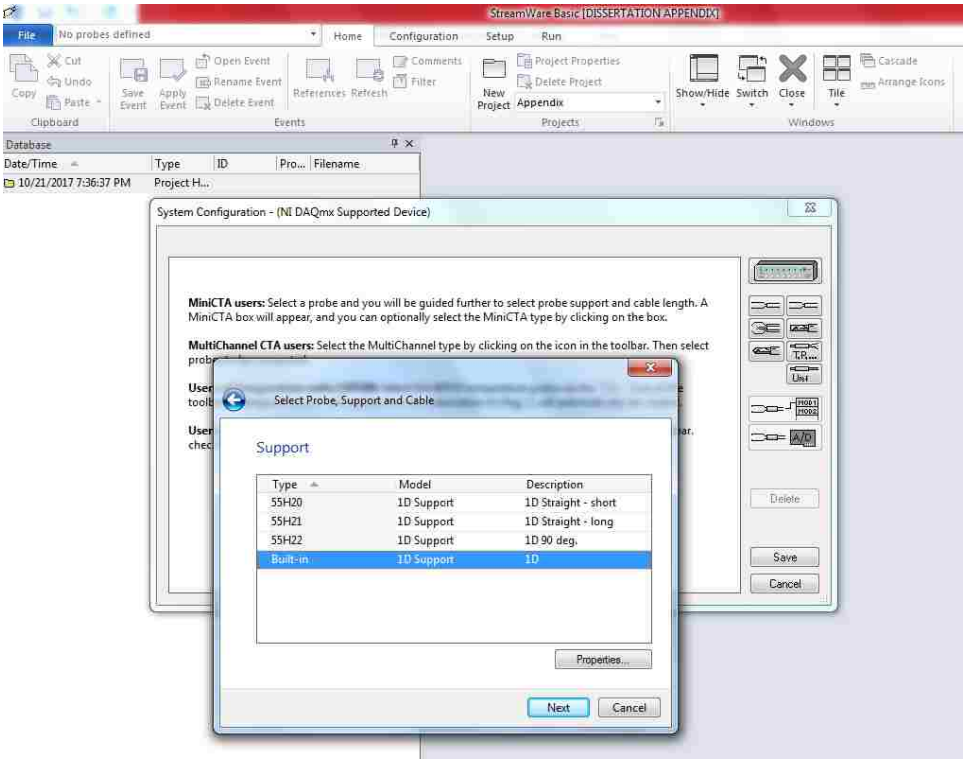

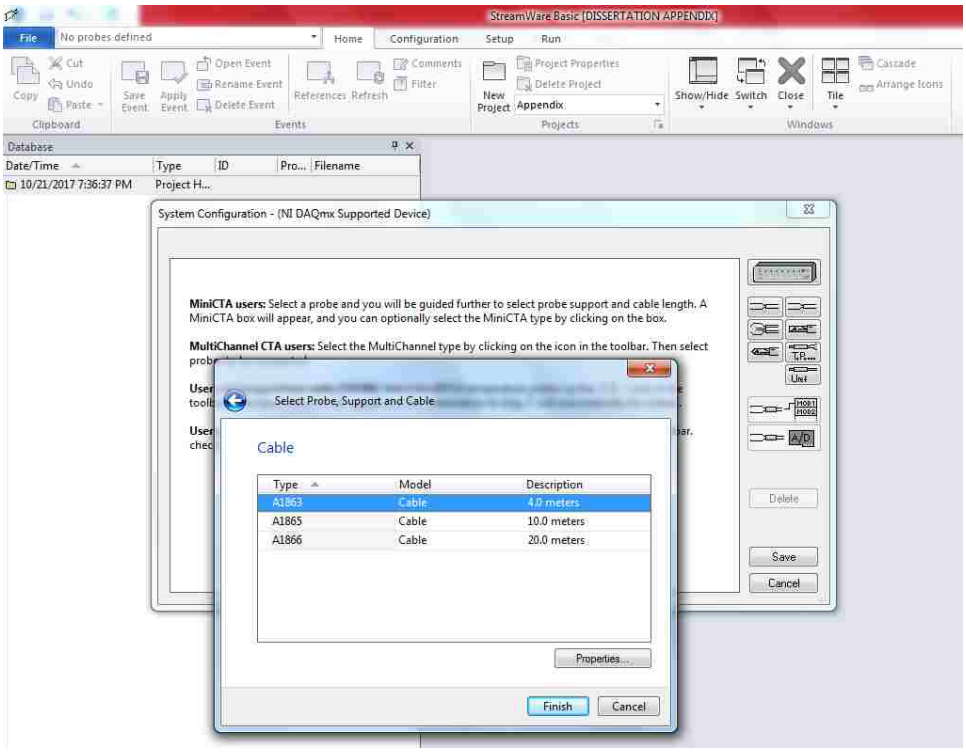

- At this stage, all HWA components are defined and the following page appears.

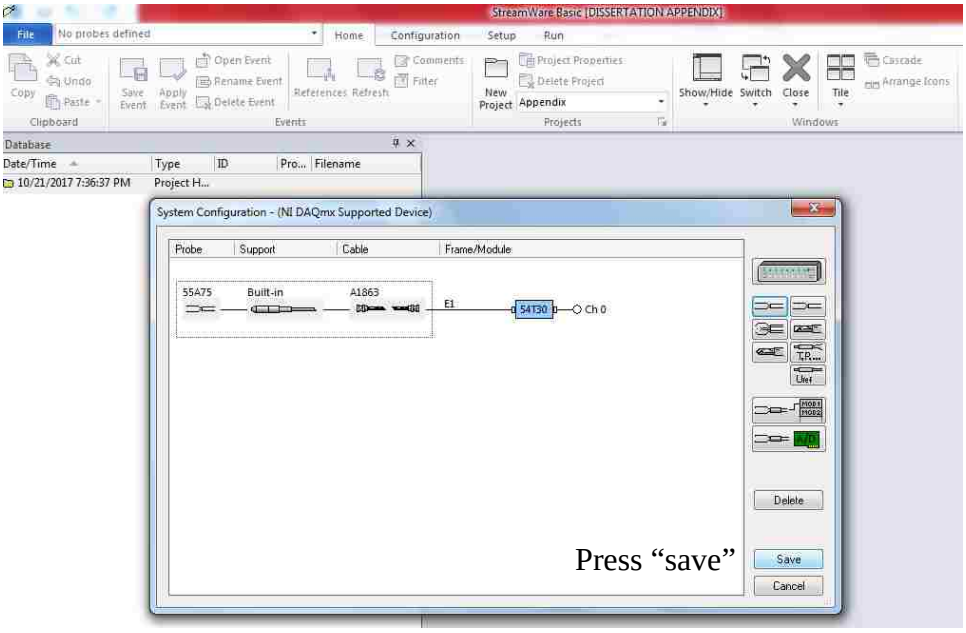

- Afterwards, the software will ask to setup the hardware and the DAQ as follows:

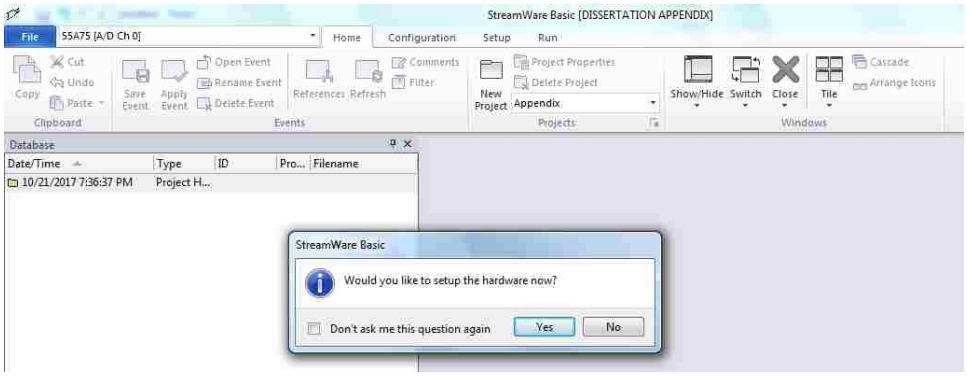

- After pressing “yes”, the following window appears.

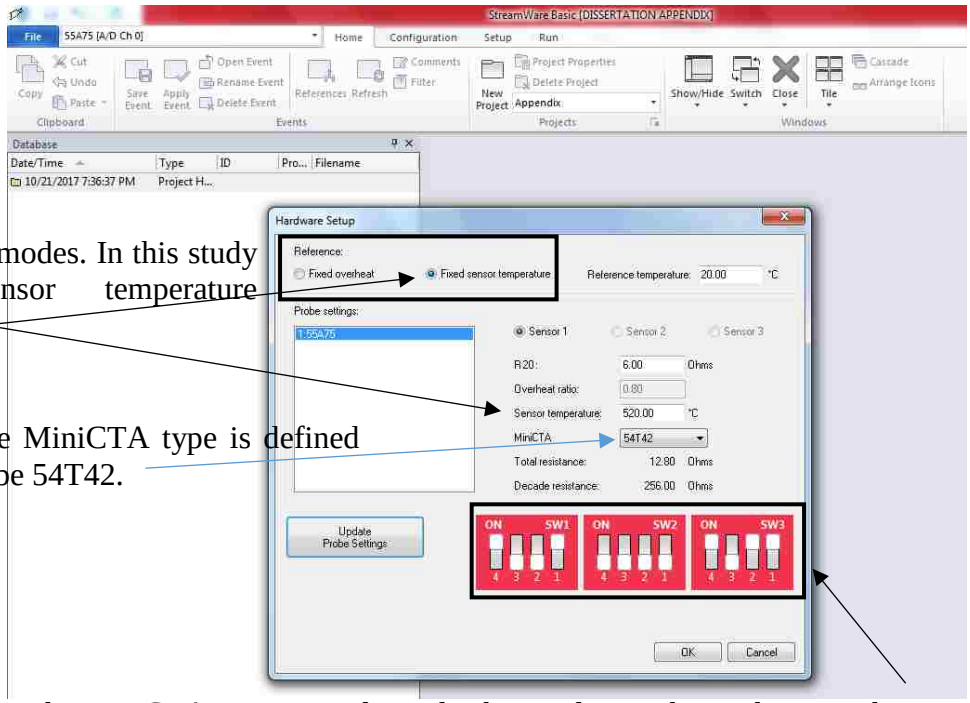

Operating modes. In this study fixed sensor temperature of 520°C.

The MiniCTA type is defined to be 54T42.

The MiniCTA pattern in adjusted to be similar to what is shown in this window.

Picture of the MiniCTA showing the pattern to be adjusted.

- Afterwards, the next window appears asking for the calibration type which is velocity calibration to be selected.

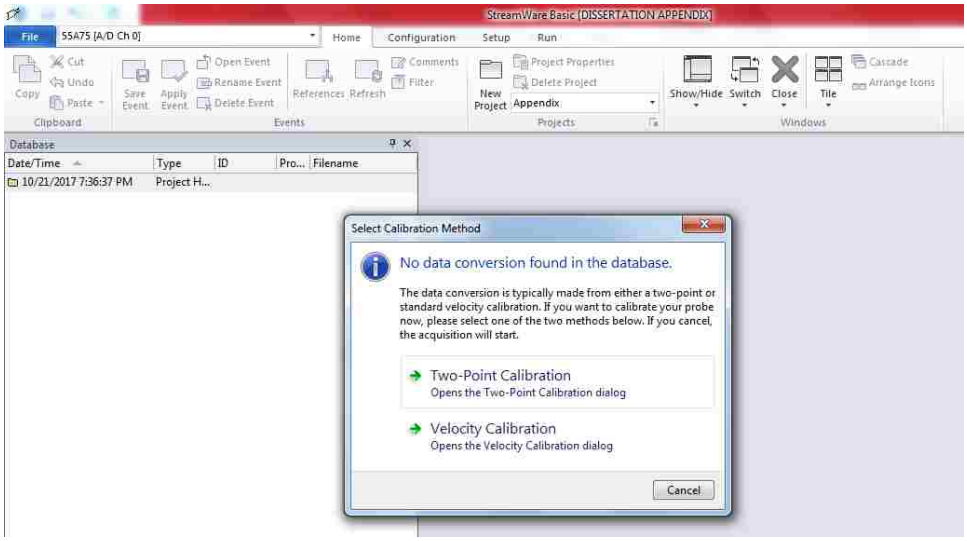

- The following window now appears asking for defining the velocity calibration range. For instance, the experimental velocity is expected to be around 0.3 m/s, then calibration must be conducted for a range covers this expected values (i.e., 0.02 to 0.5 m/s). Also, the number of calibration points is defined to be 10 points. More points will increase the calibration time.

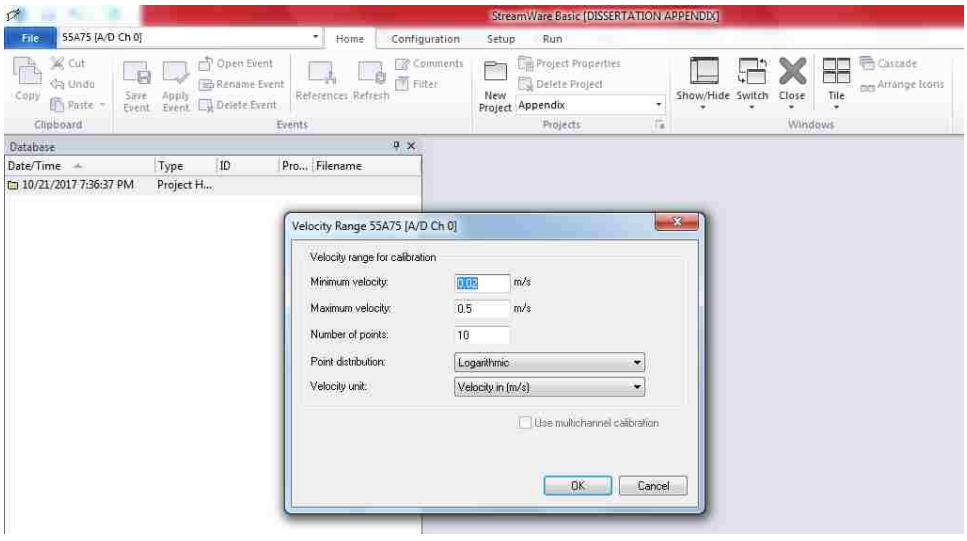

- Now make sure of the following points, shown on the picture, for the calibration unit. It is worth mentioning that the calibrator is covered with a plexiglass box to minimize calibration error resulting from interaction with surroundings.

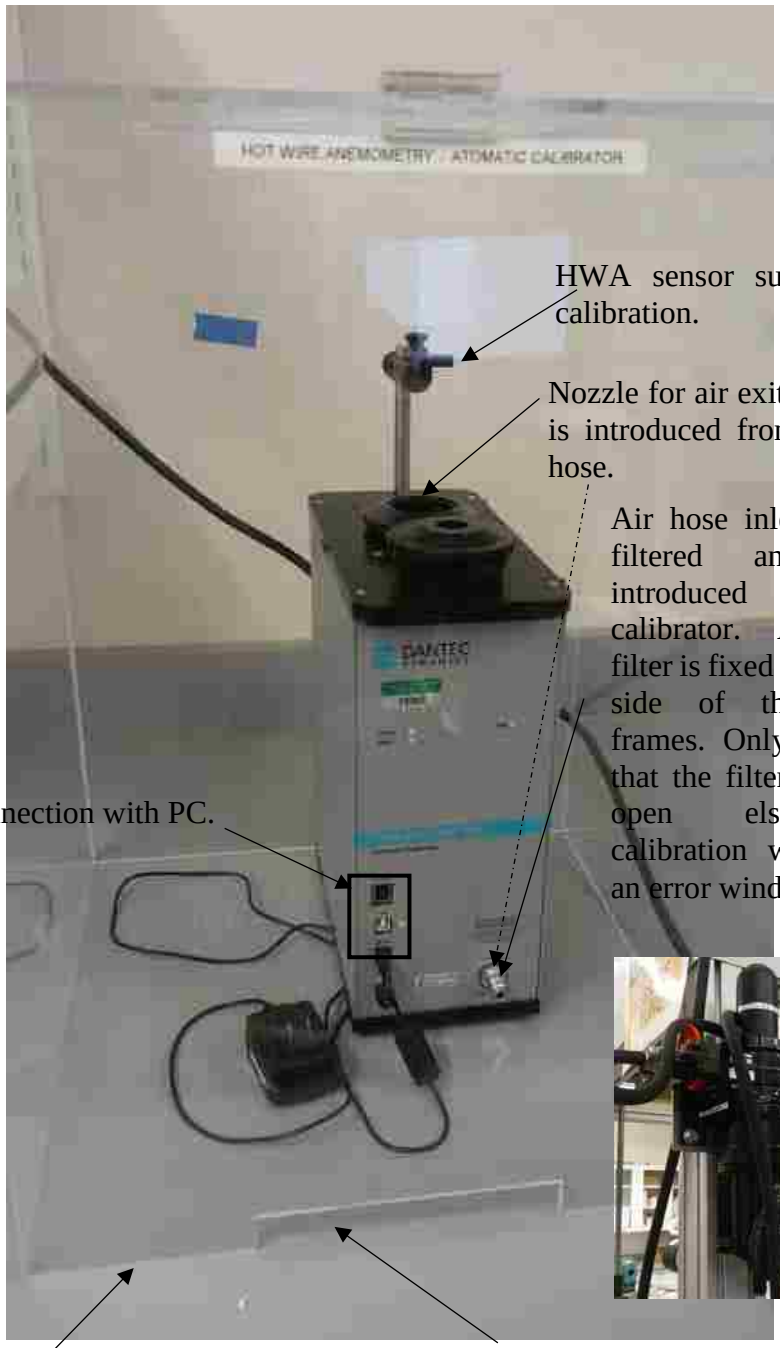

- All previous steps must be concocted before pressing “start” button on the following window else an error message will appear.

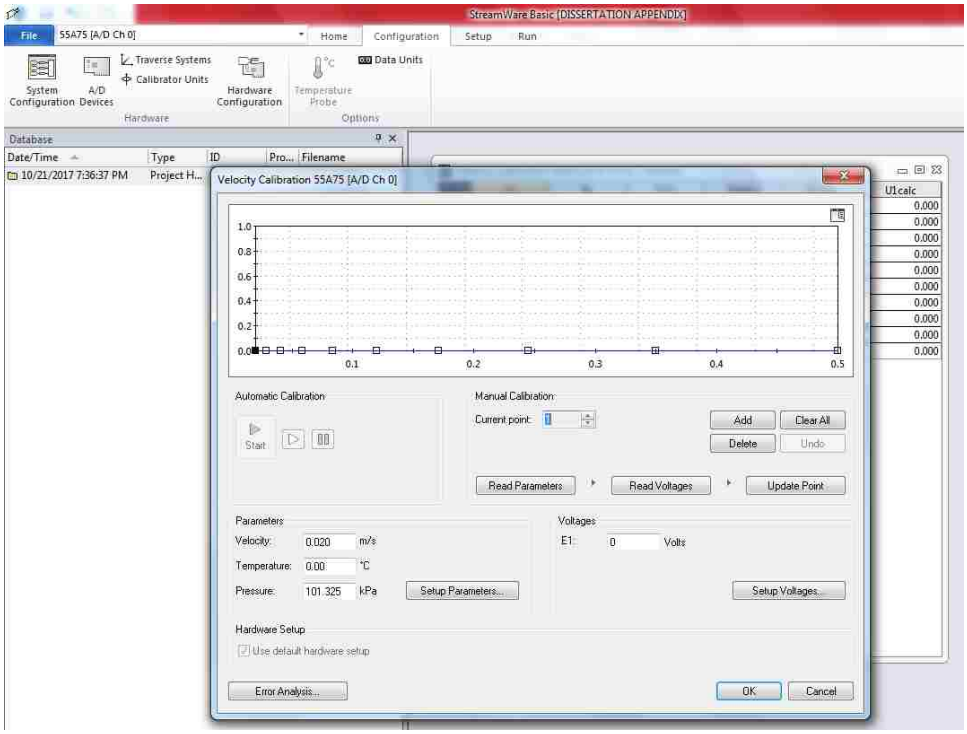

- After completing of calibration, the following window will appear.

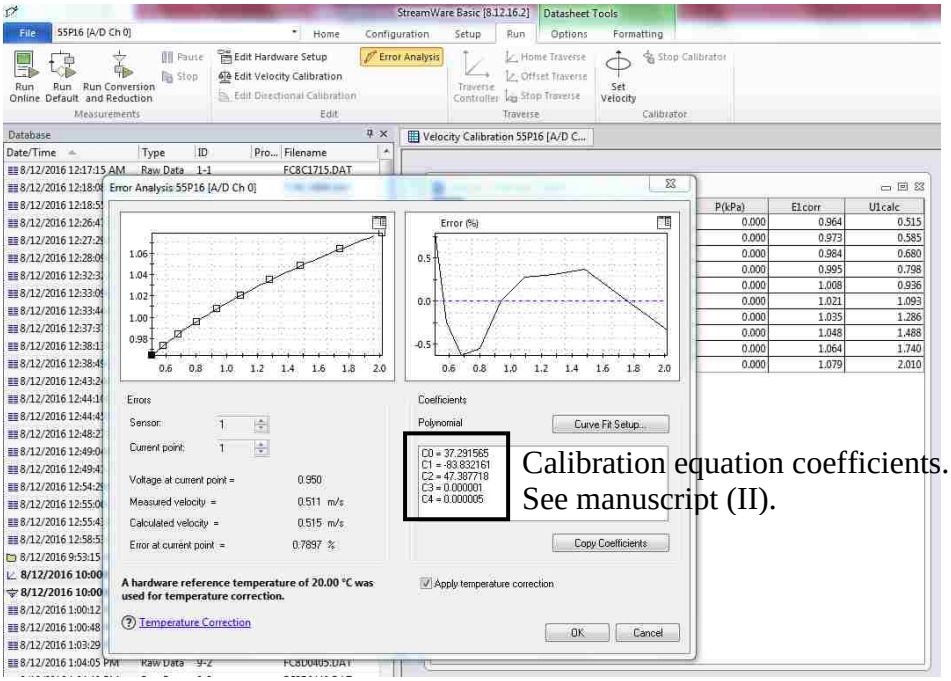

Calibration equation coefficients. See manuscript (II).

- Now system is ready for experiments. There are 2 modes of running experiments (1) run online which will show the velocity variation online while experiment is in operation and (2) run default which is selected to obtain time series velocity measurements.

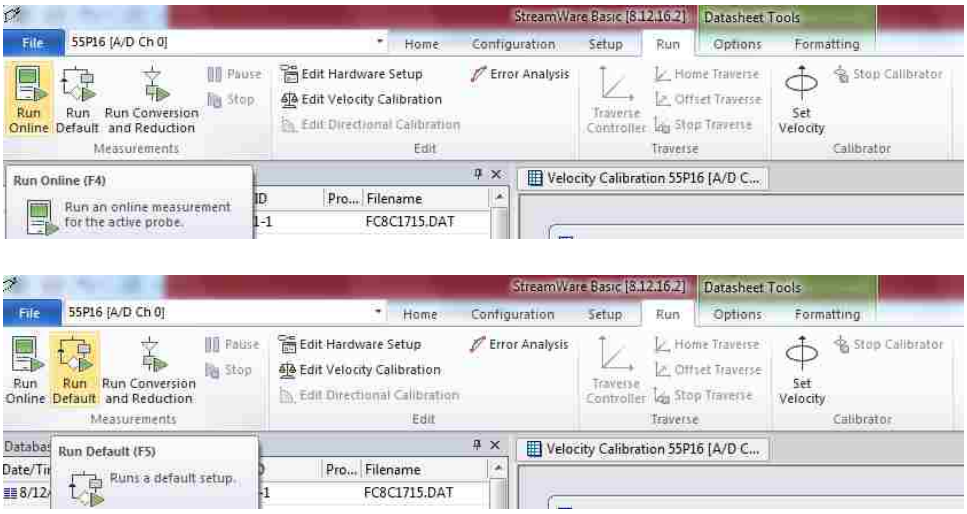

- By selecting run default, you can change the frequency and sampling points be selecting setup from the following window.

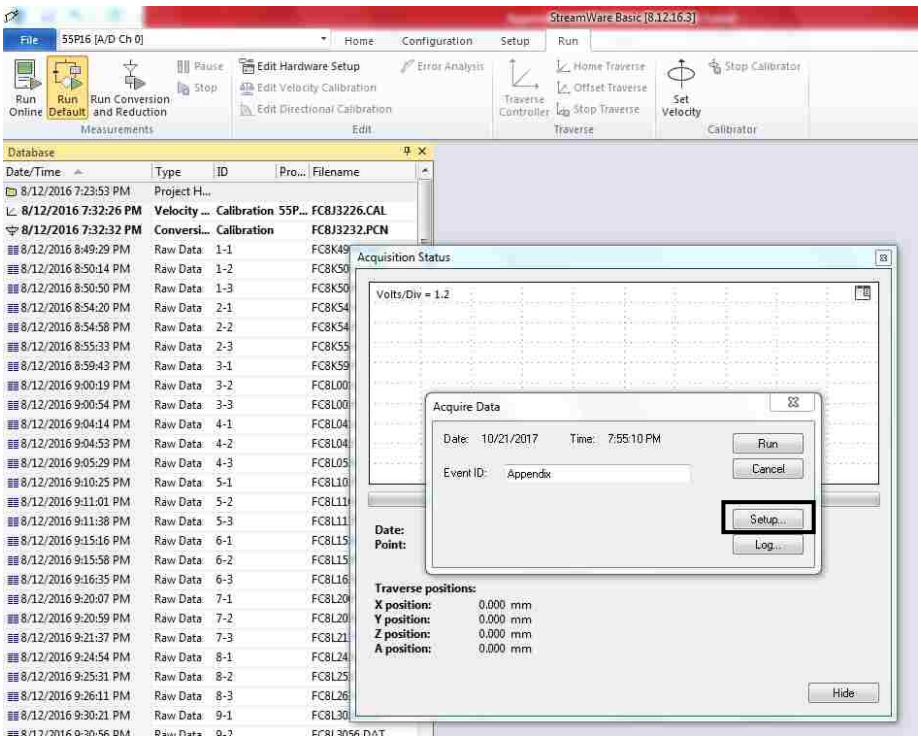

- From the default setup window select “A/D” icon that will open another window called “A/D Device setup” in which you can vary the sampling frequency and number of points.

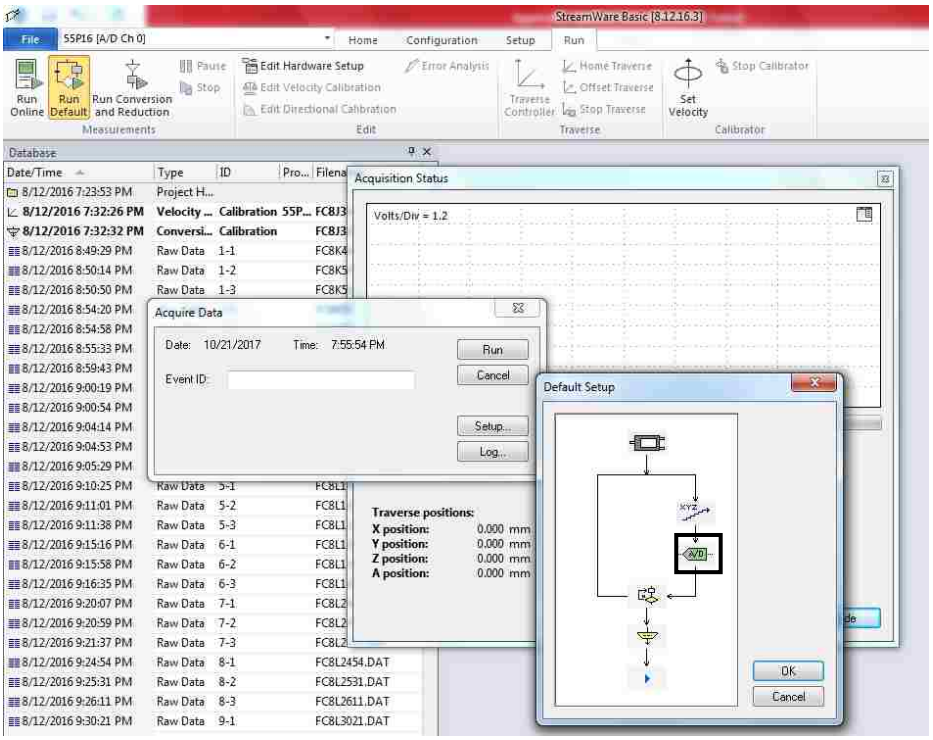

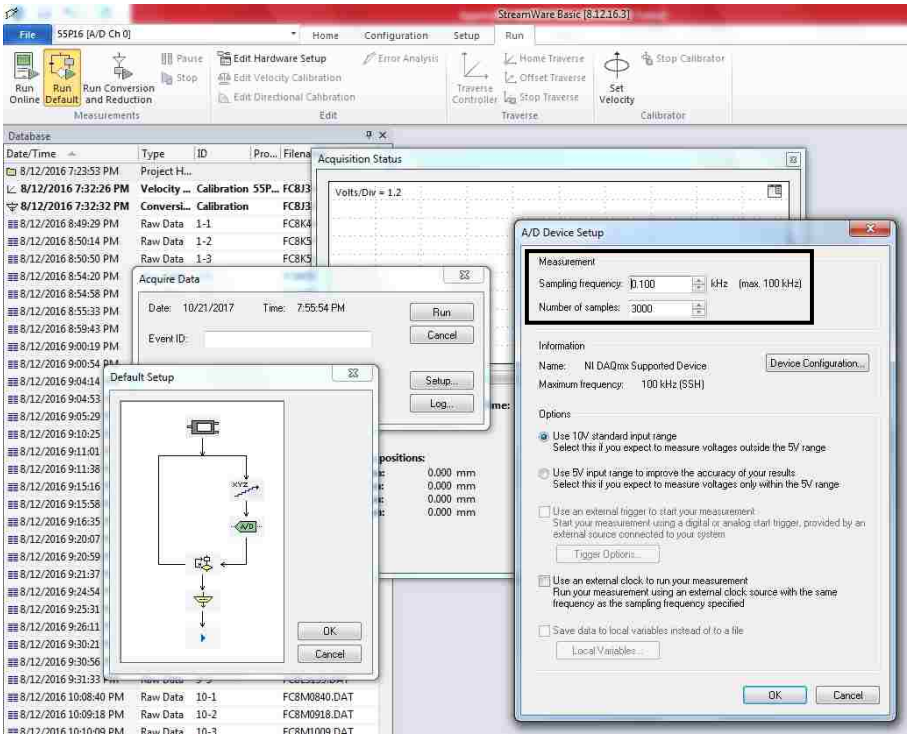

- After finalizing these steps, the obtained results will appear on the left side of the screen. You can select any file and exclude the results in terms of the velocity or the voltage. In the current study voltage results are obtained and corrected to compensate temperature differences between calibration and experimental conditions as discussed in manuscript (II).

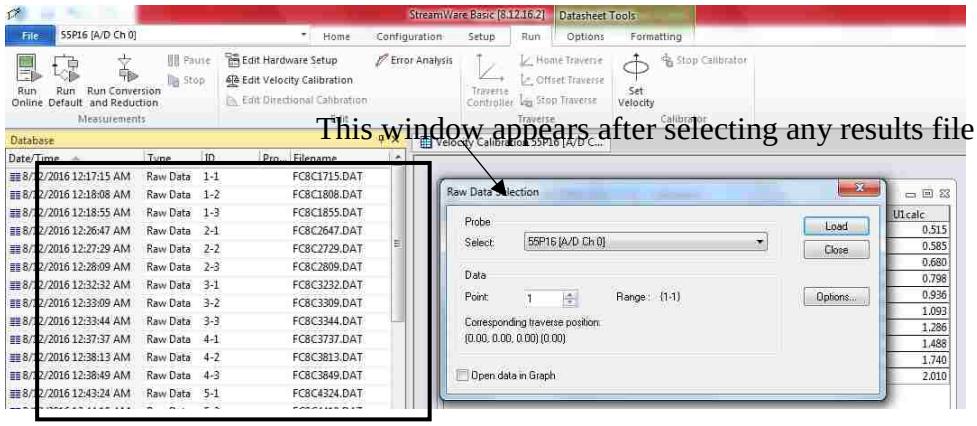

- Now select load to choose the results to be listed as velocity or voltages as follows:

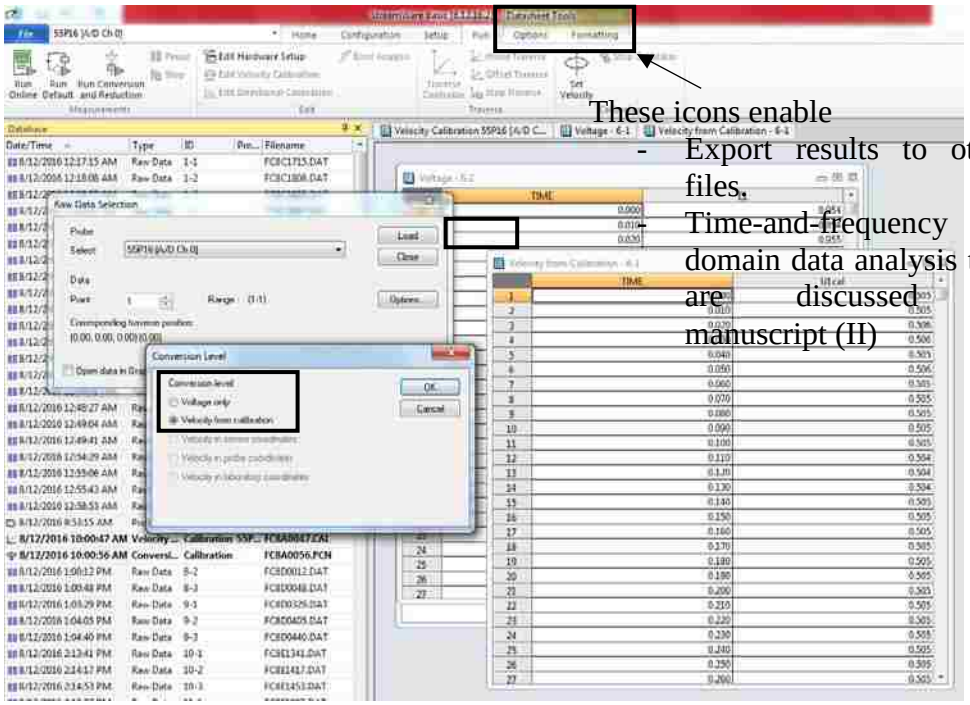

BIBLIOGRAPHY

Koster, A., Matzner, H. D., and Nicholsi, D. R., (2003). "PBMR design for the future." Nuclear Engineering and Design 222: 231–245.

Abdulmohsin, R. (2013). Gas dynaimcs and heat transfer in a packed pebble-bed reactor for the 4th generation nuclear energy. PhD, Missouri University S&T.

Aung, W. (1972). "Fully developed laminar free convection between vertical plates heated asymmetrically." International Journal of Heat and Mass Transfer 15(8): 1577-1580.

Aung, W., L. S. Fletcher and V. Sernas (1972). "Developing laminar free convection between vertical flat plates with asymmetric heating." International Journal of Heat and Mass Transfer 15(11): 2293-2308.

Badr, H. M., M. A. Habib, S. Anwar, R. Ben-Mansour and S. A. M. Said (2006). "Turbulent natural convection in vertical parallel-plate channels." Heat and Mass Transfer/Waerme- und Stoffuebertragung 43(1): 73-84.

Bejan, A. and J. L. Lage (1990). "Prandtl number effect on the transition in natural convection along a vertical surface." Journal of Heat Transfer 112(3): 787-790.

Celataa, G. P., F. Dannibale, A. Chiaradia and M. Cumo (1998). "Upflow turbulent mixed convection heat transfer in vertical pipes." International Journal of Heat and Mass Transfer 41(24): 4037-4054.

Cheng, C.-H., W.-H. Huang and H.-S. Kou (1988). "Laminar free convection of the mixing flows in vertical channels." Numerical Heat Transfer 14(4): 447-463.

Choi, J.-H., J. Cleveland and N. Aksan (2011). "Improvement in understanding of natural circulation phenomena in water cooled nuclear power plants." Nuclear Engineering and Design 241(11): 4504-4514.

Doug Chapin, S. K., and Jim Nestell (2004). The very hight temperature reactor: A technical summary, MPr Associates, Inc.

Dyer, J. R. (1975). "The development of laminar natural-convective flow in a vertical uniform heat flux duct." International Journal of Heat and Mass Transfer 18(12): 1455-1465.

Elenbaas, W. (1942). "Heat dissipation of parallel plates by free convection." Physica 9(1): 1-28.

Fedorov, A. G. and R. Viskanta (1997). "Turbulent natural convection heat transfer in an asymmetrically heated, vertical parallel-plate channel." International Journal of Heat and Mass Transfer 40(16): 3849-3860.

Fu, W.-S., W.-S. Chao, T.-E. Peng and C.-G. Li (2016). "Flow downward penetration of vertical parallel plates natural convection with an asymmetrically heated wall." International Communications in Heat and Mass Transfer 74: 55-62.

Fujii, T., S. Koyama and N. S. Buenconsejo (1988). "Laminar free convection flow rate in a vertical tube." International Journal of Heat and Mass Transfer 31(4): 831-841.

Espinosa-Paredes, G., Castillo-Jimenez, V., Herranz-Puebla, L. E., and Vázquez-Rodríguez, R., (2014). "Surface energy equation for heat transfer process in a pebble fuel." Nuclear Engineering and Design 280: 269–284.

Gradecka, M. J. and B. G. Woods (2016). "Development of thermal mixing enhancement method for lower plenum of the High Temperature Test Facility." Nuclear Engineering and Design 305: 81-103.

Frewer, H., Keller, W., and Pruschek, R., (1985). "The Modular High-Temperature Reactor." Nuclear Science and Engineering 90: 411-410.

Habib, M. A., S. A. M. Said, S. A. Ahmed and A. Asghar (2002). "Velocity characteristics of turbulent natural convection in symmetrically and asymmetrically heated vertical channels." Experimental Thermal and Fluid Science 26(1): 77-87.

Kelly, J., Dujardin, T., and Paillere, H., (2013). GIF's rule in developing the nuclear technologies of the future, NEA news.

Beck, J. M., Pincock, L. F., (2011). High Temperature Gas-Cooled Reactors Lessons Learned Applicable to the Next Generation Nuclear Plant, Idaho National Laboratory.

Jackson, R. B., E. Smith and B. G. Woods (2009). FLUENT modeling for heat transfer in upper plenum of VHTR. Transactions of the American Nuclear Society.

Jaluria, Y. and B. Gebhart (1974). "On transition mechanisms in vertical natural convection flow." Journal of Fluid Mechanics 66: 309-337.

Khane, V. b. (2014). Experimental and computational investigation of flow of pebbles in a pebble bed nuclear reactor. PhD, Missouri University S&T.

Kihm, K. D., J. H. Kim and L. S. Fletcher (1995). "Onset of flow reversal and penetration lengths of natural convective flow between isothermal vertical walls." Journal of Heat Transfer 117(3): 776-779.

Kim, M.-H. and H.-S. Lim (2011). "Evaluation of the influence of bypass flow gap distribution on the core hot spot in a prismatic VHTR core." Nuclear Engineering and Design 241(8): 3076-3085.

LaBar, M. P., A. S. Shenoy, W. A. Simon and E. M. Campbell (2003). "The Gas Turbine-Modular Helium Reactor." Nuclear News 46(11): 28-37.

LaBar, M. P., A. S. Shenoy, W. A. Simon and E. M. Campbell (2004). "Introducing the GT-MHR." Nuclear Engineering International 49(596): 18-23.

Lau, G. E., V. Timchenko, C. Menezo, S. Giroux-Julien, M. Fossa, E. Sanvicente, J. A. Reizes and G. H. Yeoh (2012). "Numerical and Experimental Investigation of Unsteady Natural Convection in a Vertical Open-Ended Channel." Computational Thermal Sciences 4(5): 443-456.

Lee, J. H., S. J. Yoon, H. K. Cho, M. Jae and G. C. Park (2015). "Experimental investigation and CFD analysis on cross flow in the core of PMR200." Annals of Nuclear Energy 83: 422-435.

Lee, J. H., S. J. Yoon, E. S. Kim and G. C. Park (2014). "CFD analysis and assessment for cross-flow phenomena in VHTR prismatic core." Heat Transfer Engineering 35(11-12): 1152-1160.

Lohnert, G. H. (1990). "Technical design features and essential safety-related properties of the HTR-module." Nuclear Engineering and Design 121(2): 259–275.

Martineau, R. C. and R. A. Berry (2010). "A preliminary investigation of rapid depressurization phenomena following a sudden DLOFC in a VHTR." Nuclear Engineering and Design 240(5): 1013-1021.

Martynenko, O. G., A. A. Berezovsky and Y. A. Sokovishin (1984). "Laminar free convection from a vertical plate." International Journal of Heat and Mass Transfer 27(6): 869-881.

McDonald, C. F. (2014). "Power conversion system considerations for a high efficiency small modular nuclear gas turbine combined cycle power plant concept (NGTCC)." Applied Thermal Engineering 73(1): 80-101.

McLlroy Jr, H. M., D. M. McEligot and R. J. Pink (2009). Idaho national laboratory experimental program to measure the flow phenomena in a scaled model of a prismatic gas-cooled reactor lower plenum for validation of CFD codes. 2008 Proceedings of the 4th International Topical Meeting on High Temperature Reactor Technology, HTR 2008.

McVay, K. L., J.-H. Park, S. Lee, Y. A. Hassan and N. K. Anand (2015). "Preliminary tests of particle image velocimetry for the upper plenum of a scaled model of a very high temperature gas cooled reactor." Progress in Nuclear Energy 83: 305-317.

Miyamoto, M., Y. Katoh, J. Kurima and H. Sasaki (1986). Turbulent free convection heat transfer from vertical parallel plates in air (heat transfer characteristics). Proceedings of the 8th Internation Heat Transfer Conference.

Moses, D. L. (2010). Very High-Temperature Reactor (VHTR) Proliferation Resistance and Physical Protection (PR&PP) ORNL.

Mycle Schneider, A. F., Yurika Ayukawa, Shaun Burnie, Raffaele Piria, Steve Thomas, Julie Hazemann (2014). The World Nuclear Industry Status Report Paris, London, Washington, D.C., A Mycle Schneider Consulting Project.

Reyes Jr, J. T., Groomer, B. G. woods, B. Jackson, and T. D. Marshall, (2010). "Scaling analysis for the high temperature Gas Reactor Test Section (GRTS)." Nuclear Engineering and Design 240(2): 397-404.

Rodriguez, S. B. and M. S. El-Genk (2010). On enhancing VHTR lower plenum heat transfer and mixing via swirling jets. International Congress on Advances in Nuclear Power Plants 2010, ICAPP 2010.

Rycroft, C. (2007). Multi-scale Modeling in Granular Flow. PhD, Massachusetts Institute of Technology (MIT).

Sabharwall, P., T. Marshall, K. Weaver and H. Gougar (2007). CFD Analysis for Flow Behavior Characteristics in the Upper Plenum during low flow/low pressure transients for the Gas Cooled Fast Reactor (GCFR), Idaho National Laboratory (INL).

Sanvicente, E., S. Giroux-Julien, C. Ménézo and H. Bouia (2013). "Transitional natural convection flow and heat transfer in an open channel." International Journal of Thermal Sciences 63: 87-104.

Sato, H., R. Johnson and R. Schultz (2010). "Computational fluid dynamic analysis of core bypass flow phenomena in a prismatic VHTR." Annals of Nuclear Energy 37(9): 1172-1185.

Schulten, R. (1978). "Pebble bed HTRs." Annals of Nuclear Energy 5(8-10): 357–374.

Schulten, R. (1985). "The AVR Nuclear Power Plant —A Milestone in High-Temperature Reactor Development." Nuclear Science and Engineering 90: 388-357.

Southworth, F. H., P. E. MacDonald, P. D. Bayless, H. D. Gougar, R. L. Moore, M. Ougouag, R. L. Sant, J. W. Sterbentz and W. K. Terry (2004). Next generation nuclear plant (NGNP) project - Preliminary assessment of two possible designs. Abstracts of the Pacific Basin Nuclear Conference.

Southworth, F. H., P. E. MacDonald, D. J. Harrell, C. V. Park, E. L. Shaber, M. R. Holbrook and D. A. Petti (2003). The Next Generation Nuclear Plant (NGNP) project. Global 2003: Atoms for Prosperity: Updating Eisenhowers Global Vision for Nuclear Energy.

Sparrow, E. M. and L. F. A. Azevedo (1985). "Vertical-channel natural convection spanning between the fully-developed limit and the single-plate boundary-layer limit." International Journal of Heat and Mass Transfer 28(10): 1847-1857.

Sparrow, E. M., G. M. Chrysler and L. F. Azevedo (1984). "Observed flow reversals and measured-predicted Nusselt numbers for natural convection in one-sided heated vertical channel." Journal of Heat Transfer 106(2): 325-332.

Steinwarz, W. (1990). "Status of design of the HTR test module China." Nuclear Engineering and Design 121(2): 317–324.

Takeda, T. (2010). "Air ingress phenomena in a depressurization accident of the very-high-temperature reactor." Nuclear Engineering and Design 240(10): 2443-2450.

Thomas, S. (2011). "The pebble bed modular reactor: An obituary." Energy Policy 36: 2431-2440.

Tung, Y. H. and R. W. Johnson (2011). CFD calculations of natural circulation in a high temperature gas reactor following pressurized circulator shutdown. ASME 2011 International Mechanical Engineering Congress and Exposition, IMECE 2011.

Yang, X., W. Hu, and S. Jiang (2009). "Experimental Investigation on feasibility of two-regiondesigned pebble-bed high-temperature gas-cooled reactor." Nuclear Science and Technology 46(4): 374-381.

Yilmaz, T. and S. M. Fraser (2007). "Turbulent natural convection in a vertical parallel-plate channel with asymmetric heating." International Journal of Heat and Mass Transfer 50: 2612-2623.

Yilmaz, T. and A. Gilchrist (2007). "Temperature and velocity field characteristics of turbulent natural convection in a vertical parallel-plate channel with asymmetric heating." Heat and Mass Transfer/Waerme- und Stoffuebertragung 43(7): 707-719.

Yoon, S.-J., C.-Y. Jin, J.-H. Lee, M.-H. Kim and G.-C. Park (2011). "Study on the flow distribution in prismatic VHTR core with a multi-block experiment and CFD analysis." Nuclear Engineering and Design 241(12): 5174-5182.

Yoon, S. U. J., C. Y. Jin, M. H. Kim and G. C. Park (2011). "Experimental and computational assessment of core bypass flow in block-type very high temperature reactor." Nuclear Technology 175(2): 419-434.

Yuanhui Xu, A. K. Z. (2002). "Overview of the 10 MW high temperature gas cooled reactor - test module project." Nuclear Engineering and Design 218(13-23).

Zongxin Wu, D. L., Daxin Zhong (2002). "The design features of the HTR-10." Nuclear Engineering and Design 218: 25-32.

Zuoyi Zhang, a. S. Y. (2002). "Future HTGR developments in China after the criticality of the HTR-10." Nuclear Engineering and Design 218: 249-257.

VITA

Mahmoud Mohamed Taha Elsayed Moharam was born in Alexandria, Egypt. In 2011, he received his Bachelors of Engineering (B.E.) in Chemical Engineering from Alexandria University, Egypt. He was employed as an instructor in the Chemical Engineering Department at Alexandria University in which he earned his master's degree (M.Sc.) in 2014. In 2014, he came to the United States to pursue his Doctor of Philosophy degree (Ph.D.) in Chemical Engineering at Missouri University of Science and Technology. His main research project was funded from the United States – Department of Energy (US - DOE) and concerned with experimental investigation of thermal hydraulics natural circulation within a test facility designed with a representative geometry of prismatic modular reactor core. In December 2017, he received his Ph.D. in Chemical Engineering from Missouri University of Science and Technology. He supervised more than 10 undergraduate students. He also served as lecturer in the Chemical Engineering Department at Missouri University of Science and Technology for the course of "Structure and Properties of Polymers".